Algebraic Input-output Equations of Four-bar Kinematic Chains: Planar; Spherical; Spatial

BY

Mirja Rotzoll

A THESIS SUBMITTED TO

The Faculty of Graduate and Postdoctoral Affairs

IN PARTIAL FULFILMENT OF THE REQUIREMENTS FOR THE DEGREE OF

Doctor of Philosophy

IN

Mechanical and Aerospace Engineering

Carleton University

Ottawa, Ontario, Canada

© 2023

Mirja Rotzoll

Doctor of Philosophy (2023) Carleton University

Mechanical and Aerospace Engineering Ottawa, Ontario, Canada

TITLE:	Algebraic Input-output Equations of Four-bar Kinematic Chains: Planar; Spherical; Spatial
AUTHOR:	Mirja Rotzoll
SUPERVISOR:	Dr. M. John D. Hayes
COMMITTEE	Dr. Hans-Peter Schröcker Dr. Howard Schwartz Dr. Natalie Baddour Dr. Rishad Irani Dr. Robert G. Langlois
NUMBER OF PAGES:	xiv, 164

Abstract

Four-bar mechanisms have been investigated for hundreds, if not thousands of years. The extensive research interest stems not only from the wide use in the industry but also from the ability to generate complex kinematic trajectory profiles, one of them being the function generating input-output (IO) equation.

This thesis aims to generalise the procedure for determining the algebraic IO equations for any four-bar linkage kinematic architecture using only algebraic means. The idea is to presume the linkage as an open kinematic chain, and to describe it adopting the Denavit Hartenberg convention. The overall kinematic displacement of the open chain can be specified using Study's kinematic mapping. This mapping allows to characterise the displacement from the base to the end-effector frame as algebraic varieties in the seven-dimensional projective kinematic image space. To obtain a linkage, the open chain is conceptually closed by equating the obtained algebraic parametrisation to its identity, leaving a set of equations that completely describe the linkage. With the help of elimination theory, the given system of polynomial equations is solved such that an equation is obtained that depends only on two joint variables. These equations represent the desired algebraic IO equations for the respective linkage. In total, there are six algebraic IO equations for each four-bar linkage kinematic architecture.

While the main objective of this thesis is the derivation of the IO equations using kinematic mapping, the geometric interpretations of the coefficients of the algebraic

IO equations reveal some deep insight on some of the characteristics of the linkages. The geometric representation of these parameters is called the design parameter space, and depending on the position of the points within the design parameter space, it is possible to directly extract information on the relative mobility classification of the linkage. Moreover, the utility of the algebraic IO equations is illustrated with detailed application examples of differential kinematics.

Acknowledgements

First of all, I would like to express my deepest appreciation to my supervisor M. John D. Hayes. Without the many weekly discussions, his patience to answer all the questions I had, and his encouragement and support, this thesis would not have been accomplished. I am grateful for the countless hours that he meticulously edited my publications and provided me with valuable feedback. His dedication to research and his students has been a true inspiration. He has made my experience as a student at Carleton University unforgettable. Thank you, John.

I am also grateful to my co-examiner Hans-Peter Schröcker as well as my committee members Howard Schwartz, Natalie Baddour, Rishad Irani and Robert G. Langlois who provided me with feedback and guidance on my thesis. In addition, I acknowledge the generous financial support from the Natural Sciences and Engineering Research Council of Canada and Carleton University.

In January 2019, I went to the University of Innsbruck for 4 months to study with Manfred L. Husty and his research group. It has been a productive and extraordinary experience, and many of the results found in this thesis would not have been possible without the help and ideas of Manfred.

In this regard, I also acknowledge the financial support of this project and my stay in Austria from Mitacs Globalink. Moreover, I wish to express special thanks to Martin Pfurner, who always answered my questions and was able to translate complex

mathematics into an understandable engineering language. I am also thankful to Daniel F. Scharler, Johannes Stiegele and Thomas Stigger for helping me to develop an understanding of the subject at the beginning of my Ph.D., and the many discussions we had while sharing an office in Innsbruck, and Ottawa.

Thanks should also go to Colin Ingalls, Professor at Carleton University, and Margaret H. Regan, Assistant Research Professor at Duke University, for whom I had the pleasure of collaborating on different conference papers. Thanks to their mathematical knowledge, they helped improve the quality of my papers and confirmed some of the results found in this thesis.

I would also like to thank Zachary A. Copeland, Alia Nichol and Quinn Bucciol for the many questions and discussions we had which helped me find answers to some of the gaps in my research.

Finally, I would be remiss in not mentioning my family, especially my husband, my parents, and siblings for their moral support, constant encouragement, and the strength they gave me to complete this thesis.

Contents

List of Figures

List of Tables

Nomenclature

Acronyms

C	Cylindrical joint
DH parameters	Denavit-Hartenberg parameters
dof	Degree of freedom
H	Screw joint
ICV	Instant centre of velocity
IO equation	Input-output equation
LIA	Linear implicitisation algorithm
P	Prismatic joint
R	Revolute joint
S	Spherical joint

Symbols

α_i	Tangent half twist angle: $\tan(\tau_i/2)$
v_i	Tangent half joint angle: $\tan(\theta_i/2)$
$\mathbb{C}$	Set of complex numbers
$\mathbb{R}$	Set of real numbers
$\mathbf{A}$	Matrix (bold capital letter)
$\mathbf{a}$	Vector (bold small letter)

$\mathbf{I}$	Identity matrix
$\mathcal{S}_6^2$	Study quadric
τ_i	Twist angle as defined by the standard DH parameters
θ_i	Joint angle as defined by the standard DH parameters
a_i	link length as defined by the standard DH parameters
d_i	Link offset as defined by the standard DH parameters
A_∞	Exceptional generator
P^7	Seven-dimensional projective space / kinematic image space
$\mathbb{E}^2$	Two-dimensional Euclidean space
$\mathbb{E}^3$	Three-dimensional Euclidean space
$SE(2)$	Group of planar Euclidean displacements
$SE(3)$	Group of Euclidean displacements in $\mathbb{E}^3$
$SO(3)$	Group of rotations in $\mathbb{E}^3$
A	Kinematic image coordinates of $\mathbf{A} \in SE(3)$

Chapter 1

Introduction

Four-bar linkages can be found in a multitude of applications, including windshield wipers, pumps, and suspension systems. They consist of four rigid links coupled by lower pairs, such as revolute (R), prismatic (P), spherical (S), cylindrical (C) or screw (H) joints, forming a closed chain. These mechanisms allow for the transformation of an input motion into a desired output motion which can be described by a mathematical function: the input-output (IO) equation. There are different methods for deriving such equations that either rely on trigonometric functions, require geometric consideration throughout the derivation, or have only focused on a particular mechanism without offering a general solution approach that can be applied to a range of mechanisms. This research aims to develop a general method based on algebraic means to obtain the algebraic IO equations for any kinematic architecture of four-bar linkage: planar; spherical; or spatial.

This chapter is organised as follows. It will provide a broad overview of the topic by first discussing the background and context, then addressing the research aims, objectives and questions, the significance and finally, the limitations.

1.1 Background and Research Problem

Due to the wide usage of mechanisms, they have been studied extensively regarding position, velocity, and acceleration analysis. Traditional methods that focus on obtaining the solutions graphically are still being taught to engineering students; see, for example [1]. While manual graphical techniques do not require sophisticated mathematical skill sets, and may be suitable to analyse planar linkages, the drawbacks are evident: they are time-intensive, provide only approximate solutions, and when studying spatial linkages, they require advanced knowledge of descriptive geometry. Moreover, graphical solutions are only valid for a particular position of the linkage. For a general overview, graphical position analysis would need to be repeated for different positions of the input link.

There are also pure numerical methods found in commercial multibody dynamics software, such as ADAMS. These techniques are reliable and very computationally robust, but only provide a discrete single instance for a discrete configuration. These techniques do not provide closed form algebraic equations that characterise the input-output relationship between variables.

As a result, analytical methods are more popular among researchers. One analytical method is based on understanding the linkage's geometry and the resulting geometric constraints that are imposed by the chosen joints. Generally speaking, this method involves identifying trigonometric relations, e.g., by defining law of cosines constraints, or that an R joint is constraining the body to move on a circle, thus, using the equation of a circle. It is easy to imagine that finding geometric constraints of simple four-bar linkages can quickly lead to a desired outcome, such as the IO equation. Derivations using this technique can, for instance, be found in [2]. However, this technique must be adapted every time a different mechanism is analysed, and the geometry must be kept under consideration throughout the analysis.

Another notable analytical method is the vector loop representation. Each link is represented as a position vector, which are added and equated to zero to form a loop. For relatively simple linkages with few unknowns and planar motion, this has proven to be a useful approach. However, once the linkage becomes more complex, using vectors is no longer possible. For example, a two (three)-dimensional vector loop equation can only be solved for two (three) unknowns, respectively. Thus, as soon as more than three equations are necessary to solve for the IO equation of spatial linkages, dual quaternions or matrices must be applied. A matrix method for analysing linkages is, for instance, outlined in [3, 4]. Although this approach is interesting, one major shortcoming is that solving the equations involves trigonometric terms, which is computationally more expensive than solving algebraic expressions. Not surprisingly, the resulting IO equations are also expressed trigonometrically, which is more challenging to work with as a mechanical designer who, e.g., is synthesising the linkages that generate the desired IO functions. In contrast to trigonometric IO equations, algebraic equations can easily be adapted to continuous approximate synthesis that has proven to converge much faster [5, 6].

In fact, there exist only three algebraic IO equations in the literature, described in [7, 8, 9]. They describe the IO relations of the planar quadrilateral linkage, and the Bennett linkage. No other algebraic IO equations have been reported.

Due to the rapid rise of computing power as well as developments of algorithms that can efficiently handle polynomial equations, the area of analysing mechanisms using algebraic tools is attracting growing attention. However, none of them has considered a systematic approach, i.e., an approach that only requires taking the geometry of the linkage in the problem statement into account, to derive the IO equations for any type of four-bar linkage using algebraic geometry.

1.2 Research Aims, Objective and Questions

The aim of this work is to generalise the procedure for determining one single method to obtain the algebraic IO equation for any kinematic architecture of four-bar linkage: planar; spherical; or spatial by using only algebraic means. In contrast to previous procedures, it will follow the same main steps for every linkage architecture, does not rely on trigonometry, nor any geometric insights other than during the initial problem statement, and is not restricted to planar linkages.

In order to achieve this research aim, this work is inspired by the significant contributions of the following authors: 1. Hartenberg and Denavit [3] who developed a standardised approach to describe kinematic chains. In the proposed algorithm in this thesis, their convention will be applied to describe the linkage as an open kinematic chain. Thus, the geometry of the linkage is only considered in the initial step; 2. Study [10] who proposed to view displacements as points on a quadric surface in a seven-dimensional projective space. While Study's representation was pushed into the background for almost a century due to its computational requirements, it was rediscovered in recent years to help analyse robotic kinematic chains algebraically, for example [11, 12, 13, 14]. In short, the proposed algorithm will use Study's representation to obtain a complete explicit parametrisation of the kinematic chain by mapping the overall displacement of the end-effector into Study's kinematic image space. Afterwards, the open chain is conceptually closed by applying the closure equation, thus, equating the parametrisation to its identity, resulting in a set of polynomial equations; and finally, 3. Buchberger [15] and Walter and Husty [16] who developed algorithms to solve systems of nonlinear multivariate polynomial equations. Since this thesis is interested in obtaining the IO equations, intermediate joint angles must be eliminated from the system of polynomial equations which can be done with the help of these algorithms.

In particular, the thesis will seek to answer the following questions:

1. How can the algebraic IO equations of an arbitrary four-bar linkage be obtained using only algebraic means? What are the steps involved?

2. How does the procedure change if one is interested in another related angle pair within the linkage?

3. How can mechanical engineers profit from these algebraic IO equations? In other words, what are possible applications where the algebraic IO equations can be successfully argued to be superior compared to traditional trigonometric equations?

1.3 Significance

This thesis offers, for the first time, a generalised procedure to determine the algebraic IO equations of any four-bar linkage jointed with lower kinematic pairs. It is successfully applied to a range of linkages, covering planar, spherical and some spatial kinematic chains. Due to being completely general, the work from this thesis may also be applied to a range of other linkages to compute either the algebraic IO equation of other known linkages, or to derive the algebraic IO equations of linkages that have not yet been discovered. Either way, this work provides some solid groundwork to the field of deriving IO equations through algebraic means.

Not only does this study provide important insights into the procedure of deriving IO equations, it equally reveals for the first time the algebraic versions of some well-known IO equations. Moreover, this thesis derives all related six angle pair equations within a four-bar linkage, the v_i-v_j equations, which have never been stated in the literature. To date, research on these equations has mostly focused on developing trigonometric equations. Working with algebraic IO equations provides clear

advantages to mechanical engineers. Specifically, the algebraic IO equations are a convenient tool for differential kinematics at the velocity, acceleration, jerk, or any level. They provide an excellent alternative to traditional vector analysis and trigonometric methods. In addition, mechanical designers of linkages profit from using algebraic IO equations when having to synthesise functional relationships. Even though specific examples for synthesis are not presented in this thesis, it is widely accepted that continuous approximate synthesis is the most accurate technique to simultaneously minimise the design and structural errors to generate desired functions by determining the most appropriate design parameters of the linkage [17]. The processing time of continuous approximate synthesis decreases if algebraic rather than trigonometric equations are implemented as the optimiser only has to integrate algebraic terms which is computationally less complex.

Finally, the algebraic IO equations offer a new tool of the design parameter space interpretation for analysing the linkage's mobility. In particular, this thesis offers a first investigation of the algebraic design parameter space of the quadrilateral, slider-crank and spherical linkage where the space is spanned by the different link design parameters. It turns out that the coefficients of the algebraic IO equation of planar and spherical 4R linkages can be interpreted as the faces of a stellated octahedron which partitions the space into regions that completely define the mobility of each of the links. This fact has never been observed before. Hence, as every point in the design parameter space represents a particular linkage, mechanical designers can use this space as a visual tool to immediately extract the relative mobility of every link.

1.4 Claim of Originality

The author claims the originality of the ideas and results presented herein, the main contributions to the field are as follows:

1. This thesis offers a generalised procedure for determining the algebraic IO equations of the quadrilateral, slider-crank, double slider, spherical, Bennett and RSSR linkage using algebraic geometry tools.

2. This is the first work providing all six of the algebraic IO equations of each of the quadrilateral, slider-crank, double slider, spherical and RSSR linkage.

3. Another outcome of this work is the derivation of the algebraic IO equations relating the four distinct joint variable parameters in the quadrilateral, slider-crank, double slider and the spherical linkage. The resulting algebraic v_i-v_j equations have never been stated in the literature.

4. The new algebraic IO equations significantly reduce the effort of differential kinematics. This approach is original, and, e.g., has been applied exemplary to the RSSR in order to find the extreme angular accelerations.

5. This work provides the velocity and acceleration level kinematics of the quadrilateral, covering the velocity and acceleration IO equations relating all angle pairings. It agrees with previously known four trigonometric velocity ratios and offers all six velocity and acceleration ratios.

6. The thesis provides a new interpretation of the algebraic design parameter spaces for the quadrilateral, slider-crank and spherical linkage. It also explores important insights into the different regions of the design parameter space which helps analysing linkages regarding the mobility of every link.

Some of the research presented in this work has been published in 13 peer-reviewed journal or conference articles: [6, 18, 19, 20, 21, 22, 23, 24, 25, 26, 27, 28, 29].

1.5 Limitations

While the algorithm presented is a general algorithm, it is only applied to a limited number of four-bar linkages in this thesis, including all planar linkages, the spherical linkage and two spatial linkages. It is always possible that the algorithm reaches its limits with other linkages, e.g., due to special geometric constellations, high complexity, limited processing capacity, etc. A case by case study would provide more insights, but considering the limited time, the focus is set on some of the most common linkages.

In addition, it is well-known that the DH parameters are not unique. Hence, depending on how they are chosen in the problem statement, they can influence the resulting IO equations. This does not denote that the results are wrong, the DH parameters are rather measured differently which needs to be kept in mind when comparing results from other sources, or when proceeding with the linkage position, velocity and acceleration analysis. A similar consideration must be made when deciding whether the coordinate systems are assigned clockwise versus counterclockwise as this may also influence the DH parameters.

To support this work and the benefit of using algebraic IO equations, some applications have been included, such as mobility analysis, the establishment of the design parameter space and computing differential kinematics. The procedure of this type of analysis remains the same for each algebraic IO equation. However, due to the limited time and space, this work focuses on a selection of examples. Hence, the findings presented in Chapter 5 might not be transferable to other algebraic IO equations, or might require different considerations, e.g., when analysing the design parameter space of the RSSR.

1.6 Structural Outline

This thesis is organised as follows:

Chapter 1: This chapter introduces the topic, and explains the research aims, objectives and questions. It also outlines the significance and limitations of this research.

Chapter 2: This chapter reviews some common kinematics terminology. In addition, all linkages to be examined are introduced: the quadrilateral, slider-crank, double slider, spherical, Bennett and the RSSR linkages. This chapter also discusses the most important works on the IO equations in the literature.

Chapter 3: This chapter presents the mathematical background required for the proposed algorithm. This includes the introduction of Denavit-Hartenberg (DH) parameters, the concept of Study's kinematic mapping as well as elimination techniques in algebraic geometry.

Chapter 4: This chapter focuses on the proposed algorithm for finding the algebraic IO equations of different linkages, i.e., all possible planar four-bar, the spherical and two spatial linkages: the Bennett and the RSSR. For each kinematic architecture there are six v_i-v_j IO equations.

Chapter 5: This chapter covers some applications the algebraic IO equations which are advantageous over trigonometric equations, as well as some new discoveries that the algebraic equations have exposed. This includes singularity analysis, the mobility classification and velocity and acceleration level kinematics. While it is technically possible to examine every IO equation presented in Chapter 4, this chapter is reduced to an exemplary selection of IO equations to demonstrate its effectiveness.

Chapter 6: In the conclusion chapter the results are briefly summerised and the research questions from the introduction are answered.

Chapter 2

Literature Review

Before diving into the in-depth literature of planar, spherical and spatial linkages, the following section will give an overall picture of the research area and simultaneously a clarification of the necessary terminology.

2.1 Kinematics

2.1.1 Terminology

Kinematics is a branch of mechanics and is the science that investigates the motion of bodies and points without considering the forces that cause them [30]. It is sometimes described as an extension of geometry, thus, would fall into the branch of mathematics. However, geometry itself is static: relative positions and orientations; relative distances and directions. When continuous changes in position and orientation are required, then differential geometry and kinematics can be used to investigate velocities and accelerations [31].

In mechanical engineering, kinematics allows the description of the motion of several rigid bodies, known as *links*, connected by joints. These systems are called

kinematic chains. If the kinematic chain forms a closed loop, i.e., every link is at least connected to two other links, the system is known as a *closed kinematic chain*. If the chain remains open, i.e., there exists at least one link that is only coupled to one other link, the chain is called an *open kinematic chain*. A closed kinematic chain is referred to as a *mechanism* if it has one link that is *fixed*, meaning this link is chosen as a reference to determine the motion of all other points in the system with respect to that link. Open and closed kinematic chains are often called *serial* and *parallel* kinematic chains, respectively [32].

The type of joint, also known as a kinematic pair, chosen in a kinematic chain determines the relative motion of points on the joint pair of rigid bodies, thus, imposes different types of kinematic constraints. Reuleaux differentiates between *lower kinematic pairs* and *higher kinematic pairs* [33], where the former allows surface contact and the latter line or point contact between pair elements. He identified exactly six lower kinematic pairs, any other joint is considered a higher kinematic pair. Accord-

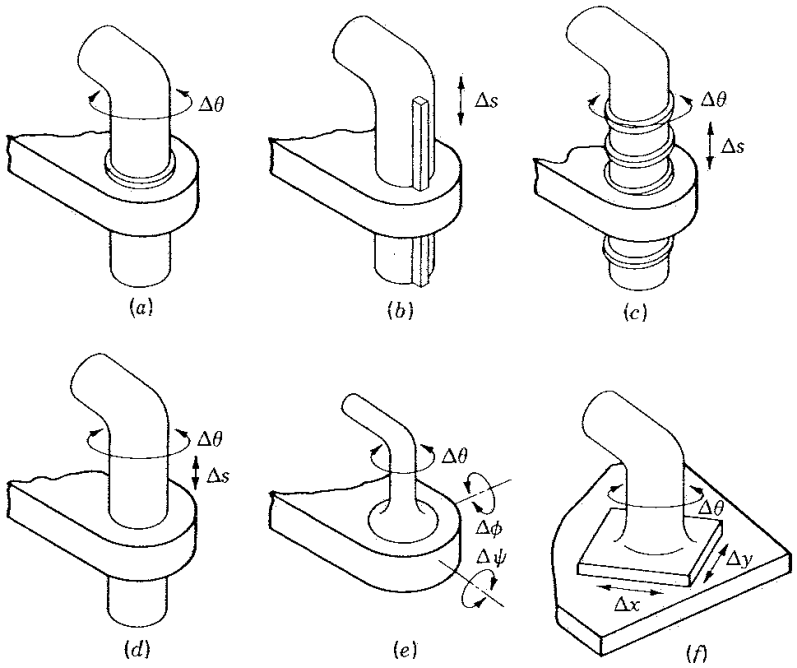

Figure 2.1: Lower kinematic pairs [31].

ing to Fig. 2.1, the six lower kinematic pairs, their relative constrained motion and

degree of freedom (dof) are [33]:

(a) **Revolute pair** ***R***: circular motion with 1 dof and 2 constraints in the plane, 5 in space;

(b) **Prismatic pair** ***P***: rectilinear motion with 1 dof and 2 constraints in the plane, 5 in space;

(c) **Screw pair** ***H***: helical motion with 1 dof and 5 constraints in space;

(d) **Cylindrical pair** ***C***: cylindrical motion with 2 dof and 4 constraints in space;

(e) **Spherical pair** ***S***: spherical motion with 3 dof and 3 constraints in space;

(f) **Planar pair** ***E***: planar motion with 3 dof and 3 constraints in space.

If all pairs of a mechanism are lower kinematic pairs, then the mechanism is called a *linkage* [31]. Linkages can be categorised in different ways, one according to the characteristics of the motion of the links: planar, spherical or spatial [34].

A linkage is called planar if each point describes a plane curve in space and all curves of all points are parallel to one reference plane. A linkage is called spherical if each of its points describes a curve on a spherical surface, and if these curves are all concentric with a single reference sphere. Finally, a linkage is called spatial if the motion of each point is not subjected to any restrictions. Hence, spherical and planar linkages are special cases of spatial mechanisms where the joint axes are directed in a special geometric constellation.

Generally, the purpose of a linkage is to transfer a motion of an input link into a desired motion of an output link [33]. The equation that describes the relation between input and output is obtained by establishing a kinematic closure equation, which in this work is called the IO equation.

If the IO equation contains n different circuits that do not intersect, then the

linkage has n different *assembly modes*. In order for the linkage to trace the points in each circuit it must be taken apart and reassembled in a different way. *Working modes* are subtly different. In theory, a linkage can change from one working mode into another working mode by passing through a singular configuration [35]. A complete disassembly is not necessary. In practice, passing through a singular configuration, i.e. passing from one working mode into another, is difficult as the linkage becomes uncontrollable when operating close to this configuration. Hence, the study of singular configurations of mechanisms is extremely important and is covered in a variety of books, theses and articles, for example, in [11, 36, 37, 38].

2.1.2 Kinematic Analysis and Synthesis

Generally, in four-bar mechanism kinematics there exist two distinct types of problems [39]: *kinematic analysis* and *kinematic synthesis*. In the former problem, a mechanism with specified link types and lengths joined with specified types of pairs is given: the goal is to analyse the prescribed motion. In the latter problem, a desired task is given and the goal is to identify the mechanism that "best" performs the task.

The nature of the task can be divided into the following three distinct types.

1. **Function generation**: The motion of the output link is correlated to the motion of the input link according to a specified function over a specified range of motion of the output link.

2. **Path generation**: The path of a point on, or rigidly attached to, a link is confined to a specified curve.

3. **Motion generation**: A desired motion of the link coupling the input to the output link is generated by the motion of the input link.

Moreover, kinematic synthesis is subdivided into three different categories [3].

1. **Type synthesis**: The aim is to determine the appropriate type of mechanism, such as a serial or parallel linkage, gear or cam system, as well as the joint types to perform the desired task.

2. **Number synthesis**: The aim is to determine the appropriate number of links and joints to perform the desired task.

3. **Dimensional synthesis**: The aim is to determine the appropriate geometric parameters, such as link lengths, to perform the desired task.

Once the type and number of links and joints have been chosen, the dimensions of the distances and possibly the angles between the joints must be determined. The kinematic closure equation for the linkage must generally be derived. The equation, or equations, obtained are typically trigonometric functions in terms of the input and output joint values. The coefficients are undetermined distances and angles. We call these coefficients *design parameters*, since a unique linkage with well-defined motion capabilities is determined by choosing a distinct set of design parameters. Similarly, we refer to variable joint rotation and translation parameters as *motion parameters*. For example, in a 4R planar linkage, the link lengths are design parameters, and the link angles are motion parameters.

Suppose that there are three non-linear equations in the three design parameters. In this case, there are three distinct kinematic loops in the chain. Then there are three independent design parameters in each chain, and nine unique values may be identified for a desired specified task.

Suppose further that the output value(s) must be a specified function of the input value(s), i.e., there may be more than 1 dof. Exact synthesis will result in nine distinct values of the input and nine distinct values of the output that satisfy the function, thereby generating a set of 27 equations in nine design parameters. These

types of identification problems can be solved by employing Gröbner bases to identify a univariate polynomial in terms of one of the design parameters, the remaining eight parameters can be identified with back substitution [40]. In this case, there will be more than one solution. However, for each set of design parameters, real or imaginary, the specified function will be exactly generated by the linkage at the prescribed input and output values, but for all other inputs the generated function will not be exact.

Now, let us consider a four-bar 4R function generator. In this case there is one input and one output parameter, but only three ratios of the link lengths [41]. In this case there will be three unknown design parameters and only three IO pairs can be specified that satisfy the desired function. Only at the specified IO pairs will the function be generated exactly by the identified 4R mechanism.

If more IO pairs, which satisfy the function, are specified than the number of design parameters, an exact solution cannot, in general, be obtained. However, the parameters can be identified with numerical approximation techniques. The identified linkage will not, in general, satisfy the function exactly. Hence, this approach to the identification of design parameters is called *approximate synthesis*.

There exist two main methods to solve dimensional synthesis problems: graphical and algebraic. In the past, graphical solutions were obtained using hand drawings, and more recently they are obtained using different CAD software. Algebraic solutions are obtained by manipulating the geometric constellation using algebra software [39].

With a few exceptions, notably [42, 43], all earlier research in this area uses trigonometric IO equations which occludes the algebraic-geometry interpretation of equations. The proposed research aims to find a generalised procedure to derive the algebraic IO equation that applies to all three types of linkages: planar, spherical and spatial; to investigate the structure of these algebraic equations and motion capabilities of the links implied by this structure. Hence, this research is classified into

the area of function generation using algebraic as opposed to trigonometric means.

Before looking at the relevant research on the linkages that will be examined in this thesis, they are narrowed down to the ones that provide practicality in the industry. This requires examining the linkage's relative dof, which will be covered in the following section.

2.2 Relative dof

To determine the relative dof of a kinematic chain, which is one of the crucial first steps in both synthesis and analysis of linkages, Chebychev, Grübler and Kutzbach independently developed a criterion [44]. It is also known as the *mobility formula* and in a three-dimensional space it is given by

$$m = 6(n-1) - 5j_1 - 4j_2 - 3j_3 - 2j_4 - j_5 \tag{2.1}$$

where

$$\begin{aligned} m &= \text{relative dof of mechanism} \\ n &= \text{number of links} \\ j_i &= \text{number of joints having } i \text{ degrees of freedom.} \end{aligned}$$

In planar or spherical kinematics, the criterion reduces to

$$m = 3(n-1) - 2j_1 - j_2. \tag{2.2}$$

Generally, a dof of zero indicates that the given mechanism is a structure and hence cannot move. A dof of one indicates that the mechanism can be driven by one input actuator, while a dof of two requires two input actuators to produce a constrained

output [34].

To be of practical value and to be able to generate a well-defined IO equation, most research on function generation, including this thesis, focusses on the types of mechanism with a dof of one. In the case of planar four-bar linkages, this includes the quadrilateral, slider-crank, and double slider. Hence, the following sections highlight some of the ground-breaking research on IO equations and IO classification schemes of planar, spherical and spatial four-bar linkages. As there exist many different kinds of spatial linkages, the research is narrowed down to two well-known types, i.e., the Bennett and the RSSR linkage.

2.3 Planar Four-bar Linkages

Planar four-bar linkages consist of four connected rigid bodies to form a closed kinematic chain. As mentioned earlier, a linkage is called planar if each point describes a plane curve in space, and all curves of all points are parallel to one reference plane. This limits the usage to R and P joints, whose joint axis are in the case of the R joint perpendicular to the moving plane or in the case of the P joint located at the line at infinity of all planes normal to the direction of translation. Hence, depending on the choice of joints, it can be differentiated between three types of planar linkages: the quadrilateral linkage which contains four R joints, the slider-crank which is equipped with three R and one P joint, and the double slider whose links are connected by two R and two P joints[2]. Applying Eq. (2.2) to each of these three linkages reveals a dof of one, allowing one input to constrain the motion of the linkage.

Linkages with greater than two P joints will not be considered in the thesis since such linkages can only generate curvilinear translations.

2.3.1 Quadrilateral Linkage

In 1954 F. Freudenstein developed an elegant trigonometric equation for planar quadrilateral linkages [41]. The equation, nowadays known as the *Freudenstein equation*, is widely used in function-generation analysis and synthesis theory. It gives designers a tool to identify the link lengths of mechanisms that optimally transform, typically in a least-squares sense, a specific input angle into a desired output angle governed by a specified functional relation, $f(\theta_1) = \theta_4$. Let a_4 be the distance between the centres of the R joints connected to the relatively non-moving base; a_1 the driver or input link length which is moving with an angle θ_1; a_3 the follower or output link length which is moving with an angle θ_4; and a_2 the coupler length of a planar 4R linkage, see Fig. 2.2, then the displacement of the linkage in terms of the link lengths a_1, a_2, a_3, a_4, the input angle θ_1, and the output angle θ_4 is governed by the following IO equation

$$k_1 + k_2 \cos(\theta_4) - k_3 \cos(\theta_1) \quad = \quad \cos(\theta_1 - \theta_4). \tag{2.3}$$

Eq. (2.3) is linear in the k_i Freudenstein parameters, which are defined in terms of the link length ratios as

$$k_1 \equiv \frac{(a_1^2 + a_2^2 + a_4^2 - a_3^2)}{2a_1a_2}; \quad k_2 \equiv \frac{a_4}{a_1}; \quad k_3 \equiv \frac{a_4}{a_2}.$$

The *Freudenstein equation* replaced manual graphical approaches with an analytical mathematical tool to design linkages for a variety of applications, such as braking and steering systems in cars, space and aircraft systems, or even laparoscopic surgical tools. In addition, it became the basis for numerous four-bar analysis and synthesis publications, for example [2, 3, 45, 46].

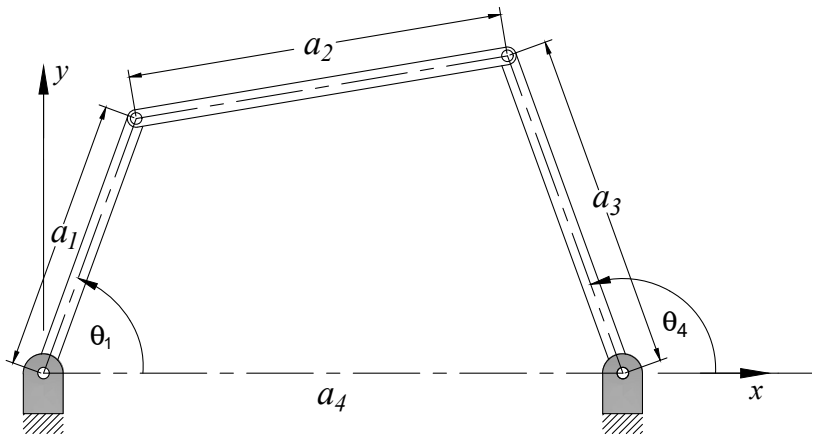

Figure 2.2: Planar 4R function generator.

The first algebraic IO equation for planar quadrilateral linkages was presented in [8] by Bottema and Roth. Their derivation is purely trigonometric. However, by substituting $\tan(\theta_1/2) = u/w$ and $\tan(\theta_4/2) = v/w$ the authors map the IO motion in a (u, v, w)-plane which results in an algebraic version of the equation.

In [7] the authors Hayes, Husty, and Pfurner provided an alternative derivation of a general algebraic IO equation for the same type of mechanism. It was obtained by mapping the linkage constraint equations of the input and output links, i.e., circular motion for the distal R joints, into Study's soma coordinates [10, 8], converting the trigonometric expressions into algebraic ones by applying the tangent of the half-angle, or Weierstraß, substitutions [47], and finally eliminating the Study coordinates to obtain the quartic IO curve [7, 48]. The resulting equation is an algebraic quartic equation in terms of input and output joint angle parameters v_1 and v_4 and is given by

$$Av_1^2v_4^2 + Bv_1^2 + Cv_4^2 - 8a_1a_2v_1v_4 + D = 0 \tag{2.4}$$

where

$$
\begin{aligned}
A &= (a_1 - a_2 - a_3 + a_4)(a_1 - a_2 + a_3 + a_4) = A_1 A_2; \\
B &= (a_1 + a_2 - a_3 + a_4)(a_1 + a_2 + a_3 + a_4) = B_1 B_2; \\
C &= (a_1 + a_2 - a_3 - a_4)(a_1 + a_2 + a_3 - a_4) = C_1 C_2; \\
D &= (a_1 - a_2 + a_3 - a_4)(a_1 - a_2 - a_3 - a_4) = D_1 D_2; \\
v_1 &= \tan\frac{\theta_1}{2}; \\
v_4 &= \tan\frac{\theta_4}{2}.
\end{aligned}
$$

In the design process of linkages for function generation it is equally common to classify the driver and the follower according to their mobility. For obvious reasons, this is an important consideration if e.g., the driver is actuated by a motor that requires full rotations. Hence, it can generally be differentiated between a *crank* which allows a full rotation of the respective link, and a *rocker* whose rotation is bounded by a specified range. Additionally, some authors further divide rockers into 0-rocker and π-rocker. The 0-rocker allows a rotation through $0°$, but does not allow a rotation through $180°$. Contrarily, the π-rocker allows a rotation through $180°$, but does not rotate through $0°$. Classification schemes are not new in the design of linkages and available in many textbooks or publications, for example [49, 50, 51] . Of particular interest is the derivation of a classification scheme presented in [52] as the authors are able to extract three parameters that not only help classifying the planar four-bar linkages but also spherical quadrilateral linkages which will be covered later in the section on spherical linkages. The three parameters T_i derived by Murray and

$$
\begin{aligned}
T_1 &= -a_1 + a_2 - a_3 + a_4 \\
T_2 &= -a_1 - a_2 + a_3 + a_4 \\
T_3 &= -a_1 + a_2 + a_3 - a_4
\end{aligned}
$$

lead to the classification scheme shown in Tab. 2.1.

	Linkage type	T_1	T_2	T_3
1.	crank-rocker	+	+	+
2.	rocker-crank	+	-	-
3.	double-crank	-	-	+
4.	Grashof double-rocker	-	+	-
5.	00 double-rocker	-	-	-
6.	0π double-rocker	+	+	-
7.	$\pi 0$ double-rocker	+	-	+
8.	$\pi\pi$ double-rocker	-	+	+

Table 2.1: Classification of planar 4R linkages

2.3.2 Slider-crank Linkage

Another well investigated planar four-bar linkage is the slider-crank whose most famous application is the piston engine. The linkage allows transforming the reciprocating motion of the piston into a rotary motion of the crankshaft. Inversely, in, e.g., a hand pump, a rotary motion is transformed into a reciprocating linear motion of the piston in the suction pipe [53].

Similar to the quadrilateral linkage, the slider-crank consists of four rigid links, i.e., the driver a_1, the coupler a_2, the follower (or slider) a_3 and the fixed frame a_4 [3]. In contrast to the quadrilateral linkage, the fourth joint is exchanged with a prismatic joint. A general illustration is shown in Fig. 2.3.

The literature differentiates between two slider-crank linkages, the *in-line* or *cen-*

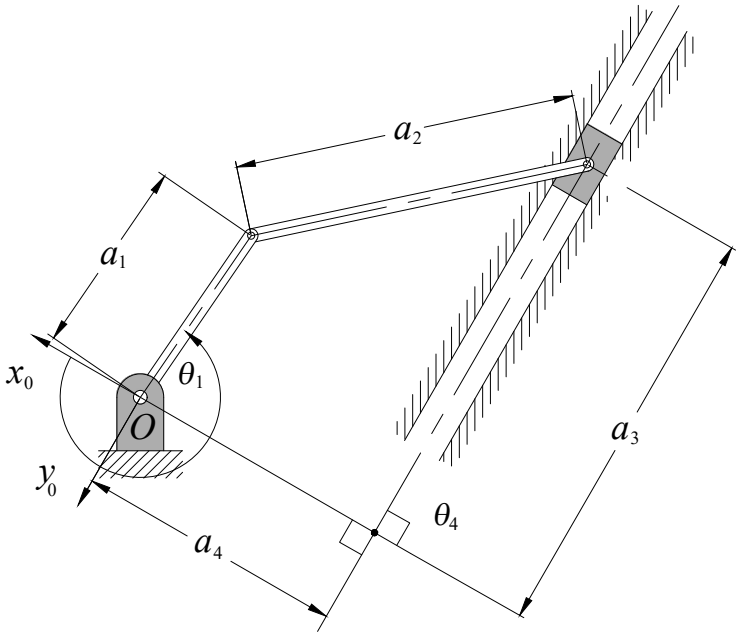

Figure 2.3: Planar RRRP function generator.

tral, and the *offset* or *eccentric* slider-crank linkages [54]. It is considered central if the extended line of the slider intersects the rotation centre of the crank. On the other hand, an eccentric slider-crank exists if $a_4 \neq 0$ [31]. Thus, a central slider-crank is a special case of the eccentric slider-crank.

Centric slider-crank IO equations for function generation can be found in every basic mechanics book. Two different trigonometric derivations that also apply to the *eccentric* linkage are shown in [2, 8]. They use trigonometric constraints to derive a trigonometric and an algebraic expression of the IO equation, respectively. As, e.g., demonstrated in [2], the slider-crank linkage can be classified according to its mobility of the input link. The two parameters derived by McCarthy and Soh using the law of cosines yield

$$\begin{aligned} S_1 &= -a_1 + a_2 + a_4 \\ S_2 &= -a_1 + a_2 - a_4. \end{aligned}$$

With these two parameters they obtain the full classification scheme shown in Tab. 2.2.

	Linkage type	S_1	S_2
1.	crank	+	+
2.	0-rocker	+	-
3.	π-rocker	-	+
4.	rocker	-	-

Table 2.2: Classification of planar RRRP linkages

2.3.3 Double Slider

The double slider, or PRRP linkage, consists of one P, two R, and another P joint. In addition to a translational output motion a_3, the input motion a_1 of the function generator is also a translation governed by a functional relation expressed by $f(a_1) = a_3$. The most common configuration is the *trammel of Archimedes* whose prismatic joint directions are perpendicular to each other, but for a general PRRP mechanism the P joint axes may have any non-zero angle between them, as illustrated in Fig. 2.4. This general configuration is also known as the *oblique trammel*.

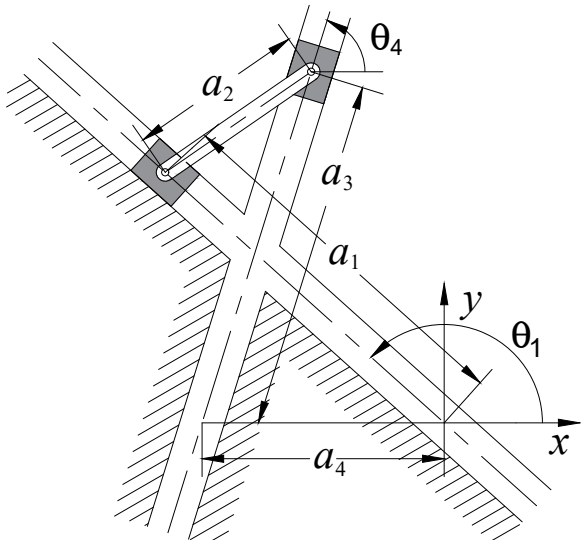

Figure 2.4: Planar PRRP function generator.

By extending the coupler of the mechanism, the trammel of Archimedes has been used to draw ellipses for hundreds, if not thousands, of years. Without any complex calculation, it is evident that the IO equation of the trammel of Archimedes yields a circle governed by

$$a_1^2 + a_3^2 - a_2^2 = 0. \tag{2.5}$$

Since 1646 it was also proven by van Schooten [55] that the coupler curve of oblique trammels also generates ellipses. A general IO equation for the oblique trammel, however, is not explicitly stated anywhere in the literature up to the author's knowledge.

2.4 Spherical Four-bar Linkages

While not as commonly used as planar four-bar linkages, spherical four-bar linkages are also found in diverse applications, for example, as a three-degree of freedom camera movement device proposed in [56], or to model the human knee [57]. The kinematic architecture of the classical spherical manipulators, also known as spherical quadrilateral or spherical 4R linkage, consists of four R joints whose joint axes intersect at the centre of a sphere. The intersection point of these axes is known as the *geometric centre* of the manipulator as shown in Fig. 2.5. In theory, other configurations of spherical four-bar manipulators exist, e.g., the planar linkages, discussed in the previous section, can all exist in spherical kinematics. The corresponding mechanisms are known as spherical crank-rockers, spherical double rockers or spherical slider-cranks. However, in these cases, the prismatic joints can no longer be "real" P joints conducting a linear translation, but they rather slide on the arc of the sphere [58].

As stated by McCarthy [59], planar kinematics is, in fact, a special case of spherical

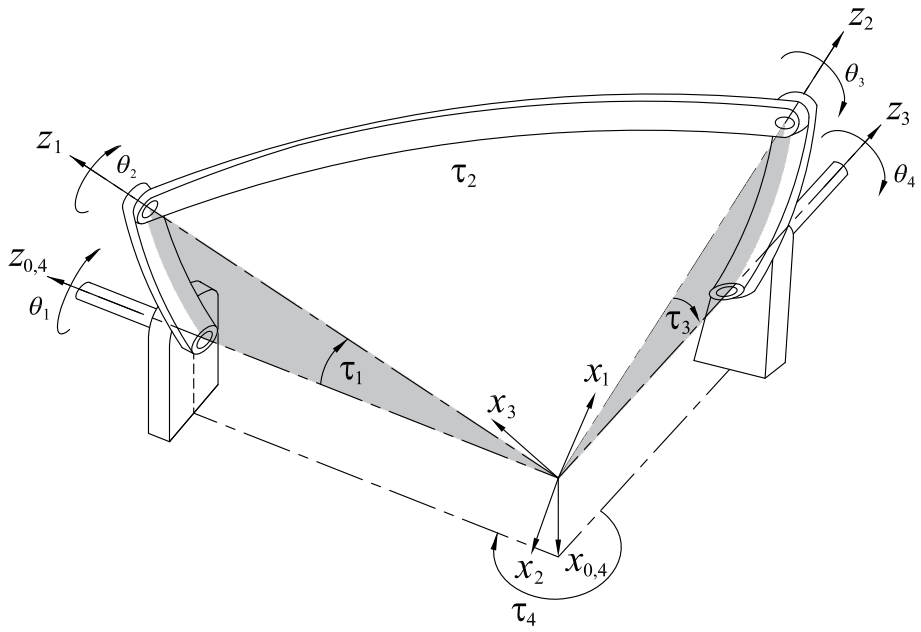

Figure 2.5: Spherical 4R function generator.

kinematics. He successfully demonstrated that the motion of planar kinematics can be described by the motion in the limits of spherical kinematics. While the joint axes of the spherical 4R linkage intersect in the centre of the sphere, the joint axes of the planar 4R linkage are all parallel. In Euclidean space $\mathbb{E}^3$ parallel lines never intersect, however, they do meet in a point at infinity in any projective extension of $\mathbb{E}^3$ [60, 61]. This suggests that if the radius of a spherical linkage approaches infinity, the linkage becomes a planar mechanism in the limit [59].

Applying Eq. (2.2) to the spherical 4R linkage reveals a relative dof of 1 [34]. Hence, in general, one given input angle would generate a specific output angle depending on the chosen design parameters τ_i.

The derivation of an IO equation for spherical 4R linkages has been examined by several authors. For example, Denavit [4] used Cayley-Klein parameters to describe the transformation between coordinate frames, Yang [62] used dual quaternions, Pin et al. [63] used unitary matrices, and McCarthy and Soh [2] used basic coordinate rotation matrices and trigonometric constraints to derive an IO equation. Not sur-

prisingly, they all yield the same IO equation. Let τ_1 be the twist angle of the driver, τ_2 the twist angle of the coupler, τ_3 the twist angle of the follower, τ_4 the twist angle between the fixed ground joints, and θ_1 and θ_4 the input and output angles, respectively, then the IO equation for spherical 4R linkages becomes

$$A(\theta_1)\cos(\theta_4) + B(\theta_1)\sin(\theta_4) = C(\theta_1) \tag{2.6}$$

where

$$\begin{aligned} A &= \cos(\theta_1)\sin(\tau_1)\cos(\tau_4)\sin(\tau_3) - \cos(\tau_1)\sin(\tau_4)\sin(\tau_3) \\ B &= \sin(\theta_1)\sin(\tau_1)\sin(\tau_3) \\ C &= \cos(\tau_2) - \cos(\theta_1)\sin(\tau_1)\sin(\tau_4)\cos(\tau_3) - \cos(\tau_1)\cos(\tau_4)\cos(\tau_3)\ . \end{aligned}$$

The classification scheme for spherical quadrilaterals by [52] and [2] yield the same table with the parameters T_i as for planar quadrilaterals. In addition, the authors consider the case where the linkage *wraps* around the sphere, which is the case if the sum of the angular arc lengths exceeds 2π.

2.5 Spatial Four-bar Linkages

The list for spatial four-bar linkage kinematic architectures is long. Harrisberger identified 132 different kinds of spatial four-bar linkage that have one dof according to Eq. (2.1) [64]. Out of these linkages, only a few have received special attention by researchers, either due to their practical potential, or because of their paradoxical nature that violates the Kutzbach criterion, Eq. (2.1). Two of these special linkages will be used to demonstrate the applicability of the generalised approach to derive an IO equation, i.e. the paradoxical overconstrained yet movable Bennett and the RSSR

spatial linkages.

2.5.1 Bennett Linkage

The Bennett linkage is, as the spherical and the planar quadrilateral, composed of four rigid links that are connected by four R joints. In addition, the linkage satisfies the following conditions, established by Bennett himself [65]

$$\begin{aligned} a_1 &= a_3 & a_2 &= a_4 \\ \tau_1 &= \tau_3 & \tau_2 &= \tau_4 \\ \frac{\sin(\tau_1)}{a_1} &= \frac{\sin(\tau_2)}{a_2} \end{aligned} \tag{2.7}$$

An exemplary Bennett linkage is shown in Fig. 2.6. According to Eq. (2.1) the Bennett

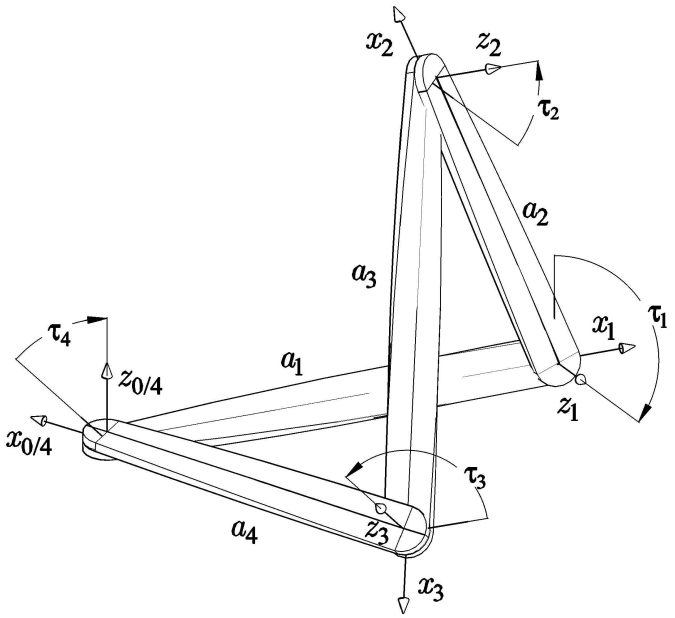

Figure 2.6: Spatial 4R function generator: the Bennett linkage.

linkage has a dof of -2, which in theory makes it unable to move. However, its actual dof is 1, and thereby, it is the only known paradoxical mobile spatial 4R linkage.

The IO equation is well known, for example [4, 9, 65, 66, 67] show different deriva-

tions. While the former authors favoured a geometric approach, Denavit used Cayley-Klein parameters, and Pfurner et al. used an algebraic method to first derive the Bennett conditions and second, obtain an IO equation in terms of the tangent half input and output angles.

An important characteristic of the Bennett IO equation is that it only depends on the twist angles, and not on the link length parameters. The equation is bilinear in the variables θ_1 and θ_4. For example this bilinear dependency is illustrated in the IO equation found in [67]

$$\tan\frac{\theta_1}{2}\tan\frac{\theta_4}{2} = \frac{\sin\dfrac{\tau_1+\tau_2}{2}}{\sin\dfrac{\tau_1-\tau_2}{2}} \quad . \tag{2.8}$$

The product of the tangent half-angle of the input and the output angle is constant. A classification scheme for the Bennett linkage is not required since a Bennett linkage is always a double crank [66].

2.5.2 RSSR Linkage

The RSSR linkage is another interesting spatial linkage. The Kutzbach criterion, Eq. (2.1) yields a dof of 2. However, one dof is the rotation of the coupler about its own axis. This rotation does not change or influence the IO equation in any way, and thus, engineers refer to it as an *idle* dof. However, the idle dof can have a positive effect on the durability of the linkage as it helps an even wear of the S joints [34].

Similar to the previous linkages, the IO equation of the RSSR linkage has been examined by several authors, for example, by [2, 3]. In addition to the link lengths a_i and twist angle parameters τ_i, the linkage can only be fully described by introducing an additional parameter, i.e., the link offset d_i. Hartenberg and Denavit's derivation of the IO equation uses their well-known parameters as well as trigonometric relations.

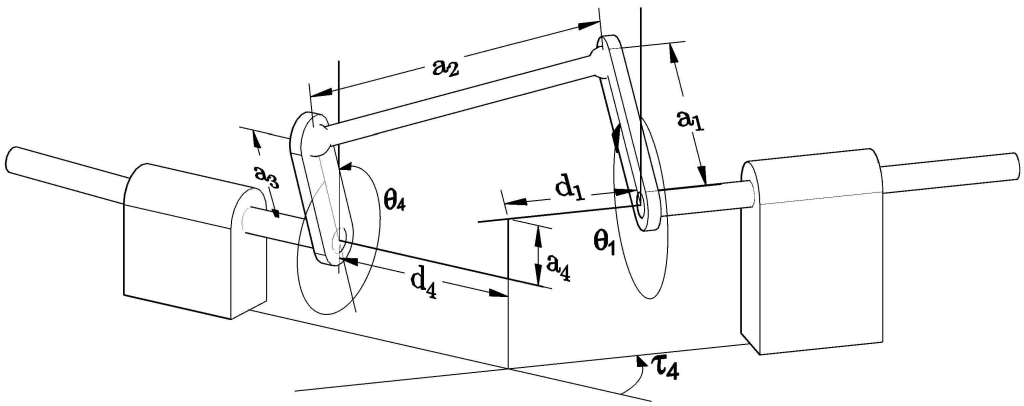

Figure 2.7: Spatial RSSR function generator.

Following the notation in Fig. 2.7 the IO equation yields

$$A(\theta_1)\sin(\theta_4) + B(\theta_1)\cos(\theta_4) = C(\theta_1) \tag{2.9}$$

where

$$\begin{aligned} A &= -\cos(\tau_4)\sin(\theta_1) + \frac{d_1\sin(\tau_4)}{a_1} \\ B &= -\frac{a_4}{a_1} - \cos(\theta_1) \\ C &= -\frac{a_1^2 - a_2^2 + a_3^2 + a_4^2 + d_1^2 + d_4^2 + 2d_1d_4\cos(\tau_4)}{2a_1a_3} - \frac{a_4}{a_3}\cos(\theta_1) - \frac{d_4\sin(\tau_4)}{a_3}\sin(\theta_1)\ . \end{aligned}$$

The RSSR linkage can also be classified according to its input and output mobility. This problem has been solved using different methods, for instance [68, 69, 70]. Of particular interest is the algebraic method presented by Bottema who evaluated the double points of a special constellation of the homogeneous IO equation, and subsequently extracted the conditions when the input and output links are rockers, or cranks [71]. A classification for the general RSSR linkage was finally presented by Freudenstein and Primose [72].

Both the Bennett and the spherical linkages can be considered as special cases of

the RSSR linkage. While Hunt [66] views the RSSR as a projection on a unit sphere, McCarthy and Soh [2] add additional constraints to the RSSR linkage, such that the offset between the R joints disappears, the distance between the R joints is restricted to unity, and the axes of the S joints are directed towards the intersection of the R joint axes. As a result of these constraints made on the RSSR IO equation, the authors are able to derive a version of the spherical IO equation.

A direct conversion of the IO equation from the RSSR linkage to the planar quadrilateral was further demonstrated by Hartenberg and Denavit who were equating the linkage offsets and link twist of the RSSR to zero, making the planar quadrilateral linkage a special case of the RSSR as well [3].

Chapter 3

Mathematical Background

3.1 Research Approach and Strategy

As mentioned in the introduction, the main research objective is to generalise the procedure for determining one single method to obtain the algebraic IO equation for any kinematic architecture of four-bar linkage: planar; spherical; or spatial.

To achieve this, this research is building on [7] who proposed an algebraic IO equation for planar 4R mechanisms. Their equation is derived by mapping the circular constraints inherent to this mechanism into a spatial projection of planar rigid body displacements, in this case into a projection obtained with Study's soma coordinates [10]. Using the method of Study's kinematic mapping, where the constraints of a mechanism are represented as algebraic varieties in the three- and seven-dimensional projective kinematic image space representing planar and spatial displacements, respectively, allows for the use of different algebraic geometry tools for analysis.

One shortcoming of [7] is that the geometric constraints of different types of mechanism can vary such that a different initial geometric description using line, circle and sphere equations has to be chosen for different mechanisms. The general approach

suggested in this thesis is therefore to consider the linkage as an open kinematic chain which can be described using the well-known standard Denavit-Hartenberg parameters. The overall displacement of the end-effector of this chain is subsequently mapped into Study's kinematic image space and algebraically closed resulting in a complete and general description of any four-bar linkage. The polynomial equations can be manipulated with, e.g., different elimination techniques, such as Gröbner basis to eliminate intermediate joint variables to obtain the desired IO equation.

The most crucial methods I will be using to achieve my research objective, i.e., describing the constraints of mechanisms using Denavit-Hartenberg parameters, the concept of kinematic mapping as well as elimination techniques in algebraic geometry, are described in the following sections.

3.2 Euclidean Displacements

It is convenient to consider a general displacement of a rigid body as the displacement of a reference coordinate system Σ_2 that moves with the rigid body relative to a fixed frame Σ_1. Moreover, let the coordinates of points in Σ_2 be described by the lower case pairs (x, y) and those in Σ_1 by the uppercase pairs (X, Y). A general displacement of Σ_2 relative to Σ_1 is described by three numbers (a, b, ϕ), where (a, b) are the coordinates of the origin of Σ_2 expressed in Σ_1, and ϕ is the angle the x-axis makes with respect to the X-axis, with counterclockwise rotations considered as positive. The position of a point in Σ_2 described in Σ_1 can be given by

$$\begin{bmatrix} X' \\ Y' \end{bmatrix} = \begin{bmatrix} \cos(\phi) & -\sin(\phi) \\ \sin(\phi) & \cos(\phi) \end{bmatrix} \begin{bmatrix} x' \\ y' \end{bmatrix} + \begin{bmatrix} a \\ b \end{bmatrix}. \tag{3.1}$$

Eq. (3.1) is **not** a linear transformation because the translation of the sum of the two vectors $\vec{x}$ and $\vec{y}$ by the amount $\vec{d}$ is $\vec{x} + \vec{y} + \vec{d}$ and not the sum of the translation of

each vector separately, which is $(\vec{x}+\vec{d})+(\vec{y}+\vec{d}) = \vec{x}+\vec{y}+2\vec{d}$. This violates the definition of a linear transformation:

If $T: V \mapsto S$ is a function from the vector space V to the vector space S, then T is a linear transformation if and only if

(i) $T(\vec{u}+\vec{v}) = T(\vec{u}) + T(\vec{v}) \quad \forall\, \vec{u}, v \vec{\in} V$

(ii) $T(k\vec{u}) = Tk(\vec{u}) \quad \forall\, \vec{u} \in V$ and all scalars.

Clearly, Eq. (3.1) violates (i). Moreover, it is not a linear transformation because Eq. (3.1) cannot be represented by an $n \times n$ matrix. This situation can be remedied by the use of *homogeneous coordinates*. They replace cartesian coordinate pairs (x', y') with triples of ratios $(x_0 : x_1 : x_2)$, such that

$$\begin{aligned} x' &= \frac{x_1}{x_0}, \quad y' = \frac{x_2}{x_0} \\ X' &= \frac{X_1}{X_0}, \quad Y' = \frac{X_2}{X_0}. \end{aligned}$$

Substituting these into Eq. (3.1) gives

$$\begin{aligned} \frac{X_1}{X_0} &= \frac{x_1}{x_0}\cos\phi - \frac{x_2}{x_0}\sin\phi + a \\ \frac{X_2}{X_0} &= \frac{x_1}{x_0}\sin\phi + \frac{x_2}{x_0}\cos\phi + b. \end{aligned} \tag{3.2}$$

The first coordinate, X_0 and x_0 may be thought of simply as scaling factors. As long as $X_0 \neq 0$, we can set $X_0 = x_0$, multiply Eq. (3.2) through by x_0 and write Eq. (3.1) as a linear transformation, which is computationally extremely convenient:

$$\begin{bmatrix} X_0 \\ X_1 \\ X_2 \end{bmatrix} = \begin{bmatrix} 1 & 0 & 0 \\ a & \cos(\phi) & -\sin(\phi) \\ b & \sin(\phi) & \cos(\phi) \end{bmatrix} \begin{bmatrix} x_0 \\ x_1 \\ x_2 \end{bmatrix} \tag{3.3}$$

Eq. (3.3) represents a planar displacement of reference frame Σ_2 with respect to Σ_1 in the Euclidean plane $\mathbb{E}^2$. It should be noted that in North America the convention for homogeneous coordinates is slightly different from the European convention presented herein. In North America x_0/X_0 usually corresponds to the last, while in the European convention it corresponds to the first coordinate. As we will see later, the dimensions of the spaces and points that represent the homogeneous coordinates in this thesis and therefore, the indices of the last coordinate, may vary. For that reason, this thesis favors European convention.

The concept of using homogeneous coordinates can be extended to three-dimensional Euclidean space, $\mathbb{E}^3$. The linear transformation, preserving orientation and displacements, results in

$$\begin{bmatrix} X_0 \\ X_1 \\ X_2 \\ X_3 \end{bmatrix} = \left[\begin{array}{c|ccc} 1 & 0 & 0 & 0 \\ \hline & & & \\ \mathbf{t} & & \mathbf{A} & \\ & & & \end{array}\right] \begin{bmatrix} x_0 \\ x_1 \\ x_2 \\ x_3 \end{bmatrix} \tag{3.4}$$

where $\mathbf{A}$ is a proper orthogonal 3×3 rotation matrix, and $\mathbf{t}$ is a 3×1 position vector.

Surely, as shown above it is one way of interpreting the transformation as a three-dimensional rotation of $\mathbf{A}$ with a subsequent translation by vector $\mathbf{t}$. However, a different geometric interpretation is known as *screw displacement* where the spatial displacement consists of a rotation about a line, the *screw axis*, and a translation along the same line. To validate this statement the translation vector $\mathbf{t}$ is decomposed into a vector that is parallel to the rotation axis of $\mathbf{A}$ and a vector that is perpendicular to the rotation axis of $\mathbf{A}$ [2]. Hence, the displacement can be rewritten as

$$\mathbf{D}(x) = \mathbf{A}(x) + \mathbf{t} = \mathbf{A}(x) + \mathbf{t}_\perp + \mathbf{t}_\parallel \tag{3.5}$$

Consider $\mathbf{D}^*(x) = \mathbf{A}(x) + \mathbf{t}_\perp$ which represents a transformation about the axis defined

by $\mathbf{A}(x)$. All points undergo a transformation within the plane that is perpendicular to the axis of rotation. In contrast to $\mathbf{D}(x)$, the transformation $\mathbf{D}^*(x)$ contains an invariant point C since the component of $\mathbf{t}_\perp$ which is pointing along the rotation axis is zero. Thus, the screw axis is passing through C and because of $\mathbf{D}(x) = \mathbf{D}^*(x) + \mathbf{t}_\parallel$, the screw axis is pointing along $\mathbf{t}_\parallel$. One important aspect of this theory is that the axis of rotation remains invariant and is defined by the rotation matrix elements a_{ij} of $\mathbf{A}$ alone. The concept is visualised in Fig. (3.1) which was inspired by [73].

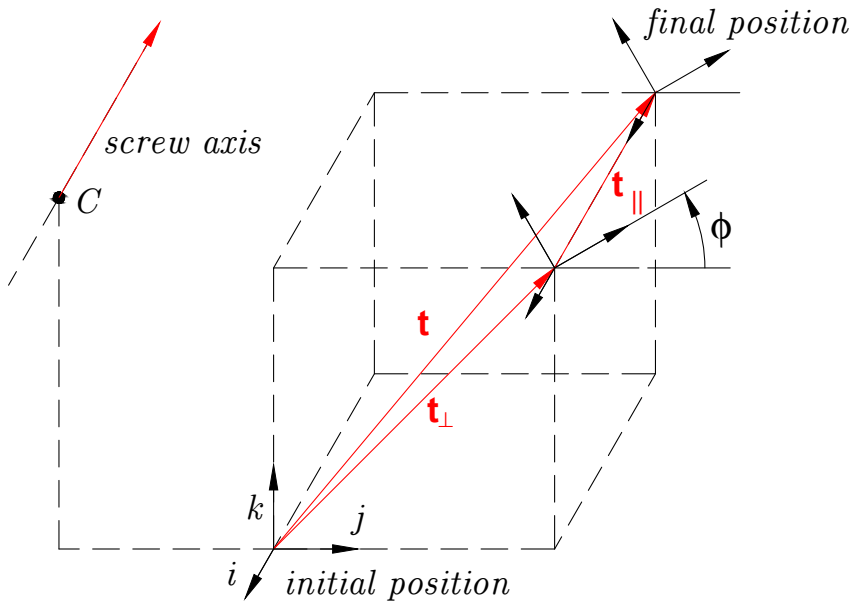

Figure 3.1: Concept of a screw displacement.

In general, the axis of rotation $\vec{v}$ and the rotation angle ϕ of a 3×3 orthogonal matrix $\mathbf{A}$ are defined by [74]

$$v_1 : v_2 : v_3 = (a_{32} - a_{23}) : (a_{13} - a_{31}) : (a_{21} - a_{12}) \tag{3.6}$$

$$\cos(\phi) = \frac{1}{2}(a_{11} + a_{22} + a_{33} - 1). \tag{3.7}$$

3.3 Study's Kinematic Mapping

Using matrices, such as Eq. (3.4), is one possibility of representing Euclidean displacements where orientation and distances are preserved. Another possibility was introduced by Eduard Study in 1903 [10]. He demonstrated that rigid body displacements can be represented as points on a hyper-surface in a seven-dimensional space, known as *kinematic mapping*. These points require eight homogeneous coordinates known as *Study parameters* or *soma coordinates*, $x = [x_0 : x_1 : x_2 : x_3 : y_0 : y_1 : y_2 : y_3]^\mathsf{T} \in P^7$, soma being the greek word for body. While Study used kinematic mapping for spatial displacement, Grünwald [75] and Blaschke [76] applied kinematic mapping to planar kinematics, and Müller to spherical kinematics [77]. For many decades kinematic mapping was not the preferred choice to solve synthesis or analysis problems of mechanisms. Kinematicians used matrix or vector methods instead. However, with the rise of robotic manipulators, computer algebra systems, and the accompanying ability to solve complex systems of polynomial equations, kinematic mapping is seeing a revival in recent decades [2, 8, 74, 78].

Given a rotation matrix $\mathbf{A}$ and a translation vector $\mathbf{t}$, as it is shown in Eq. (3.4), then the first four entries of the Study array x_i are defined as one of the following linear combinations of the rotation matrix elements a_{ij} of $\mathbf{A}$

$$x_0 : x_1 : x_2 : x_3 \quad = \quad \begin{cases} 1 + a_{11} + a_{22} + a_{33} : a_{32} - a_{23} : a_{13} - a_{31} : a_{21} - a_{12}, \\ a_{32} - a_{23} : 1 + a_{11} - a_{22} - a_{33} : a_{12} + a_{21} : a_{31} + a_{13}, \\ a_{13} - a_{31} : a_{12} + a_{21} : 1 - a_{11} + a_{22} - a_{33} : a_{23} + a_{32}, \\ a_{21} - a_{12} : a_{31} + a_{13} : a_{23} + a_{32} : 1 - a_{11} - a_{22} + a_{33}. \end{cases} \tag{3.8}$$

Study showed that four different combinations of the rotation matrix elements are needed since certain displacements make one or more of the relations lead to $(0 : 0 : 0 : 0)$, the exceptional generator in P^7 which does not correspond to any displacement

in $\mathbb{E}^3$. Once the x_i have been determined, the remaining four entries are computed as linear combinations of the vector elements of the translation $\mathbf{t}$ and the x_i determined above, giving

$$\begin{aligned} y_0 &= \tfrac{1}{2}(t_3x_3 + t_2x_2 + t_1x_1), & y_1 &= \tfrac{1}{2}(t_3x_2 - t_2x_3 - t_1x_0), \\ y_2 &= \tfrac{1}{2}(-t_3x_1 + t_1x_3 - t_2x_0), & y_3 &= \tfrac{1}{2}(-t_3x_0 + t_2x_1 - t_1x_2). \end{aligned} \tag{3.9}$$

These eight Study parameters must fulfil the Study condition in order to represent a Euclidean displacement, meaning the eight ratios represent a point on Study's seven-dimensional quadric $\mathcal{S}_6^2$

$$x_0y_0 + x_1y_1 + x_2y_2 + x_3y_3 = 0 \tag{3.10}$$

excluding the exceptional generator A_∞

$$(x_0 : x_1 : x_2 : x_3) = (0 : 0 : 0 : 0). \tag{3.11}$$

As, e.g., demonstrated in [79], the mapping from Euclidean displacements to Study's coordinates that fulfil $\mathcal{S}_6^2$, with A_∞ being excluded, is bijective. Thus, it is straightforward to perform the inverse mapping from P^7 to $\mathbb{E}^3$, known as computing the pre-image, from given coordinates of an image point $x = [x_0 : x_1 : x_2 : x_3 : y_0 : y_1 :$

$y_2 : y_3]^{\mathsf{T}} \in P^7$ with

$$\mathbf{D} = \Delta^{-1} \begin{pmatrix} x_0^2 + x_1^2 + x_2^2 + x_3^2 & 0 & 0 & 0 \\ l & x_0^2 + x_1^2 - x_2^2 - x_3^2 & 2(x_1x_2 - x_0x_3) & 2(x_1x_3 + x_0x_2) \\ m & 2(x_1x_2 + x_0x_3) & x_0^2 - x_1^2 + x_2^2 - x_3^2 & 2(x_2x_3 - x_0x_1) \\ n & 2(x_1x_3 - x_0x_2) & 2(x_2x_3 + x_0x_1) & x_0^2 - x_1^2 - x_2^2 + x_3^2 \end{pmatrix}, \tag{3.12}$$

where

$$\begin{aligned} \Delta &= x_0^2 + x_1^2 + x_2^2 + x_3^2 \\ l &= 2(-x_0y_1 + x_1y_0 - x_2y_3 + x_3y_2) \\ m &= 2(-x_0y_2 + x_1y_3 + x_2y_0 - x_3y_1) \\ n &= 2(-x_0y_3 - x_1y_2 + x_2y_1 + x_3y_0). \end{aligned}$$

In the following section, the derivation of the Study parameters will be presented. This will help to relate Study's parametrisation of Euclidean displacements to other parametrisations, such as Euler parameters, Rodrigues parameters, and dual quaternions. The derivation is mainly based on [74] and influenced by [13, 14].

3.3.1 First Four Study Parameters x_i

As mentioned, the first four Study parameters are combinations of the elements a_{ij} of $\mathbf{A}$. According to Cayley's theorem an orthogonal matrix $\mathbf{A}$ can be expressed as

$$\mathbf{A} = (\mathbf{I} - \mathbf{S})^{-1}(\mathbf{I} + \mathbf{S}) \tag{3.13}$$

where S is a skew symmetric matrix given by

$$\mathbf{S} = \begin{pmatrix} 0 & -b_3 & b_2 \\ b_3 & 0 & -b_1 \\ -b_2 & b_1 & 0 \end{pmatrix}.$$

Thus, this clearly demonstrates that $\mathbf{A}$ only depends on three different parameters, b_1, b_2 and b_3. Expanding Eq. (3.13) yields

$$\mathbf{A} = (\mathbf{I} - \mathbf{S})^{-1}(\mathbf{I} + \mathbf{S}) = \begin{pmatrix} 1 & b_3 & -b_2 \\ -b_3 & 1 & b_1 \\ b_2 & -b_1 & 1 \end{pmatrix}^{-1} \begin{pmatrix} 1 & -b_3 & b_2 \\ b_3 & 1 & -b_1 \\ -b_2 & b_1 & 1 \end{pmatrix}$$

$$\mathbf{A} = \Delta^{-1} \begin{pmatrix} 1 + b_1^2 - b_2^2 - b_3^2 & 2(b_1 b_2 - b_3) & 2(b_1 b_3 + b_2) \\ 2(b_1 b_2 + b_3) & 1 - b_1^2 + b_2^2 - b_3^2 & 2(b_2 b_3 - b_1) \\ 2(b_1 b_3 - b_2) & 2(b_2 b_3 + b_1) & 1 - b_1^2 - b_2^2 + b_3^2 \end{pmatrix} \tag{3.14}$$

where

$$\Delta = 1 + b_1^2 + b_2^2 + b_3^2.$$

The rotation angle of Eq. (3.14) can be evaluated by substituting the matrix elements into Eq. (3.7)

$$\cos(\phi) = \frac{-b_1^2 - b_2^2 - b_3^2 + 1}{b_1^2 + b_2^2 + b_3^2 + 1}.$$

With the tangent half-angle substitution, the expression becomes

$$\tan\left(\frac{\phi}{2}\right) = \pm\sqrt{\frac{1 - \cos\phi}{1 + \cos\phi}} = \pm\sqrt{b_1^2 + b_2^2 + b_3^2}. \tag{3.15}$$

Similarly, the rotation axis can be evaluated by substituting the matrix elements into Eq. (3.6), resulting in

$$v_1 : v_2 : v_3 = b_1 : b_2 : b_3. \tag{3.16}$$

This shows that the rotation axis of Eq. (3.14) is defined by $\mathbf{b} = (b_1, b_2, b_3)$, which can also easily be verified by multiplying $\mathbf{A}$ with $\mathbf{b}$ resulting in $\mathbf{b}$ showing that $\mathbf{b}$ is invariant. The elements of $\mathbf{b}$ are also known as Rodrigues parameters, and Eq. (3.14) is the corresponding Rodrigues parametrisation [8].

Normalising vector $\mathbf{b}$ by $\vec{e} = \dfrac{\vec{b}}{|\vec{b}|}$ and substituting Eq. (3.15) for $|\vec{b}|$, the vector coordinates can be rewritten as

$$\begin{aligned} b_1 &= e_x \tan\frac{\phi}{2} \\ b_2 &= e_y \tan\frac{\phi}{2} \\ b_3 &= e_z \tan\frac{\phi}{2}. \end{aligned}$$

The expression can be generalised further by homogenising $b_i = \dfrac{c_i}{c_0}$. After defining $c_0 = \cos\dfrac{\phi}{2}$, and substituting $\tan\dfrac{\phi}{2} = \sin\dfrac{\phi}{2}/\cos\dfrac{\phi}{2}$, it leads to

$$c_0 = \cos\frac{\phi}{2} \tag{3.17}$$

$$\begin{aligned} c_1 &= e_x \sin\frac{\phi}{2} \\ c_2 &= e_y \sin\frac{\phi}{2} \\ c_3 &= e_z \sin\frac{\phi}{2}. \end{aligned} \tag{3.18}$$

The parameters c_i are known as Euler parameters [8]. Similar to the derivation of

$\times$	1	$\mathbf{i}$	$\mathbf{j}$	$\mathbf{k}$
1	1	$\mathbf{i}$	$\mathbf{j}$	$\mathbf{k}$
$\mathbf{i}$	$\mathbf{i}$	-1	$\mathbf{k}$	$-\mathbf{j}$
$\mathbf{j}$	$\mathbf{j}$	$-\mathbf{k}$	-1	$\mathbf{i}$
$\mathbf{k}$	$\mathbf{k}$	$\mathbf{j}$	$-\mathbf{i}$	-1

Table 3.1: Multiplication table for quaternions

the Rodrigues parametrisation above, the Euler parametrisation results in

$$\mathbf{A} = \Delta^{-1} \begin{pmatrix} c_0^2 + c_1^2 - c_2^2 - c_3^2 & 2(c_1c_2 - c_0c_3) & 2(c_1c_3 + c_0c_2) \\ 2(2c_1c_2 + c_0c_3) & c_0^2 - c_1^2 + c_2^2 - c_3^2 & 2(c_2c_3 - c_0c_1) \\ 2(c_1c_3 - c_0c_2) & 2(c_2c_3 + c_0c_1) & c_0^2 - c_1^2 - c_2^2 + c_3^2 \end{pmatrix} \tag{3.19}$$

where

$$\Delta = c_0^2 + c_1^2 + c_2^2 + c_3^2.$$

Without loss of generality, the parametrisation is normalised by setting $\Delta = 1$.

A different way of representing the Euler parametrisation can be achieved via unit quaternions. Quaternions were discovered independently by B.O. Rodrigues in 1840 [80] and W.R. Hamilton in 1844 [81]. On the basis of complex numbers which had already been known to represent points in the plane and which could undergo certain operations, Hamilton wanted to extend this concept to higher dimensions. He discovered quaternions, a new number system denoted as $\mathbb{H}$, that he defined as

$$Q = q_0 + q_1\mathbf{i} + q_2\mathbf{j} + q_3\mathbf{k}$$

where q_i are real numbers and $\mathbf{i}$, $\mathbf{j}$ and $\mathbf{k}$ are quaternion units. q_0 is known as the scalar part, and the imaginary part consisting of $\mathbf{q} = (q_1, q_2, q_3)$ is also known as the vector part. While addition and scalar multiplication can be performed componentwise, the multiplication of two quaternions follows the multiplication table given in Tab. 3.1.

Similar to complex numbers, the conjugate of a quaternion is defined as

$$Q^* = q_0 - q_1\mathbf{i} - q_2\mathbf{j} - q_3\mathbf{k};$$

and the norm of a quaternion is defined as

$$\|Q\| = \sqrt{QQ^*} = \sqrt{Q^*Q} = \sqrt{q_0^2 + q_1^2 + q_2^2 + q_3^2}.$$

If $\|Q\| = 1$ then Q is a unit quaternion.

According to Euler [82], a rotation of a vector $\mathbf{p} = p_1\mathbf{i}+p_2\mathbf{j}+p_3\mathbf{k}$ can be computed with the following quaternion multiplication

$$\begin{aligned} Q\mathbf{p}Q^* &= (q_0 + q_1\mathbf{i} + q_2\mathbf{j} + q_3\mathbf{k})(p_1\mathbf{i} + p_2\mathbf{j} + p_3\mathbf{k})(q_0 - q_1\mathbf{i} - q_2\mathbf{j} - q_3\mathbf{k}) \\ &= ((q_0^2 + q_1^2 - q_2^2 - q_3^2)p_1 + (-2q_0q_3 + 2q_1q_2)p_2 + (2q_0q_2 + 2q_1q_3)p_3)\mathbf{i} \\ &\quad +((2q_0q_3 + 2q_1q_2)p_1 + (q_0^2 - q_1^2 + q_2^2 - q_3^2)p_2 + (-2q_0q_1 + 2q_2q_3)p_3)\mathbf{j} \\ &\quad +((-2q_0q_2 + 2q_1q_3)p_1 + (2q_0q_1 + 2q_2q_3)p_2 + (q_0^2 - q_1^2 - q_2^2 + q_3^2)p_3)\mathbf{k}. \end{aligned}$$

Rewriting this expression in matrix form yields

$$Q\mathbf{p}Q^* = \begin{pmatrix} q_0^2 + q_1^2 - q_2^2 - q_3^2 & 2(q_1q_2 - q_0q_3) & 2(q_1q_3 + q_0q_2) \\ 2(q_1q_2 + q_0q_3) & q_0^2 - q_1^2 + q_2^2 - q_3^2 & 2(q_2q_3 - q_0q_1) \\ 2(q_1q_3 - q_0q_2) & 2(q_2q_3 + q_0q_1) & q_0^2 - q_1^2 - q_2^2 + q_3^2 \end{pmatrix} \begin{pmatrix} p_1 \\ p_2 \\ p_3 \end{pmatrix}. \tag{3.20}$$

Comparing Eq. (3.19) with Eq. (3.20), it follows that $q_0^2 + q_1^2 + q_2^2 + q_3^2 = 1$ in order for Eq. (3.20) to be a rotation matrix. Hence, it was shown that unit quaternions Q are another possibility to represent Euclidean rotations.

We have seen different parametrisations, all resulting in the same rotation matrix. In the following steps, the procedure continues with the notation chosen in the Euler

parametrisation. Evaluating the rotation axis of Eq. (3.19) with Eq. (3.6) will already provide three of the first Study parameters

$$x_1 : x_2 : x_3 = a_{32} - a_{23} : a_{13} - a_{31} : a_{21} - a_{12} = 4c_0c_1 : 4c_0c_2 : 4c_0c_3. \tag{3.21}$$

However, an additional homogenising coordinate x_0 is required which is evaluated with an auxiliary variable λ such that

$$(x_0 : x_1 : x_2 : x_3) = \lambda(c_0 : c_1 : c_2 : c_3).$$

It follows that $\lambda = 4c_0$ and thus, $x_0 = \lambda c_0 = 4c_0^2$. Recall the first Euler parameter, Eq. (3.17), which can be reformulated with the half-angle substitution

$$c_0 = \cos\frac{\phi}{2} = \pm\sqrt{\frac{1+\cos\phi}{2}}.$$

With Eq. (3.7) c_0 becomes

$$c_0 = \pm\frac{1}{2}\sqrt{\frac{1+\left(\frac{1}{2}\left(a_{11}+a_{22}+a_{33}-1\right)\right)}{2}} = \pm\frac{1}{2}\sqrt{a_{11}+a_{22}+a_{33}+1}. \tag{3.22}$$

Finally, substituting Eq. (3.22) into the expression for x_0 yields

$$x_0 = 4c_0^2 = a_{11}+a_{22}+a_{33}+1. \tag{3.23}$$

This concludes the derivation for the first four Study parameters of the first line as shown in Eq. (3.8). As mentioned, other combinations are required if the rotation matrix would result in $x_i = (0:0:0:0)$. The derivations of the remaining three possibilities of Eq. (3.8) are similar to its first line. They will not be discussed here, but can be found, for example, in [14].

3.3.2 Latter Four Study Parameters y_i

The derivation of the remaining Study parameters y_i requires some understanding of the algebra of dual quaternions. They were discovered by W.K. Clifford in 1873 [83], and later it was shown by Study how Clifford's algebra could be applied to describe displacements in three-dimensional space. Let ϵ denote the dual unit, which is a quasi-imaginary number defined as having the following two properties

$$\epsilon \neq 0, \quad \text{and} \quad \epsilon^2 = 0.$$

Then a dual number can be written as

$$\hat{d} = x_i + \epsilon y_i.$$

As the name suggests, a dual quaternion is a regular quaternion whose coefficients are not real numbers but instead consist of dual numbers. Thus, a dual quaternion, or sometimes referred to as a biquaternion, consists of eight different elements forming an eight-dimensional vector space over the real numbers

$$\begin{aligned} \hat{Q} &= x_0 + y_0\epsilon + (x_1 + y_1\epsilon)\mathbf{i} + (x_2 + y_2\epsilon)\mathbf{j} + (x_3 + y_3\epsilon)\mathbf{k} \\ &= x_0 + x_1\mathbf{i} + x_2\mathbf{j} + x_3\mathbf{k} + \epsilon(y_0 + y_1\mathbf{i} + y_2\mathbf{j} + y_3\mathbf{k}) \\ &= x_0 + \mathbf{x} + \epsilon(y_0 + \mathbf{y}). \end{aligned}$$

Just as in the addition and scalar multiplication of quaternions, these operations are conducted componentwise. Furthermore, the multiplication of dual quaternions follow the same table given in Tab. 3.1, while also considering the definition of the dual unit $\epsilon^2 = 0$.

There are two types of conjugates for dual quaternions. Following the defini-

tion of the conjugate for regular quaternions, the vector part of the two embedded quaternions change their signs. Hence, one conjugate for dual quaternions is defined as

$$\hat{Q}^* = x_0 - \mathbf{x} + \epsilon y_0 - \epsilon \mathbf{y}.$$

In addition, there exists the dual number conjugate where the sign of the dual part changes. Hence, the dual number conjugate is defined as

$$\hat{Q}_\epsilon = x_0 + \mathbf{x} - \epsilon y_0 - \epsilon \mathbf{y}.$$

The norm of the dual quaternion is defined as

$$\|\hat{Q}\| = \sqrt{\hat{Q}\hat{Q}^*}.$$

Expanding the norm and requiring that it equates to one, i.e., $(1+\epsilon 0)$, the expression yields

$$\hat{Q}\hat{Q}^* = (x_0^2 + x_1^2 + x_2^2 + x_3^2) + \epsilon(2x_0y_0 + 2x_1y_1 + 2x_2y_2 + 2x_3y_3) := 1.$$

Therefore, unit dual quaternions undergo two algebraic constraints, namely

$$x_0^2 + x_1^2 + x_2^2 + x_3^2 = 1 \tag{3.24}$$

$$x_0y_0 + x_1y_1 + x_2y_2 + x_3y_3 = 0. \tag{3.25}$$

Similar to the above quaternion product representing rotations about the origin, let us define that the product of dual quaternions $\hat{Q}_\epsilon \mathbf{p} \hat{Q}^*$ represents Euclidean displacements, where $\mathbf{p}$ is a vector in Euclidean 3-space given as $\mathbf{p} = 1+\epsilon(p_1\mathbf{i}+p_2\mathbf{j}+p_3\mathbf{k})$.

Following the multiplication rules, the expression becomes

$$\begin{aligned}
\hat{Q}_\epsilon \mathbf{p} \hat{Q}^* &= (x_0 + x_1\mathbf{i} + x_2\mathbf{j} + x_3\mathbf{k} + \epsilon(-y_0 - y_1\mathbf{i} - y_2\mathbf{j} - y_3\mathbf{k}))(1 + \epsilon(p_1\mathbf{i} + p_2\mathbf{j} + p_3\mathbf{k})) \\
&\quad (x_0 - x_1\mathbf{i} - x_2\mathbf{j} - x_3\mathbf{k} + \epsilon(y_0 - y_1\mathbf{i} - y_2\mathbf{j} - y_3\mathbf{k})) \\
&= (x_0^2 + x_1^2 + x_2^2 + x_3^2) \\
&\quad +((x_0^2 + x_1^2 - x_2^2 - x_3^2)p_1 + (-2x_0x_3 + 2x_1x_2)p_2 + (2x_0x_2 + 2x_1x_3)p_3 \\
&\qquad -2x_0y_1 + 2x_1y_0 - 2x_2y_3 + 2x_3y_2)\epsilon\mathbf{i} \\
&\quad +((2x_0x_3 + 2x_1x_2)p_1 + (x_0^2 - x_1^2 + x_2^2 - x_3^2)p_2 + (-2x_0x_1 + 2x_2x_3)p_3 \\
&\qquad -2x_0y_2 + 2x_1y_3 + 2x_2y_0 - 2x_3y_1)\epsilon\mathbf{j} \\
&\quad +((-2x_0x_2 + 2x_1x_3)p_1 + (2x_0x_1 + 2x_2x_3)p_2 + (x_0^2 - x_1^2 - x_2^2 + x_3^2)p_3 \\
&\qquad -2x_0y_3 - 2x_1y_2 + 2x_2y_1 + 2x_3y_0)\epsilon\mathbf{k}.
\end{aligned}$$

If $\hat{Q}$ is a unit quaternion, we can substitute Eq. (3.24) and reformulate the dual quaternion product in matrix form

$$\hat{Q}_\epsilon \mathbf{p} \hat{Q}^* = \begin{pmatrix} 1 & 0 & 0 & \\ l & x_0^2 + x_1^2 - x_2^2 - x_3^2 & 2(x_1x_2 - x_0x_3) & 2(x_1x_3 + x_0x_2) \\ m & 2(x_1x_2 + x_0x_3) & x_0^2 - x_1^2 + x_2^2 - x_3^2 & 2(x_2x_3 - x_0x_1) \\ n & 2(x_1x_3 - x_0x_2) & 2(x_2x_3 + x_0x_1) & x_0^2 - x_1^2 - x_2^2 + x_3^2 \end{pmatrix} \begin{pmatrix} 1 \\ p_1 \\ p_2 \\ p_3 \end{pmatrix} \tag{3.26}$$

where

$$\begin{aligned}
l &= 2(-x_0y_1 + x_1y_0 - x_2y_3 + x_3y_2); \\
m &= 2(-x_0y_2 + x_1y_3 + x_2y_0 - x_3y_1); \\
n &= 2(-x_0y_3 - x_1y_2 + x_2y_1 + x_3y_0).
\end{aligned}$$

Eq. (3.26) can be compared to the linear transformation, Eq. (3.4), revealing that the

translation part $\mathbf{t}$ can be expressed as a linear combination of the dual quaternion coefficients, i.e., $\mathbf{t} = (l, m, n)$. Therefore, Euclidean displacements can be represented with the above defined product of unit dual quaternions. As, e.g., shown in [79], the translation $\mathbf{t}$ can subsequently be converted into Study's image coordinates y_i as it was previously given in Eq. (3.9). This concludes the algebraic derivation of the 8-tupel Study array.

Even though Study's parameters and dual quaternions can be viewed as analytically identical, it is important to note that their geometric interpretation differs. Dual quaternions are two vectors in a dual three-space and Study's parameters are points on a quadric in a seven-dimensional space [84].

3.3.3 Geometry of Study's Quadric

The previous sections unveiled some information on the derivation of Study's parametric representation of Euclidean rigid body displacements. It was also put into perspective with regard to other representations. To understand the main advantage of Study's representation when studying the kinematics of linkages, it is beneficial to have some fundamental understanding of the geometry of the mapping which is the focus of this section. Since Study's array is homogeneous, the mapping can be viewed as a point in a seven-dimensional projective space, P^7. All these points lie on the constraint imposed by Eq. (3.10), known as Study's quadric $\mathcal{S}_6^2$. As mentioned, points on Eq. (3.25) where $x_0 = x_1 = x_2 = x_3 = 0$, having the parametric representation

$$[0 : 0 : 0 : 0 : y_0 : y_1 : y_2 : y_3],$$

are known as the exceptional generator, A_∞, and do not represent any real displacements. Thus, these points are technically not part of $\mathcal{S}_6^2$. Hence, there exists a one-to-one correspondence between a point on Study's quadric and a Euclidean

displacement, $SE(3) \setminus A_\infty$. Study called the points "soma", a Greek word meaning "body". The entirety of all possible displacements in $SE(2)$ and $SE(3)$ must map to points, curves, surfaces or higher-dimensional objects on $\mathcal{S}_6^2$ which are represented as algebraic polynomials, known as constraint equations [12]. In contrast to classical trigonometric approaches the algebraic constraint equations contain all information of the manipulator which allows to determine all solutions to kinematic analysis problems [85]. Hence, with the appropriate algebraic tools it is possible to perform different analyses, such as singularity analysis or identifying the number of assembly modes of the mechanisms generating the displacements.

Admittedly, it is not straightforward to picture, not to mention illustrate $\mathcal{S}_6^2$ on a two-dimensional piece of paper, as it is a six-dimensional quadric surface in a seven-dimensional space. However, some geometric insights leading to a symbolic sketch can be observed from Eq. (3.10). The equation consists of bilinear cross-terms, which suggest that it has been rotated out of its standard position, or normal form [86, 87]. With the help of the principle axes theorem, the cross-terms can be eliminated and the equation can be transformed into its *canonical form*, which in return provides information on its nature [88]. In essence, the theorem states that if $\mathbf{M}$ is a symmetric $n \times n$- matrix, then its quadratic form of $\mathbf{x}^T\mathbf{M}\mathbf{x}$ can be rewritten using an orthogonal change of variable $\mathbf{x} = \mathbf{P}\mathbf{y}$, such that the new equation becomes $\mathbf{y}^T\mathbf{D}\mathbf{y}$ where $\mathbf{D}$ is a diagonal matrix and hence, cross-terms are no longer present in the quadric form.

Concretely, rewriting Eq. (3.10) using a 8×8 symmetric matrix yields

$$\mathbf{x}^T\mathbf{M}\mathbf{x} = [x_0 \dots y_3] \begin{bmatrix} 0 & 0 & 0 & 0 & 1/2 & 0 & 0 & 0 \\ 0 & 0 & 0 & 0 & 0 & 1/2 & 0 & 0 \\ 0 & 0 & 0 & 0 & 0 & 0 & 1/2 & 0 \\ 0 & 0 & 0 & 0 & 0 & 0 & 0 & 1/2 \\ 1/2 & 0 & 0 & 0 & 0 & 0 & 0 & 0 \\ 0 & 1/2 & 0 & 0 & 0 & 0 & 0 & 0 \\ 0 & 0 & 1/2 & 0 & 0 & 0 & 0 & 0 \\ 0 & 0 & 0 & 1/2 & 0 & 0 & 0 & 0 \end{bmatrix} \begin{bmatrix} x_0 \\ \vdots \\ y_3 \end{bmatrix}. \quad (3.27)$$

$\mathbf{M}$ is called the *matrix of the quadratic form*. Introducing a change of variable such that

$$\mathbf{x} = \mathbf{P}\mathbf{y} \quad \text{or} \quad \mathbf{y} = \mathbf{P}^{-1}\mathbf{x}, \quad (3.28)$$

where $\mathbf{P}$ is an invertible matrix and $\mathbf{y} = [z_0 : z_1 : z_2 : z_3 : w_0 : w_1 : w_2 : w_3]^T$ is a new 8×1 vector in P^7, the quadratic expression can be written as

$$\mathbf{x}^T\mathbf{M}\mathbf{x} = (\mathbf{P}\mathbf{y})^T \mathbf{M} (\mathbf{P}\mathbf{y}) = \mathbf{y}^T\mathbf{P}^T\mathbf{M}\mathbf{P}\mathbf{y} = \mathbf{y}^T \left(\mathbf{P}^T\mathbf{M}\mathbf{P}\right) \mathbf{y}. \quad (3.29)$$

Since $\mathbf{M}$ is symmetric, it is orthogonally diagonalisable, which can be expressed by

$$\mathbf{M} = \mathbf{P}\mathbf{D}\mathbf{P}^T = \mathbf{P}\mathbf{D}\mathbf{P}^{-1}, \quad (3.30)$$

where $\mathbf{P}$ is a proper orthogonal matrix and $\mathbf{D}$ is a diagonal matrix. Rearranging Eq. (3.30) reveals that there must be an orthogonal matrix $\mathbf{P}$ such that the expression in the brackets of Eq. (3.29) is a diagonal matrix,

$$\mathbf{P}^T\mathbf{M}\mathbf{P} = \mathbf{D}. \quad (3.31)$$

One option to derive $\mathbf{P}$ is to compute the eigenvectors of $\mathbf{M}$ since the eigenvectors of different eigenspaces must be orthogonal to each other. Hence, $\mathbf{P}$ becomes

$$\mathbf{P} = \begin{bmatrix} 0 & 0 & 0 & 1 & -1 & 0 & 0 & 0 \\ 0 & 0 & 1 & 0 & 0 & 0 & 0 & -1 \\ 0 & 1 & 0 & 0 & 0 & 0 & -1 & 0 \\ 1 & 0 & 0 & 0 & 0 & -1 & 0 & 0 \\ 0 & 0 & 0 & 1 & 1 & 0 & 0 & 0 \\ 0 & 0 & 1 & 0 & 0 & 0 & 0 & 1 \\ 0 & 1 & 0 & 0 & 0 & 0 & 1 & 0 \\ 1 & 0 & 0 & 0 & 0 & 1 & 0 & 0 \end{bmatrix}. \tag{3.32}$$

It may be necessary to interchange two columns of $\mathbf{P}$ to ensure that $\det(\mathbf{P}) = 1$. This allows us to compute $\mathbf{D}$ using Eq. (3.31)

$$\mathbf{D} = \begin{bmatrix} 1 & 0 & 0 & 0 & 0 & 0 & 0 & 0 \\ 0 & 1 & 0 & 0 & 0 & 0 & 0 & 0 \\ 0 & 0 & 1 & 0 & 0 & 0 & 0 & 0 \\ 0 & 0 & 0 & 1 & 0 & 0 & 0 & 0 \\ 0 & 0 & 0 & 0 & -1 & 0 & 0 & 0 \\ 0 & 0 & 0 & 0 & 0 & -1 & 0 & 0 \\ 0 & 0 & 0 & 0 & 0 & 0 & -1 & 0 \\ 0 & 0 & 0 & 0 & 0 & 0 & 0 & -1 \end{bmatrix} \tag{3.33}$$

as well as the expression for $\mathcal{S}_6^2$ in the rotated coordinate system $\mathbf{y}$

$$\mathbf{x}^T\mathbf{M}\mathbf{x} = \mathbf{y}^T\mathbf{D}\mathbf{y} = z_0^2 + z_1^2 + z_2^2 + z_3^2 - w_0^2 - w_1^2 - w_2^2 - w_3^2. \tag{3.34}$$

Clearly, this expression unveils that the Study quadric $\mathcal{S}_6^2$ is an hyperboloid of one

sheet. Similar to the hyperboloid of one sheet in the Euclidean 3-space, this quadric contains two sets of generator spaces. While the generator lines of the hyperboloid of one sheet in $\mathbb{E}^3$ are skew lines in two reguli, the generator spaces of $\mathcal{S}_6^2$ are 3-spaces in two opposite reguli, which are called A-planes and B-planes, after [78]. However, the 3-spaces in one regulus are not skew in a sense, since some of the 3-spaces intersect others in the same regulus. In total, there are $3 + 2\infty^4$ different generator spaces contained on the Study quadric [89]. A- and B-planes follow a right-handed and left-handed coordinate system, respectively, which makes A-planes significantly more interesting to applied kinematics. A symbolic sketch of $\mathcal{S}_6^2$ that is showing the A-planes as generator spaces is displayed in Fig. 3.2. As the A-planes are mostly skew, they generally do not intersect. However, there are exceptions where they can intersect in a line [90].

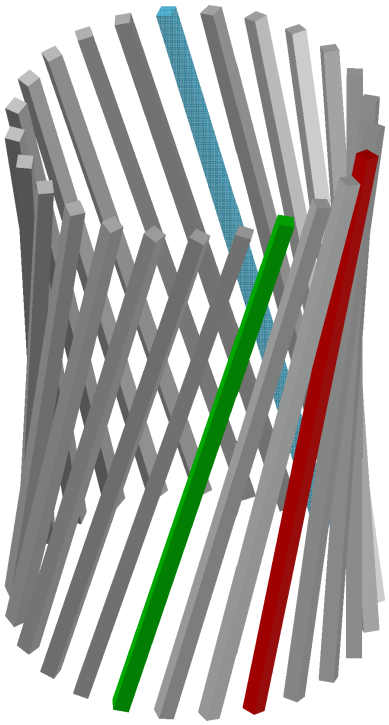

Figure 3.2: Symbolic sketch of the Study quadric $\mathcal{S}_6^2$.

In this thesis, emphasis should be placed on three generator spaces: A_∞, $SO(3)$

and $SE(2)$. The exceptional generator A_∞ is highlighted in blue in Fig. 3.2. Even though A_∞ does not represent real displacements, it plays an important role in determining the type of other A-planes. An A-plane corresponds to $SO(3)$ if it contains the identity array $[1:0:0:\ldots:0]^T$, which Study called the "protosoma", and its intersection with A_∞ is the empty set. As there are no translational elements in $SO(3)$, the generator is characterised by $y_0 = y_1 = y_2 = y_3 = 0$. An A-plane corresponds to $SE(2)$ if it contains the identity and intersects A_∞ in a line. It can easily be shown that the $SE(2)$ generator is characterised by $x_1 = x_2 = y_0 = y_3 = 0$ [90]. Symbolically, $SO(3)$ and $SE(2)$ are highlighted in red and green in Fig. 3.2, respectively.

As e.g., demonstrated in [89], the maximum dimension of linear subspaces on S_6^2 is three. Thus, in addition to the three-dimensional generator spaces discussed above, there also exists two-dimensional and one-dimensional subspaces on S_6^2. Three-dimensional generator spaces correspond to a three-parametric set of rotations or translations, two-dimensional subspaces are planes corresponding to a two-parametric set of rotations or translations and one-dimensional subspaces are lines corresponding to a one-parameter set of translations or rotations [78, 91]. Since two A-planes may intersect in a line, lines are the connecting link between generator spaces of the same type. For a line on Study's quadric to represent a rotation or translation of $SE(3)$, it must pass the "protosoma", thus, intersect with the hyperplane where $y_0 = 0$. Eberharter and Ravani classify the straight lines on S_6^2 into three categories [89].

1. Simple rotations: these have a proper axis through the origin and the lines are parametrised by $y_0 = y_1 = y_2 = y_3 = 0$.

2. General rotations: these have a proper axis that does not pass through the origin. These lines are parametrised by $y_0 = 0$.

3. Translations: these displacements have an improper axis which lies at infinity perpendicular to the direction of translation. These lines are parametrised by

$$x_1 = x_2 = x_3 = y_0 = 0.$$

3.3.4 Transformations in the Kinematic Image Space

This section examines the different coordinate transformations in the kinematic image space which will greatly facilitate the computations when working with kinematic chains. Considering coordinate transformations in Cartesian space, we can distinguish between two types. The first type is taking place in the fixed reference frame, or non-moving base frame. Hence, rotations and translations are all conducted about and along the fixed base frame coordinate axes, respectively, and are performed using pre-multiplication. The second type is taking place in the moving coordinate frame of the preceding frame in the kinematic chain. Hence, rotations and translations are conducted about and along the axis resulting from the previous transformation. This procedure is performed using post-multiplication [92].

Pfurner [14] demonstrates in his PhD thesis how the two transformations can be written in the kinematic image space, and due to its importance for this thesis, the derivations will be briefly summarised. Let us consider an arbitrary Euclidean displacement matrix $\mathbf{A} \in SE(3)$ with image coordinates of $A[a_0 : a_1 : a_2 : a_3 : a_4 : a_5 : a_6 : a_7] \in \mathcal{S}_6^2 \setminus A_\infty$, then following Eq. (3.12) the homogeneous matrix representation with the normalising condition of $a_0^2 + a_1^2 + a_2^2 + a_3^2 = 1$ corresponding to its pre-image can be written as

$$\mathbf{A} = \begin{pmatrix} a_0^2 + a_1^2 + a_2^2 + a_3^2 & 0 & 0 & 0 \\ 2(-a_0a_5 + a_1a_4 - a_2a_7 + a_3a_6) & a_0^2 + a_1^2 - a_2^2 - a_3^2 & 2(a_1a_2 - a_0a_3) & 2(a_1a_3 + a_0a_2) \\ 2(-a_0a_6 + a_1a_7 + a_2a_4 - a_3a_5) & 2(a_1a_2 + a_0a_3) & a_0^2 - a_1^2 + a_2^2 - a_3^2 & 2(a_2a_3 - a_0a_1) \\ 2(-a_0a_7 - a_1a_6 + a_2a_5 + a_3a_4) & 2(a_1a_3 - a_0a_2) & 2(a_2a_3 + a_0a_1) & a_0^2 - a_1^2 - a_2^2 + a_3^2 \end{pmatrix}. \tag{3.35}$$

Moreover, consider a fixed transformation $\mathbf{T} \in SE(3)$ with image coordinates of $T[t_0 : t_1 : t_2 : t_3 : t_4 : t_5 : t_6 : t_7] \in \mathcal{S}_6^2 \setminus A_\infty$. The coordinate transformation in terms of the Study parameters is given as

$$\mathbf{T} = \begin{pmatrix} t_0^2+t_1^2+t_2^2+t_3^2 & 0 & 0 & 0 \\ 2(-t_0t_5+t_1t_4-t_2t_7+t_3t_6) & t_0^2+t_1^2-t_2^2-t_3^2 & 2(t_1t_2-t_0t_3) & 2(t_1t_3+t_0t_2) \\ 2(-t_0t_6+t_1t_7+t_2t_4-t_3t_5) & 2(t_1t_2+t_0t_3) & t_0^2-t_1^2+t_2^2-t_3^2 & 2(t_2t_3-t_0t_1) \\ 2(-t_0t_7-t_1t_6+t_2t_5+t_3t_4) & 2(t_1t_3-t_0t_2) & 2(t_2t_3+t_0t_1) & t_0^2-t_1^2-t_2^2+t_3^2 \end{pmatrix}. \tag{3.36}$$

If the transformation is required in the fixed frame, pre-multiplication of the transformation matrix $\mathbf{T}$, i.e., $\mathbf{T} \cdot \mathbf{A}$, where the $\cdot$ operator indicates matrix multiplication, yields a 4×4 matrix. This matrix can be normalised by dividing by $(t_0^2+t_1^2+t_2^2+t_3^2)(a_0^2+a_1^2+a_2^2+a_3^2)$ and mapped onto Study's quadric using Eq. (3.8) and Eq. (3.9). Mapping $\mathbf{T} \cdot \mathbf{A}$ on $\mathcal{S}_6^2$ will be symbolised by the operator $\circ$, i.e., $T \circ A$. The computation of the first four Study parameters is straightforward. However, the latter four require some additional manipulation as follows. To ensure that $\mathbf{A}$ and $\mathbf{T}$ are contained on the Study quadric substituting some variations of Eq. (3.10), such as $t_1t_5+t_2t_6+t_3t_7 = -t_0t_4$, $t_0t_4+t_2t_6+t_3t_7 = -t_1t_5$, $a_1a_5+a_2a_6+a_3a_7 = -a_0a_4$ and $a_0a_4+a_2a_6+a_3a_7 = -a_1a_5$ greatly simplify the expressions. The final matrix product

in Study parameters then becomes

$$T \circ A = \Delta \begin{pmatrix} a_0t_0 - a_1t_1 - a_2t_2 - a_3t_3 \\ a_0t_1 + a_1t_0 - a_2t_3 + a_3t_2 \\ a_0t_2 + a_1t_3 + a_2t_0 - a_3t_1 \\ a_0t_3 - a_1t_2 + a_2t_1 + a_3t_0 \\ a_0t_4 - a_1t_5 - a_2t_6 - a_3t_7 - a_4t_0 - a_5t_1 - a_6t_2 - a_7t_3 \\ a_0t_5 + a_1t_4 - a_2t_7 + a_3t_6 + a_4t_1 + a_5t_0 - a_6t_3 + a_7t_2 \\ a_0t_6 + a_1t_7 + a_2t_4 - a_3t_5 + a_4t_2 + a_5t_3 + a_6t_0 - a_7t_1 \\ a_0t_7 - a_1t_6 + a_2t_5 + a_3t_4 + a_4t_3 - a_5t_2 + a_6t_1 + a_7t_0 \end{pmatrix} \tag{3.37}$$

where

$$\Delta = \frac{a_0t_0 - a_1t_1 - a_2t_2 - a_3t_3}{(t_0^2 + t_1^2 + t_2^2 + t_3^2)(a_0^2 + a_1^2 + a_2^2 + a_3^2)}.$$

Since Study parameters are homogeneous Δ can be omitted. Rewriting Eq. (3.37) as a matrix product where $\mathbf{a}$ corresponds to an 8×1 vector according to

$$T \circ A = \mathbf{T}_b \mathbf{a}, \tag{3.38}$$

the basis transformation matrix $\mathbf{T}_b$ becomes

$$\mathbf{T}_b = \begin{pmatrix} t_0 & -t_1 & -t_2 & -t_3 & 0 & 0 & 0 & 0 \\ t_1 & t_0 & -t_3 & t_2 & 0 & 0 & 0 & 0 \\ t_2 & t_3 & t_0 & -t_1 & 0 & 0 & 0 & 0 \\ t_3 & -t_2 & t_1 & t_0 & 0 & 0 & 0 & 0 \\ t_4 & -t_5 & -t_6 & -t_7 & -t_0 & -t_1 & -t_2 & -t_3 \\ t_5 & t_4 & -t_7 & t_6 & t_1 & t_0 & -t_3 & t_2 \\ t_6 & t_7 & t_4 & -t_5 & t_2 & t_3 & t_0 & -t_1 \\ t_7 & -t_6 & t_5 & t_4 & t_3 & -t_2 & t_1 & t_0 \end{pmatrix}. \tag{3.39}$$

Following the same procedure for the coordinate transformation in the moving frame, the matrix product $\mathbf{A} \cdot \mathbf{T}$ can be mapped onto Study's quadric. After simplification and rewriting the Study vector that resulted from $A \circ T$ as the matrix product $\mathbf{T}_m \mathbf{a}$, i.e.,

$$A \circ T = \mathbf{T}_m \mathbf{a}, \tag{3.40}$$

the matrix describing this type of transformation reads

$$\mathbf{T}_m = \begin{pmatrix} t_0 & -t_1 & -t_2 & -t_3 & 0 & 0 & 0 & 0 \\ t_1 & t_0 & t_3 & -t_2 & 0 & 0 & 0 & 0 \\ t_2 & -t_3 & t_0 & t_1 & 0 & 0 & 0 & 0 \\ t_3 & t_2 & -t_1 & t_0 & 0 & 0 & 0 & 0 \\ t_4 & -t_5 & -t_6 & -t_7 & t_0 & -t_1 & -t_2 & -t_3 \\ t_5 & t_4 & t_7 & -t_6 & t_1 & t_0 & t_3 & -t_2 \\ t_6 & -t_7 & t_4 & t_5 & t_2 & -t_3 & t_0 & t_1 \\ t_7 & t_6 & -t_5 & t_4 & t_3 & t_2 & -t_1 & t_0 \end{pmatrix}. \tag{3.41}$$

The conclusion drawn from the derivation of $\mathbf{T}_b$ and $\mathbf{T}_m$ is that any coordinate transformation, both in the fixed and the moving frame, can be expressed as a projective transformation in Study's kinematic image space. It turns out that the elements of the transformation matrices are linear in the Study parameters and therefore, provide an efficient tool to compute coordinate transformation in $SE(3)$. Further inspection of these two matrices show that they commute, i.e., $\mathbf{T}_b \cdot \mathbf{T}_m = \mathbf{T}_m \cdot \mathbf{T}_b$, thus, as in Euclidean space the order of these two transformations does not affect the result [14].

3.4 Denavit-Hartenberg Parameterisation

3.4.1 DH Parametrisation and the Euclidean space

Displacements of kinematic chains are often parametrised using the Denavit-Hartenberg (DH) convention [93]. They were first introduced by Denavit and Hartenberg in 1955, and are still widely used in the field of robotics. Nowadays, the literature contains many variations of the original DH coordinate system and parameter assignment convention. Subtly different coordinate frame attachment rules and parameter definitions have been devised for mechanical system calibration, dynamic analysis, accounting for misalignment of joint axis directions, etc., see [92, 94, 95, 96] for several examples. Therefore, it is important to precisely define the convention used in this work to avoid confusion and misinterpretation since the corresponding coordinate transformations are all different from those of Denavit and Hartenberg.

The first step in the DH parametrisation of an arbitrary kinematic chain is to identify and number all the joint axes. Next comes the allocation of coordinate systems to each link in the chain using a set of rules to locate the origin of the coordinate system and the orientation of the basis vectors. The position and orientation of consecutive links are defined by a homogeneous transformation matrix that maps coordinates of points in the coordinate system attached to link i to those of the same points described in the coordinate system attached to link $i-1$. Symbolically, the coordinate transformation matrix is denoted

$$ {}^{i-1}_{i}\mathbf{T}. $$

The forward and inverse kinematics of serial chains are the concatenations of the individual transformation matrices in the appropriate order [97]. For example, the forward kinematics problem of determining the position and orientation of the nth link in a serial kinematic chain described in a relatively fixed non-moving base

coordinate system 0, given the relevant DH parameters and values for the n joint variables is conceptually straightforward as matrix multiplication.

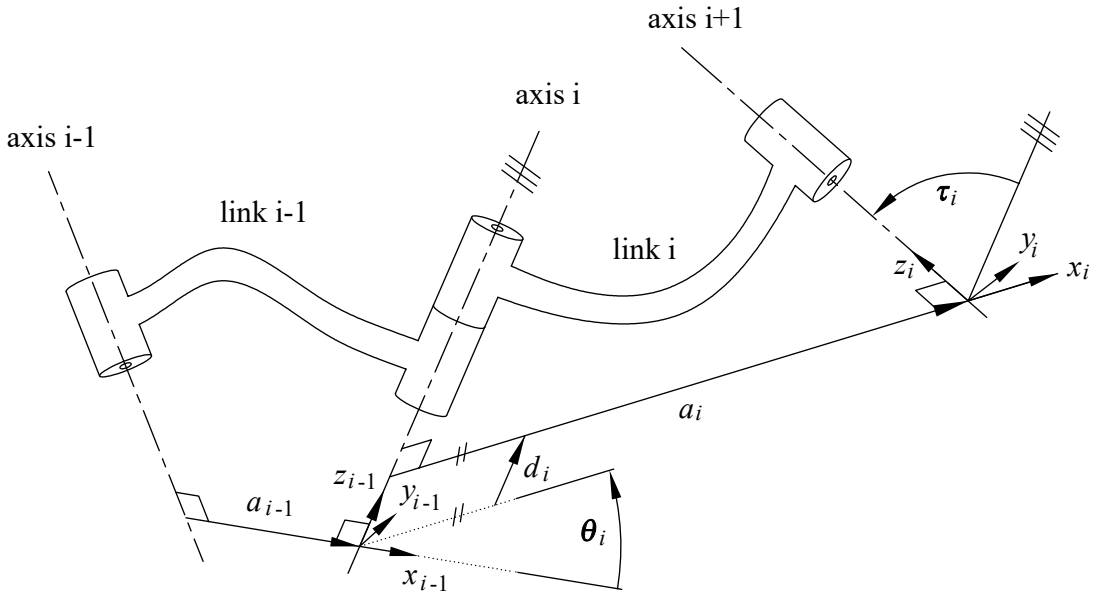

Figure 3.3: DH parameter frame assignment and its corresponding DH parameters.

To visualise the four DH parameters, consider two arbitrary sequential neighbouring links, $i-1$ and i. Two such links are illustrated in Fig. 3.3. The procedure for assigning the location of the origin and the basis vectors for the coordinate system for the ith link in which the DH parameters are defined as follows.

1. Identify all joint axes. Consider neighbours $i-1$, i, and $i+1$, illustrated in Fig. 3.3.

2. Identify the common perpendicular between the two axes i and $i+1$, or their point of intersection. At the point of intersection, or where the common perpendicular meets the $i+1^{st}$ joint axis, assign the link coordinate system origin, 0_i.

3. For coordinate systems 0 and 1, ensure the coordinate axes are aligned when $\theta_1 = 0$.

4. Assign the z_i axis to point along the joint axis $i+1$.

5. Assign the x_i axis to point along the common normal between the joint axes i and $i+1$. If the axes are parallel, any convenient normal can be selected. If the axes intersect, assign x_i to be perpendicular to the plane containing z_{i-1} and z_i.

6. Assign the y_i axis to complete a right-handed coordinate system.

Now, the four DH parameters [93] are defined in the following way.

θ_i, joint angle: the angle from x_{i-1} to x_i measured about z_{i-1}.

d_i, link offset: the distance from x_{i-1} to x_i measured along z_{i-1}.

τ_i, link twist: the angle from z_{i-1} to z_i measured about x_i.

a_i, link length: the directed distance from z_{i-1} to z_i measured along x_i.

According to this convention the coordinate transformation from the coordinate system for joint i relative to the coordinate system of the previous joint $i-1$ can be divided into two screw displacement, i.e., two pure rotations and two pure translations in terms of the DH parameter

$$\mathbf{T}(d_i) = \left[\begin{array}{c|ccc} 1 & 0 & 0 & 0 \\ \hline 0 & 1 & 0 & 0 \\ 0 & 0 & 1 & 0 \\ d_i & 0 & 0 & 1 \end{array}\right]; \quad \mathbf{T}(\theta_i) = \left[\begin{array}{c|ccc} 1 & 0 & 0 & 0 \\ \hline 0 & \cos(\theta_i) & -\sin(\theta_i) & 0 \\ 0 & \sin(\theta_i) & \cos(\theta_i) & 0 \\ 0 & 0 & 0 & 1 \end{array}\right];$$

$$\mathbf{T}(a_i) = \left[\begin{array}{c|ccc} 1 & 0 & 0 & 0 \\ \hline a_i & 1 & 0 & 0 \\ 0 & 0 & 1 & 0 \\ 0 & 0 & 0 & 1 \end{array}\right]; \quad \mathbf{T}(\tau_i) = \left[\begin{array}{c|ccc} 1 & 0 & 0 & 0 \\ \hline 0 & 1 & 0 & 0 \\ 0 & 0 & \cos(\tau_i) & -\sin(\tau_i) \\ 0 & 0 & \sin(\tau_i) & \cos(\tau_i) \end{array}\right].$$

Multiplying the rotations and translations following

$$\mathbf{T}(\theta_i) \cdot \mathbf{T}(d_i) \cdot \mathbf{T}(a_i) \cdot \mathbf{T}(\tau_i) \tag{3.42}$$

yields the transformation between two coordinate frames which is given by

$$ {}^{i-1}_{i}\mathbf{T} = \left[\begin{array}{cccc} \cos\theta_i & -\sin\theta_i\cos\tau_i & \sin\theta_i\sin\tau_i & a_i\cos\theta_i \\ \sin\theta_i & \cos\theta_i\cos\tau_i & -\cos\theta_i\sin\tau_i & a_i\sin\theta_i \\ 0 & \sin\tau_i & \cos\tau_i & d_i \\ \hline 0 & 0 & 0 & 1 \end{array}\right] = \left[\begin{array}{ccc|c} & \mathbf{A} & & \mathbf{t} \\ \hline 0 & 0 & 0 & 1 \end{array}\right]. \tag{3.43}$$

Hence, to describe the end-effector coordinate frame of a kinematic chain with respect to the base frame, the overall transformation matrix becomes

$$ {}^{0}_{i}\mathbf{T} = {}^{0}_{1}\mathbf{T}\ {}^{1}_{2}\mathbf{T}\ {}^{2}_{3}\mathbf{T}\ \ldots\ {}^{i-1}_{i}\mathbf{T}. \tag{3.44}$$

Applying this algebraic representation to simple closed chains, like a mechanism, requires that the end-effector coordinate frame coincides with the coordinate frame of the base. Hence, the overall transformation equates to the identity matrix [3].

3.4.2 DH Parametrisation and the Kinematic Projective Image Space

Depending on the number of joints and links in a kinematic chain, it can be extremely tedious to evaluate Eq. (3.44) in matrix form. Moreover, this representation may be subjected to representational singularities that are present in the trigonometric expressions. When studying kinematic chains of rigid bodies, Study's kinematic mapping aims to describe distinct three-dimensional displacements of the moving end-effector frame as distinct points in a seven-dimensional projective kinematic mapping

image space. Constraints on the motion of the end-effector frame imposed by the joints in the kinematic chain map to curves or surfaces in the image space and essentially describe the workspace of the manipulator. The equations of these curves or surfaces are known as constraint equations [12]. An efficient computation method without having to first evaluate Eq. (3.44) and subsequently map the result onto Study's quadric, builds upon Section 3.3.4. More details of the following derivation in this section are given in [14].

Without loss of generality, we can combine and rename the transformation matrices in Eq. (3.42), i.e.,

$$\mathbf{M_i} = \mathbf{T}(\theta_i) \qquad \mathbf{G_i} = \mathbf{T}(d_i) \cdot \mathbf{T}(a_i) \cdot \mathbf{T}(\tau_i) \tag{3.45}$$

For a revolute joint, the matrix $\mathbf{M_i}$ depends only on the variable motion parameter θ_i while the matrix $\mathbf{G_i}$ depends only on constant design parameters. For a prismatic joint the matrix $\mathbf{M_i}$ would depend on the variable link offset d_i while θ_i would be a constant, changing the design parameter matrix to

$$\mathbf{G_i} = \mathbf{T}(\theta_i) \cdot \mathbf{T}(a_i) \cdot \mathbf{T}(\tau_i).$$

Thus, the homogeneous transformation matrices

$$\mathbf{M_i} = \left[\begin{array}{c|ccc} 1 & 0 & 0 & 0 \\ \hline 0 & \cos(\theta_i) & -\sin(\theta_i) & 0 \\ 0 & \sin(\theta_i) & \cos(\theta_i) & 0 \\ 0 & 0 & 0 & 1 \end{array}\right]; \quad \mathbf{G_i} = \left[\begin{array}{c|ccc} 1 & 0 & 0 & 0 \\ \hline a_i & 1 & 0 & 0 \\ 0 & 0 & \cos(\tau_i) & -\sin(\tau_i) \\ d_i & 0 & \sin(\tau_i) & \cos(\tau_i) \end{array}\right] \tag{3.46}$$

are mapped onto Study's quadric using Eq. (3.8) and Eq. (3.9). It turns out that the Study parameters can be simplified by algebraising the transformations using

tangent half-angle substitutions for the angle parameters $v_i = \tan(\theta_i/2)$ and $\alpha_i = \tan(\tau_i/2)$ [47]. This implies that

$$\cos\theta_i = \frac{1-v_i^2}{1+v_i^2}, \quad \sin\theta_i = \frac{2v_i}{1+v_i^2}, \tag{3.47}$$

$$\cos\tau_i = \frac{1-\alpha_i^2}{1+\alpha_i^2}, \quad \sin\tau_i = \frac{2\alpha_i}{1+\alpha_i^2}. \tag{3.48}$$

Hence, the Study parameters for $\mathbf{M_i}$ and $\mathbf{G_i}$ reduce to

$$M_i = [1:0:0:v_i:0:0:0:0]^T; \tag{3.49}$$

$$G_i = [2:2\alpha_i:0:0:a_i\alpha_i:-a_i:-d_i\alpha_i:-d_i]^T. \tag{3.50}$$

In Section 3.3.4, the distinction between transformations in the fixed and moving frame led to two different matrices, $\mathbf{T_b}$ and $\mathbf{T_m}$, in terms of the Study parameters, respectively. Hence, the specific transformations in Eq. (3.49) and Eq. (3.50) expressed in the kinematic image space as a coordinate transformation in the fixed frame yield according to Eq. (3.39)

$$\mathbf{T_b}(M_i) = \begin{pmatrix} 1 & 0 & 0 & -v_i & 0 & 0 & 0 & 0 \\ 0 & 1 & -v_i & 0 & 0 & 0 & 0 & 0 \\ 0 & v_i & 1 & 0 & 0 & 0 & 0 & 0 \\ v_i & 0 & 0 & 1 & 0 & 0 & 0 & 0 \\ 0 & 0 & 0 & 0 & 1 & 0 & 0 & -v_i \\ 0 & 0 & 0 & 0 & 0 & 1 & -v_i & 0 \\ 0 & 0 & 0 & 0 & 0 & v_i & 1 & 0 \\ 0 & 0 & 0 & 0 & v_i & 0 & 0 & 1 \end{pmatrix} \tag{3.51}$$

$$\mathbf{T_b}(G_i) = \begin{pmatrix} 2 & -2\alpha_i & 0 & 0 & 0 & 0 & 0 & 0 \\ 2\alpha_i & 2 & 0 & 0 & 0 & 0 & 0 & 0 \\ 0 & 0 & 2 & -2\alpha_i & 0 & 0 & 0 & 0 \\ 0 & 0 & 2\alpha_i & 2 & 0 & 0 & 0 & 0 \\ a_i\alpha_i & a_i & d_i\alpha_i & d_i & 2 & -2\alpha_i & 0 & 0 \\ -a_i & a_i\alpha_i & d_i & -d_i\alpha_i & 2\alpha_i & 2 & 0 & 0 \\ -d_i\alpha_i & -d_i & a_i\alpha_i & a_i & 0 & 0 & 2 & -2\alpha_i \\ -d_i & d_i\alpha_i & -a_i & a_i\alpha_i & 0 & 0 & 2\alpha_i & 2 \end{pmatrix} \tag{3.52}$$

Hence, given a concatenation of coordinate frame transformations as in an arbitrary kinematic chain, the workspace of the end-effector can be described in P_7 by

$$\mathbf{p} = \mathbf{T_b}(M_1) \cdot \mathbf{T_b}(G_1) \cdot \mathbf{T_b}(M_2) \cdot \mathbf{T_b}(G_2) \cdot \cdots \cdot \mathbf{T_b}(M_n) \cdot \mathbf{T_b}(G_n) \cdot \mathbf{id}, \tag{3.53}$$

where **id** corresponds to the identity in the kinematic image space,

$$\mathbf{id} = [1 : 0 : 0 : 0 : 0 : 0 : 0 : 0]^T.$$

Similarly, the specific transformations in Eq. (3.49) and Eq. (3.50) expressed in the kinematic image space as a coordinate transformation in the moving frame yield

according to Eq. (3.41)

$$\mathbf{T_m}(M_i) = \begin{pmatrix} 1 & 0 & 0 & -v_i & 0 & 0 & 0 & 0 \\ 0 & 1 & v_i & 0 & 0 & 0 & 0 & 0 \\ 0 & -v_i & 1 & 0 & 0 & 0 & 0 & 0 \\ v_i & 0 & 0 & 1 & 0 & 0 & 0 & 0 \\ 0 & 0 & 0 & 0 & 1 & 0 & 0 & -v_i \\ 0 & 0 & 0 & 0 & 0 & 1 & v_i & 0 \\ 0 & 0 & 0 & 0 & 0 & -v_i & 1 & 0 \\ 0 & 0 & 0 & 0 & v_i & 0 & 0 & 1 \end{pmatrix}, \tag{3.54}$$

$$\mathbf{T_m}(G_i) = \begin{pmatrix} 2 & -2\alpha_i & 0 & 0 & 0 & 0 & 0 & 0 \\ 2\alpha_i & 2 & 0 & 0 & 0 & 0 & 0 & 0 \\ 0 & 0 & 2 & 2\alpha_i & 0 & 0 & 0 & 0 \\ 0 & 0 & -2\alpha_i & 2 & 0 & 0 & 0 & 0 \\ a_i\alpha_i & a_i & d_i\alpha_i & d_i & 2 & -2\alpha_i & 0 & 0 \\ -a_i & a_i\alpha_i & -d_i & d_i\alpha_i & 2\alpha_i & 2 & 0 & 0 \\ -d_i\alpha_i & d_i & a_i\alpha_i & -a_i & 0 & 0 & 2 & 2\alpha_i \\ -d_i & -d_i\alpha_i & a_i & a_i\alpha_i & 0 & 0 & -2\alpha_i & 2 \end{pmatrix}. \tag{3.55}$$

Using Eq. (3.54) and Eq. (3.55) to obtain the same result as in Eq. (3.53), i.e., the displacement of the end-effector in the kinematic image space, it must be written as

$$\mathbf{p} = \mathbf{T_m}(G_n) \cdot \mathbf{T_m}(M_n) \cdot \cdots \cdot \mathbf{T_m}(G_2) \cdot \mathbf{T_m}(M_2) \cdot \mathbf{T_m}(G_1) \cdot \mathbf{T_m}(M_1) \cdot \mathbf{id}. \tag{3.56}$$

3.5 Elimination Theory

Once polynomial equations for a particular mechanism have been established, they must be manipulated such that certain variables are eliminated. In the case of this thesis, these variables generally correspond to intermediate joint angles but could also include other variables, such as slider distances. Systematic elimination of variables from polynomial equations can be accomplished using *Elimination Theory* [98]. While systems of linear equations can be completely solved with Gaussian elimination, or with Cramer's rule, other methods, such as resultants [99], Gröbner bases [15] or the linear implicitisation algorithm [16], have demonstrated to be effective for solving systems of equations with non-linear polynomials. These three methods will now be explained briefly. The explanations and definitions for this section are mainly taken from [16, 98, 100, 101] if not mentioned otherwise.

Let k be any field, such as the rational numbers $\mathbb{Q}$, the real numbers $\mathbb{R}$, or the complex numbers $\mathbb{C}$. A monomial, sometimes referred to as a power product, is the product of variables $x_1, ..., x_n$ with non-negative integer powers α_i, such that

$$x_1^{\alpha_1} x_2^{\alpha_2} \cdots x_n^{\alpha_n}.$$

This leads to the definition of a multivariate polynomial $f(x_1, ..., x_n)$, which is specified as a finite sum of terms where a term is a linear combination of coefficients in k and monomials,

$$f = \sum_{\alpha} c_\alpha x^\alpha.$$

Consider a set of polynomials f_s, then the set of all solutions of the equations $f_1(x_1, ..., x_n) = \cdots = f_s(x_1, ..., x_n) = 0$ is known as the variety, i.e.,

$$\mathbf{V}(f_1, ..., f_s) = \{(a_1, ..., a_n) \in k^n \mid f_i(a_1, ..., a_n) = 0, i = 1, 2, ..., s\}.$$

While a set of equations determines a variety, a variety is not determined by a *particular* set of equations. Some generating sets leading to the same solution are, in fact, "easier" to solve than others. For example, consider a linear system of equations before and after transforming it using Gauss-Jordan elimination. Finding a better generating set of a variety requires the definition of ideals. $I \in k[x_1, ..., x_n]$ is an ideal if

1. $0 \in I$,
2. $f + g \in I$ if $f \in I$ and $g \in I$, and,
3. $pf \in I$ given that $p \in k[x_1, ..., x_n]$ and $f \in I$.

Thus, the collection of polynomials $\langle f_1, ...f_s \rangle$ defines an ideal whose generating set is the polynomials $f_1, ...f_s \in k[x_1, ..., x_n]$. It is important to understand that a variety is determined by an ideal. The goal usually is to find a "better" generating set for the ideal that is "easier" to interpret. As some generating sets of ideals allow a "better" understanding of their algebraic structure, they may allow a "better" understanding of the geometric structure of its variety.

3.5.1 Resultants

The objective of resultants is to verify whether two polynomials share a common factor or common root. Moreover, resultants can be used to eliminate a variable of two multivariate polynomials. If executed in sequence, resultants can be used to solve multivariate polynomial systems. Let f and g be two polynomials $f, g \in k[x]$ of degree l and m, respectively:

$$\begin{aligned} f = &\quad a_0 x^l + a_1 x^{l-1} + \cdots + c_l, && a_0 \neq 0, \quad l > 0; \\ g = &\quad b_0 x^m + b_1 x^{m-1} + \cdots + b_m && d_0 \neq 0, \quad m > 0. \end{aligned}$$

The resultant of these two polynomials can be computed with the determinant of the Sylvester matrix which is defined by [100]

$$Res(f,g) = det \underbrace{\begin{pmatrix} a_0 & & & & b_0 & & & \\ a_1 & a_0 & & & b_1 & b_0 & & \\ a_2 & a_1 & \ddots & & b_2 & b_2 & \ddots & \\ \vdots & a_2 & \ddots & a_0 & \vdots & b_2 & \ddots & b_0 \\ a_l & \vdots & \ddots & a_1 & b_m & \vdots & \ddots & b_1 \\ & a_l & & a_2 & & b_m & & b_2 \\ & & \ddots & \vdots & & & \ddots & \vdots \\ & & & a_l & & & & b_m \end{pmatrix}}_{m \text{ columns}} \underbrace{\qquad}_{l \text{ columns}}, \tag{3.57}$$

where the empty entries of the matrix are zero. Notice that the size of the matrix is determined by $(l+m) \times (l+m)$. The main properties of the resultant which are of significant importance for elimination are [100]:

1. $Res(f,g)$ is an integer polynomial in the coefficients of f and g.
2. Only if f and g share a non-trivial common factor, $Res(f,g)$ becomes zero.
3. There exists two polynomials $A, B \in k[x]$ that fulfil $Res(f,g) = Af + Bg$. The degrees of A and B are smaller than m and l, respectively.

To understand how the resultant can be used for elimination, consider two polynomials f, g in the field $k[x,y]$. Now, f and g can also be viewed as two polynomials in x with polynomial coefficients in y. This allows to compute the resultant with respect to x, i.e. $Res(f,g,x)$, which is by definition a polynomial free of the variable x. Because of the third property above, the resultant is part of the elimination ideal $\langle f,g \rangle \cap k[y]$. It follows that the solutions to $Res(f,g,x) = 0$ are also solutions where $f = g = 0$. For a detailed example, see [100].

3.5.2 Gröbner Basis

To begin this section, consider *Hilbert's Basis Theorem* which guarantees that the hereinafter explained algorithms will terminate and yield a solution. The theorem states that every ideal I in $k[x_1, ..., x_n]$ has a finite generating set, i.e., if I is any ideal of $k[x_1, ..., x_n]$, then there exists polynomials $f_1, ..., f_s \in k[x_1, ..., x_n]$ such that $I = \langle f_1, ...f_s \rangle$. The generating polynomials are also called the *basis* of I.

One important algorithm to fully understand Gröbner bases is known as the division algorithm, a recursive procedure which computes a quotient and a remainder. For instance, in the case of two univariate polynomials $f, g \in k[x]$, the algorithm divides f by g, resulting in a quotient q and a remainder r such that

$$\begin{aligned} f &= qg + r, \quad \text{and} \\ r &= 0 \qquad\quad \text{or} \quad deg(r) < deg(g). \end{aligned}$$

This algorithm can help to obtain a different generating set of polynomials that are describing the same variety, for example, by using it to determine the greatest common divisor $g = gcd(f_1, ...f_s)$. Since g divides every polynomial $f_1, ...f_s$, it follows that $I = \langle f_1, ..., f_s \rangle = \langle g \rangle$. This particular case is also known as the Euclidean algorithm [101].

The division algorithm also provides groundwork for solving the *ideal membership problem* which allows to verify whether a polynomial h is part of a given ideal $I = \langle f_1, ..., f_s \rangle$. It requires computing the greatest common divisor of I, i.e., $g = gcd(f_1, ...f_s)$ and subsequently h is divided by g. If the remainder is zero, it follows that $h \in I$.

The above-mentioned division algorithm can also be extended to multivariate polynomials. However, while in the previous cases with one variable the order was implied by the degree of each term, i.e. $x^m > ... > x^2 > x > 1$, multivariate

polynomials need some sort of explicit systematic ordering. There are several well-established monomial orderings of which three will now be briefly discussed.

- *Lexicographic* ordering compares the exponents of every variable to establish a distinct order of the monomials, similarly as it can be found with letters in dictionaries. The abbreviation commonly used is lex. In other words, let x^α and x^β be two monomials in $k[x_1, ..., x_n]$, then $x^\alpha >_{lex} x^\beta$ if the leftmost nonzero entry in the difference of $\alpha - \beta \in \mathbb{Z}^n$ is positive.

- *Graded lexicographic* ordering, also known as *degree lexicographic* ordering, first compares the total degree of every monomial before comparing the exponents of every variable. The abbreviation commonly used is $grlex$ or $deglex$. Concretely, let x^α and x^β be two monomials in $k[x_1, ..., x_n]$, then $x^\alpha >_{grlex} x^\beta$ if $\sum_{i=1}^n \alpha_i > \sum_{i=1}^n \beta_i$ or if $\sum_{i=1}^n \alpha_i = \sum_{i=1}^n \beta_i$ and $x^\alpha >_{lex} x^\beta$.

- Finally, another important monomial ordering often used in elimination theory is the *graded reverse lexicographic* ordering. It also compares the total degree of every monomial in the first place, but in the subordinated comparison of individual exponents, it compares the exponents of the last indeterminate x_n. The abbreviation commonly used is $grevlex$ or $tdeg$. More formally, let x^α and x^β be two monomials in $k[x_1, ..., x_n]$, then $x^\alpha >_{grevlex} x^\beta$ if $\sum_{i=1}^n \alpha_i > \sum_{i=1}^n \beta_i$ or if $\sum_{i=1}^n \alpha_i = \sum_{i=1}^n \beta_i$ and the rightmost nonzero entry in the difference of $\alpha - \beta \in \mathbb{Z}^n$ is negative.

Now that monomial orderings for nonlinear multivariate polynomials can be described, recall the division algorithm. The idea of the division algorithm in $k[x_1, ...x_n]$ is similar to the previously described division algorithm in one variable: f is divided by $f_1, ...f_s$ such that the leading terms of f are canceled until the division is no longer

possible. Thus, f can be reformulated as

$$f = q_1 f_1 + q_2 f_2 + \cdots + q_s f_s + r$$

where $r, q_i \in k[x_1, ..., x_n]$, and r is either zero, or includes solely monomials that are not divisible by any of the leading terms of $f_i,\ i = 1, ...s$.

Consider again the ideal membership problem, which verifies whether a given polynomial $f \in k[x_1, ...x_n]$ belongs to an ideal $I = \langle f_1, ..., f_s \rangle$. Clearly, if the remainder of the division of f by $F = (f_1, ..., f_s)$ is equals zero, then $f \in I$. However, it is possible that the remainder is not zero, and yet f can belong to I. Thus, to guarantee that the remainder is always zero if $f \in I$ for every $f \neq 0$, it requires computing a generating set $G = (g_1, ..., g_t) \subseteq I$ such that the leading term of f is divisible by some leading term of g_i where $i \in \{1, ..., t\}$. This is called a Gröbner basis. In essence, computing a Gröbner basis for multivariate polynomials is the analogy to computing the greatest common divisor in the univariate case. This naturally leads to the question, how can a Gröbner basis be computed? The answer was first presented by Bruno Buchberger in his PhD thesis [15]. His advisor was Wolfgang Gröbner, whom Buchberger was naming his findings after. He developed an algorithm based on S-polynomials that he uses to cancel leading terms. Let $f, g \in k[x_1, ..., x_n]$, then the S-polynomial of f, g is defined as

$$S(f, g) = \frac{L}{lt(f)} f - \frac{L}{lt(g)} g \tag{3.58}$$

where lt are the leading terms, and L the least common multiple of the leading monomials, lm, of f and g,

$$L = lcm(lm(f), lm(g)).$$

Given an ideal $I = \langle f_1, ..., f_s \rangle \subseteq k[x_1, ..., x_n]$, the algorithm requires computing the

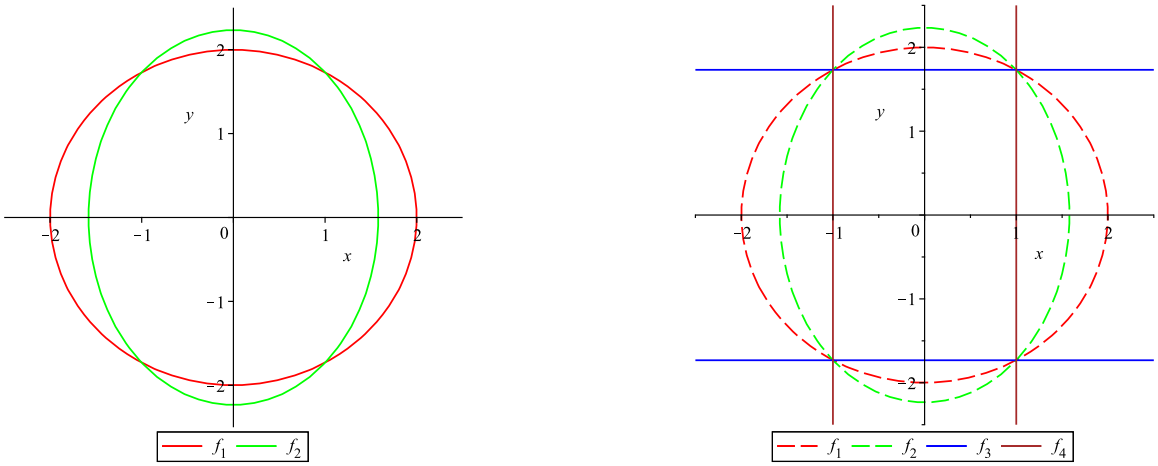

(a) Initial generating equations. (b) Gröbner bases generating equations.

Figure 3.4: Same variety: $V(f_1, f_2) = V(f_3, f_4)$.

$S(f_i, f_j)$-polynomial for every pair of polynomials, $i \neq j$, in the existing ideal, then applying the division algorithm, i.e., reducing $S(f_i, f_j)$ relative to the polynomials $f_1, ..., f_s$. If the remainder is not zero, it is added to the current ideal. The procedure is repeated until every $S(f_i, f_j) = 0, i \neq j$.

Generally, it is possible to compute different Gröbner bases for the same ideal. The outcome depends on two factors. A different monomial order, and the order of computing the S-Polynomial influences the Gröbner basis outcome. Notably, this can lead to unnecessary generating equations, such that one leading term of a generator divides the leading term of another generator. To avoid this situation, there exists the so-called *reduced* Gröbner basis. A Gröbner basis $G = \{g_1, ...g_t\}$ is called reduced if all leading coefficients in G are 1, and G is reduced with respect to $G - \{g_i\}$, meaning that no non-zero term in g_i is divisible by any leading monomial of g_j, for any $j \neq i$.

Before proceeding, consider the following illustrative example. Given are two non-linear equations, one describing a circle with radius 2, centred at the origin, i.e., $f_1 : x^2 + y^2 - 4 = 0$; and one describing an ellipse by $f_2 : 2x^2 + y^2 - 5 = 0$. The aim is to determine the real intersections, if they exist. . Plotting the two functions reveals that there are indeed four intersections, see Fig. 3.4a. However, we can also

use Gröbner bases to determine a generating set of equations that is "easier" to solve than the two polynomials of the ideal $I = \langle f_1, f_2 \rangle$. The monomial ordering is chosen as $x >_{lex} y$. First, following Eq. (3.58) the S-polynomial of f_1 and f_2 becomes

$$S(f_1, f_2) = \frac{x^2}{x^2}(x^2 + y^2 - 4) - \frac{x^2}{2x^2}(2x^2 + y^2 - 5) = \frac{y^2}{2} - \frac{3}{2}.$$

$S(f_1, f_2)$ cannot be reduced with respect to f_1 and f_2. As a result, after multiplying $S(f_1, f_2)$ by 2, it is added to the current ideal as

$$f_3 = y^2 - 3.$$

Now that there are three polynomials in the ideal, $I' = \langle f_1, f_2, f_3 \rangle$, additional S-Polynomials have to be computed and reduced with respect to I'. First,

$$S(f_1, f_3) = \frac{x^2y^2}{x^2}(x^2 + y^2 - 4) - \frac{x^2y^2}{y^2}(y^2 - 3) = 3x^2 + y^4 - 4y^2$$

can be reduced to

$$S(f_1, f_3) = 3f_1 + (y^2 - 4)f_3.$$

Note that the remainder of the division algorithm is zero. Second,

$$S(f_2, f_3) = \frac{x^2y^2}{2x^2}(2x^2 + y^2 - 5) - \frac{x^2y^2}{y^2}(y^2 - 3) = 3x^2 + \frac{1}{2}y^4 - \frac{5}{2}y^2$$

is multiplied by 2, such that $S(f_2, f_3) = 6x^2 + y^4 - 5y^2$ which can be reduced to

$$S(f_2, f_3) = 6f_1 + (y^2 - 8)f_3.$$

Again, the remainder of the division algorithm is zero which terminates the Buchberger algorithm. Therefore, the Gröbner basis is $G = \langle f_1, f_2, f_3 \rangle$. However, it is not

a reduced Gröbner basis yet as the leading monomial of f_1 and f_2 divide each other. This can be solved by

$$f_4 = f_2 - f_1 = 2x^2 + y^2 - 5 - (x^2 + y^2 - 4) = x^2 - 1$$

which yields the reduced Gröbner basis $G = \langle f_3, f_4 \rangle$. The two functions f_3 and f_4 represent four intersecting lines, and as shown in Fig. 3.4b the intersection points of these four lines compared to the original intersection of f_1 and f_2 are the same, i.e. $V(f_1, f_2) = V(f_3, f_4)$. The difference is the lower computational effort required to solve the system of f_3 and f_4.

Finally, with the understanding of what a Gröbner basis is, and how they can be computed, it is now possible to discuss how they can be leveraged to eliminate certain variables in a non-linear multivariate system of equations. The key to computing a Gröbner basis, describing the same variety, but with generating sets that no longer contain certain variables, is the choice of the monomial ordering. Let G be a Gröbner basis of $I \subseteq k[x_1, ...x_n]$, computed according to the lexicographic ordering, i.e. $x_1 > x_2 > \dots x_n$. Furthermore, let $0 \leq l \leq n$, then

$$G_l = G \cap k[x_{l+1}, ..., x_n] \tag{3.59}$$

is the l^{th} elimination ideal I_l. A detailed proof of this statement can, for instance, be found in [98].

When selecting an elimination monomial ordering, at least one of $x_1, ..., x_l$ has to be greater than all monomials with the remaining variables. This is not only the case for the lexicographic but also, e.g., for the graded reverse lexicographic ordering.

3.5.3 Linear Implicitisation Algorithm

Both resultants and Gröbner basis have some major drawbacks. Computing the resultant from multipolynomials generally yields a polynomial with high degree that includes many terms and factors, and when Gröbner bases are computed, the number of polynomials in the generating set may become very large as the algorithm continues adding polynomials until the remainder of the division algorithm of all S-polynomials equals zero. Thus, even though both algorithms terminate in theory, they might not in practice with the currently available processing power.

For that reason, an additional elimination technique shall be considered. It is known as the "linear implicitisation algorithm" (LIA) and was first presented by Walter and Husty [16] whose original publication will be briefly summerised in here. LIA was developed to have a technique that allows to change a parametric representation of a kinematic chain into an implicit representation. Of special interest are implicit representations of curves, surfaces, or higher algebraic varieties that represent the constrained movements of the kinematic chain without any parameters of the chosen parametrisation, such as the eight Study parameters. The main advantage of LIA as opposed to the elimination techniques presented above is that it is computed linearly.

Before performing LIA, let us consider the expected result, i.e., the minimal number of required polynomial equations, m, that describe the constraint variety. It is influenced by the number of dof of a kinematic chain, n. In general, the relation is given by

$$m = 6 - n,$$

which, however, should be used with caution as, e.g., redundant dofs can influence m. LIA computes these implicit constraint equations according to the following steps. Given is a parametric description of a kinematic chain, such as the Study represen-

tation

$$\begin{aligned} x_0 &= f_0(t_1, ..., t_n) \\ x_1 &= f_1(t_1, ..., t_n) \\ &\vdots \\ y_3 &= f_s(t_1, ..., t_n) \end{aligned} \tag{3.60}$$

where t_i are the *motion parameters* of the chain. If t_i is an angular measurement, it can be algebraised by expressing it as its tangent half-angle. As the name suggests, motion parameters are those parameters that are variable in the chain, e.g., θ is the motion parameter of a rotational joint. *Design parameters* on the contrary have fixed numerical values that must be decided upon when building a particular kinematic chain. In general, a typical example of a design parameter is a link length or link twist. To find the implicit equations LIA assumes a homogeneous polynomial in the parametrisation parameters with a given degree, known as the *ansatz polynomial*. For the eight Study parameters with a linear polynomial, i.e., of degree one, the general ansatz polynomial using the graded reverse lexicographic monomial ordering reads

$$C_1 y_3 + C_2 y_2 + C_3 y_1 + C_4 y_0 + C_5 x_3 + C_6 x_2 + C_7 x_1 + C_8 x_0 = 0, \tag{3.61}$$

where C_i are the unknown coefficients. If the algorithm does not yield any result for the linear ansatz, an ansatz with higher degree has to be chosen. The general ansatz polynomial of degree two and three have 36 and 120 terms, respectively. Fortunately, for simple closed kinematic chains solutions can be computed using the ansatz of degree one or two. Substituting Eq. (3.60) into Eq. (3.61) and reorganising the result, such that the expression is collected in its motion parameters, leaves an expression with coefficients in terms of C_i and the remaining design parameters. Since the motion parameters are in general non-zero, the coefficients have to vanish for the equation to be satisfied. This yields a system of linear equations with generally more equations than unknowns C_i. If solving for C_i does not yield a solution, the degree of

the ansatz polynomial must be increased by one, otherwise the solution can be back-substituted into the general ansatz polynomial which unveil the set of polynomials of the constraint variety.

Chapter 4

IO Equation Derivation Algorithm

4.1 Overview of the Algorithm

In essence, the idea of a generalised method to derive the algebraic IO equation for any kind of four-bar linkage is subclassified in several steps:

1. The linkage is opened up, and considered as an open kinematic chain.

2. The open kinematic chain is described using the standard DH convention. Moreover, the tangent half-angle substitution is adopted for angle parameters and angle variables.

3. The overall kinematic displacement, i.e., the orientation and position of the end-effector frame with respect to the base frame, is described using Study's kinematic mapping.

4. The open kinematic chain is closed by equating the overall displacement to its identity.

5. The arising set of equations generate an ideal that contains the full geometric description of the linkage. This ideal is manipulated using elimination theory

to obtain a single implicit polynomial IO equation that is free of the two intermediate variables. While applying resultants or a sequence of Gröbner bases is an effective way to eliminate variables of less involved equations, such as the slider-crank or the quadrilateral, respectively, it turns out that a single application of the elimination monomial ordering called "`lexdeg`" in Maple 2021 leads directly to the desired IO equations of all planar kinematic architectures. When the ideal generated by the system of polynomials contains coefficients that are not too large or complicated, this elimination monomial ordering is very efficient, in the sense that it does not compute an entire basis from the lexicographic ordering which can give large Gröbner bases. Even though the algorithm of computing a Gröbner basis always terminates, the processing time required varies as the intermediate polynomials can be very long. Especially when dealing with long, spatial kinematic chains, solving the set of polynomials using Gröbner bases might not be the most efficient approach. It turns out that for the RSSR linkage it is more efficient to split the kinematic chain into two parts, followed by eliminating the intermediate joint angles via the linear implicitisation algorithm in both chains.

These five steps should be kept in mind for the remaining part of this chapter as they will be followed to derive the IO equations of the different types of linkages: planar, spherical and spatial.

4.2 Planar Four-bar Linkages

4.2.1 Quadrilateral Linkage

To derive the algebraic IO equation for planar four-bar mechanisms using the DH convention [93] and Study's kinematic mapping [10], the four-bar mechanism is con-

sidered as an open kinematic chain as shown in Fig. 4.1. Following the assignments of coordinate frames as presented in Section 3.4 the origins of the frames are placed in the rotational joints with frame 0 located at the base and frame 4 at the end-effector, i.e., the tip of the last rigid body. The respective DH parameters are listed in Tab. 4.1. Note that all DH parameters have a direction including the link lengths and link offsets. Hence, the four link lengths a_i are directed line segments that can also include a negative value which is simply a link length pointing into the opposite direction as defined by the corresponding coordinate system. In the case of the 4R chain, all link twists and link offsets are identically zero. This simplifies the overall transformation matrix ${}^0_4\mathbf{T}$, which maps the coordinates of points described in the end-link coordinate frame to those of the base frame:

$$ {}^0_4\mathbf{T} = {}^0_1\mathbf{T}\ {}^1_2\mathbf{T}\ {}^2_3\mathbf{T}\ {}^3_4\mathbf{T}, \tag{4.1} $$

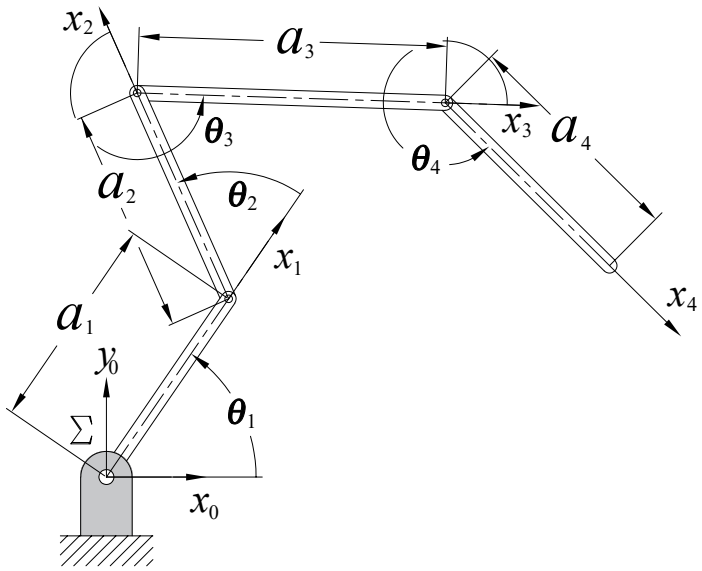

Figure 4.1: Open 4R chain.

where the transformation matrices ${}^0_1\mathbf{T}$, ${}^1_2\mathbf{T}$, ${}^2_3\mathbf{T}$ and ${}^3_4\mathbf{T}$ are evaluated according to

Table 4.1: DH parameters for open 4R chain.

joint axis i	link length a_i	link angle θ_i	link offset d_i	link twist τ_i
1	a_1	θ_1	0	0
2	a_2	θ_2	0	0
3	a_3	θ_3	0	0
4	a_4	θ_4	0	0

Eq. (3.43). The computed transformation matrix can be mapped onto Study's quadric using Eq. (3.8) and Eq. (3.9) resulting in a Study array with zero entries for x_1, x_2, y_0 and y_3. After normalizing, the remaining four Study parameters become

$$x_0 = (2v_2v_3v_4 - 2v_2 - 2v_3 - 2v_4)v_1 + (-2v_3 - 2v_4)v_2 - 2v_3v_4 + 2, \tag{4.2}$$

$$x_3 = ((-2v_3 - 2v_4)v_2 - 2v_3v_4 + 2)v_1 - 2v_2v_3v_4 + 2v_2 + 2v_3 + 2v_4, \tag{4.3}$$

$$\begin{aligned} y_1 = {} & ((v_4(a_1 - a_2 + a_3 - a_4)v_3 - a_1 + a_2 + a_3 + a_4)v_2 + (-a_1 - a_2 + a_3 + a_4)v_3 \\ & -v_4(a_1 + a_2 + a_3 - a_4))v_1 + ((a_1 - a_2 + a_3 + a_4)v_3 + v_4(a_1 - a_2 - a_3 + a_4))v_2 \\ & +v_4(a_1 + a_2 - a_3 + a_4)v_3 - a_1 - a_2 - a_3 - a_4, \end{aligned} \tag{4.4}$$

$$\begin{aligned} y_2 = {} & (((a_1 - a_2 + a_3 + a_4)v_3 + v_4(a_1 - a_2 - a_3 + a_4))v_2 + v_4(a_1 + a_2 - a_3 + a_4)v_3 \\ & -a_1 - a_2 - a_3 - a_4)v_1 + (-v_4(a_1 - a_2 + a_3 - a_4)v_3 + a_1 - a_2 - a_3 - a_4)v_2 \\ & +(a_1 + a_2 - a_3 - a_4)v_3 + v_4(a_1 + a_2 + a_3 - a_4), \end{aligned} \tag{4.5}$$

where $v_i = \tan(\theta_i/2)$.

The same Study parameters can be obtained with the knowledge from Section 3.3.4 and 3.4.2 allowing to perform the transformations directly in P^7. Thus, applying Eq. (3.53) or alternatively Eq. (3.56) to the planar 4R open chain reads

$$\mathbf{p} = \mathbf{T_b}(M_1)\cdot\mathbf{T_b}(G_1)\cdot\mathbf{T_b}(M_2)\cdot\mathbf{T_b}(G_2)\cdot\mathbf{T_b}(M_3)\cdot\mathbf{T_b}(G_3)\cdot\mathbf{T_b}(M_4)\cdot\mathbf{T_b}(G_4)\cdot\mathbf{id},$$

$$\mathbf{p} = \mathbf{T_m}(G_4)\cdot\mathbf{T_m}(M_4)\cdot\mathbf{T_m}(G_3)\cdot\mathbf{T_m}(M_3)\cdot\mathbf{T_m}(G_2)\cdot\mathbf{T_m}(M_2)\cdot\mathbf{T_m}(G_1)\cdot\mathbf{T_m}(M_1)\cdot\mathbf{id},$$

respectively. With the DH parameters from Tab. 4.1 as well as the 8×8 matrices

given in Eq. (3.52), Eq. (3.51), Eq. (3.55) and Eq. (3.54), the overall displacement $\mathbf{p}$ of the fourth coordinate frame with respect to the base frame can be calculated. As the Study array is homogeneous, it can safely be divided by any common factor, in this case 8, resulting in the Study array above, Eq. (4.2-4.5).

To close the planar four-bar chain, the first and last coordinate frames have to align in both their orientation and position. Algebraically, this is specified using the *kinematic closure equation*, where the overall transformation equates to the identity [93].

$$\prod_{i=1}^{4} {}_{i}^{i-1}\mathbf{T} = \mathbf{I}. \tag{4.6}$$

As stated earlier the identity matrix maps to $\mathbf{id} = [1 : 0 : 0 : 0 : 0 : 0 : 0 : 0]^{\mathsf{T}} \in P^7$ which can easily be verified by substituting the identity matrix into Eq. (3.8) and Eq. (3.9). Fig. 4.2 illustrates the arising planar four-bar linkage with joint angle variables θ_i that are measured according to the DH frame assignment. As a consequence of this frame assignment, the initial coordinate frame 0 must be rotated by π and the input and output angle θ_1 and θ_4 must be measured differently compared to Freudenstein's derivation, for comparison see Fig. 2.2. Equating the Study array of

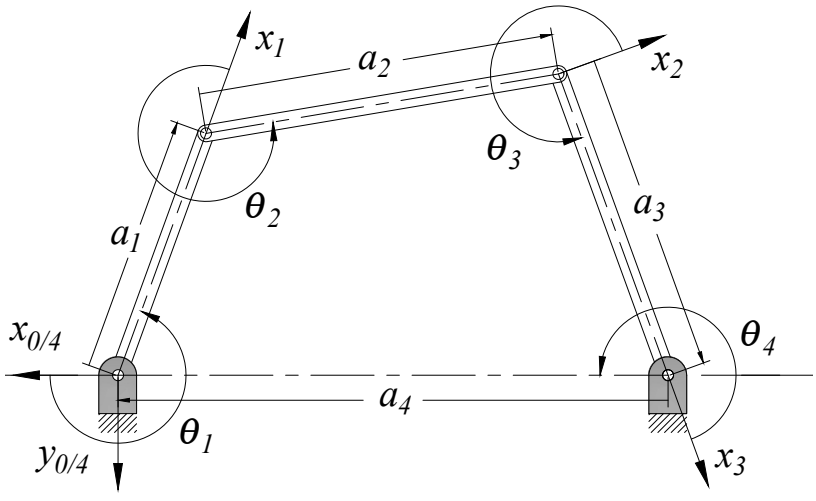

Figure 4.2: Closed 4R kinematic chain.

the overall transformation to the Study array of the identity matrix, forces

$$[x_0 : 0 : 0 : x_3 : 0 : y_1 : y_2 : 0] = [1 : 0 : 0 : 0 : 0 : 0 : 0 : 0]. \tag{4.7}$$

Recall that the Study array is homogeneous, meaning Eq. (4.2) can be equated to any number which in return allows to safely omit this equation. Hence, the three equations that are equal to zero, Eq. (4.3-4.5), define the ideal of a generic planar 4R linkage and thus, are sufficient to completely describe the linkage. This includes the IO equation but clearly also any other imaginable information on any planar 4R linkage. All that is required is to manipulate the three polynomials to extract the information of interest.

This leads to the final step of the suggested algorithm. In order to extract the IO equation from the ideal, the undesired intermediate joint angles v_2 and v_3 have to be eliminated from the generating set. Gröbner bases provide different possibilities that lead to the IO equation. For example, a two elimination procedures involving *graded reverse lexicographic* order with indeterminate ordering $v_3 > v_2 > v_4 > v_1$, followed by *pure lexicographic* ordering of the same indeterminate sequence, produces one polynomial in the new generating set that no longer contains v_2 and v_3. Alternatively, a single application of the elimination monomial ordering "`lexdeg`" in Maple 2021 leads directly to the desired planar 4R IO equation.

In both cases, after collecting the input and output angle motion parameters v_1 and v_4, the algebraic IO equation can be written as

$$Av_1^2v_4^2 + Bv_1^2 + Cv_4^2 - 8a_1a_3v_1v_4 + D = 0, \tag{4.8}$$

where

$$
\begin{aligned}
A &= (a_1 - a_2 + a_3 - a_4)(a_1 + a_2 + a_3 - a_4) = A_1 A_2, \\
B &= (a_1 + a_2 - a_3 - a_4)(a_1 - a_2 - a_3 - a_4) = B_1 B_2, \\
C &= (a_1 - a_2 - a_3 + a_4)(a_1 + a_2 - a_3 + a_4) = C_1 C_2, \\
D &= (a_1 + a_2 + a_3 + a_4)(a_1 - a_2 + a_3 + a_4) = D_1 D_2, \\
v_1 &= \tan\frac{\theta_1}{2}, \\
v_4 &= \tan\frac{\theta_4}{2}.
\end{aligned}
$$

This algebraic equation is of degree 4 in the v_1 and v_4 variable parameters, while the coefficients labelled A, B, C, and D are each products of two bilinear factors which can be viewed as eight distinct planes treating the four a_i link lengths as homogeneous coordinates. See Section 5.3 for a detailed description of this design parameter space. Furthermore, it should be noted that Eq. (4.8) is identical to Eq. (2.4) if the phase shift of the input and output angle as well as the different notation are considered.

Eq. (4.8) is an implicit equation expressing the functional relationship between v_1 and v_4. This functional relationship defines five others. Depending on the application, mechanism designers may be interested in generating functions between two other motion parameters, such as the input and transmission angle, i.e. v_1-v_3 equation. In general, all moveable four-bar linkages generate six distinct functions between the four distinct joint variable parameters taken two at a time, abstractly referred to as v_i and v_j. While this is common knowledge in the kinematics community, there do not exist convenient and consistent ways to determine and express these six functions using algebraic means. Moreover, only the v_1-v_4 and v_1-v_3 IO equations can be found in the vast body of archival literature, but they are expressed as trigonometric implicit equations, see [41, 102] for standard examples.

The five related IO equations can be determined by eliminating the relevant intermediate joint angle parameters from Eq. (4.3-4.5). By applying the "`lexdeg`"

monomial term orderings to the planar 4R variables in the appropriate disjoint lists, the v_1-v_2, v_1-v_3, v_2-v_3, v_2-v_4, and v_3-v_4 IO equations are obtained and listed as follows.

$$A_1B_2v_1^2v_2^2 + A_2B_1v_1^2 + C_1D_2v_2^2 - 8a_2a_4v_1v_2 + C_2D_1 = 0, \tag{4.9}$$

$$A_1B_1v_1^2v_3^2 + A_2B_2v_1^2 + C_2D_2v_3^2 + C_1D_1 = 0, \tag{4.10}$$

$$A_1D_2v_2^2v_3^2 + B_2C_1v_2^2 + B_1C_2v_3^2 - 8a_1a_3v_2v_3 + A_2D_1 = 0, \tag{4.11}$$

$$A_1C_1v_2^2v_4^2 + B_2D_2v_2^2 + A_2C_2v_4^2 + B_1D_1 = 0, \tag{4.12}$$

$$A_1C_2v_3^2v_4^2 + B_1D_2v_3^2 + A_2C_1v_4^2 + 8a_2a_4v_3v_4 + B_2D_1 = 0. \tag{4.13}$$

Eqs. (4.8), (4.9), (4.11), and (4.13) all contain a bilinear quadratic term because they relate adjacent angle pairs, while Eqs. (4.10) and (4.12) relate opposite angle pairs, and hence do not possess a bilinear quadratic term.

Each of these six IO equations is of degree 4 in the two variable angle parameters, defining quartic curves in the planes spanned by the different v_i-v_j angle parameter pairs. They also all have genus 1. Therefore, following Harnack [103] who developed a theorem on algebraic curves relating the genus of a curve p to the maximum number of circuits, or assembly modes, m by

$$m = p + 1, \tag{4.14}$$

one may immediately conclude that a planar 4R mechanism can never have more than two assembly modes.

For example, consider the v_1-v_4 equation of a quadrilateral with the following link lengths: $a_1 = 2$, $a_2 = 6$, $a_3 = 8$ and $a_4 = 5$. As illustrated in Fig. 4.3, for any given input angle, the linkage can be assembled in two constellations. While the input link a_1 and the base link a_4 are the same for both assembly modes, the coupler a_2 and the

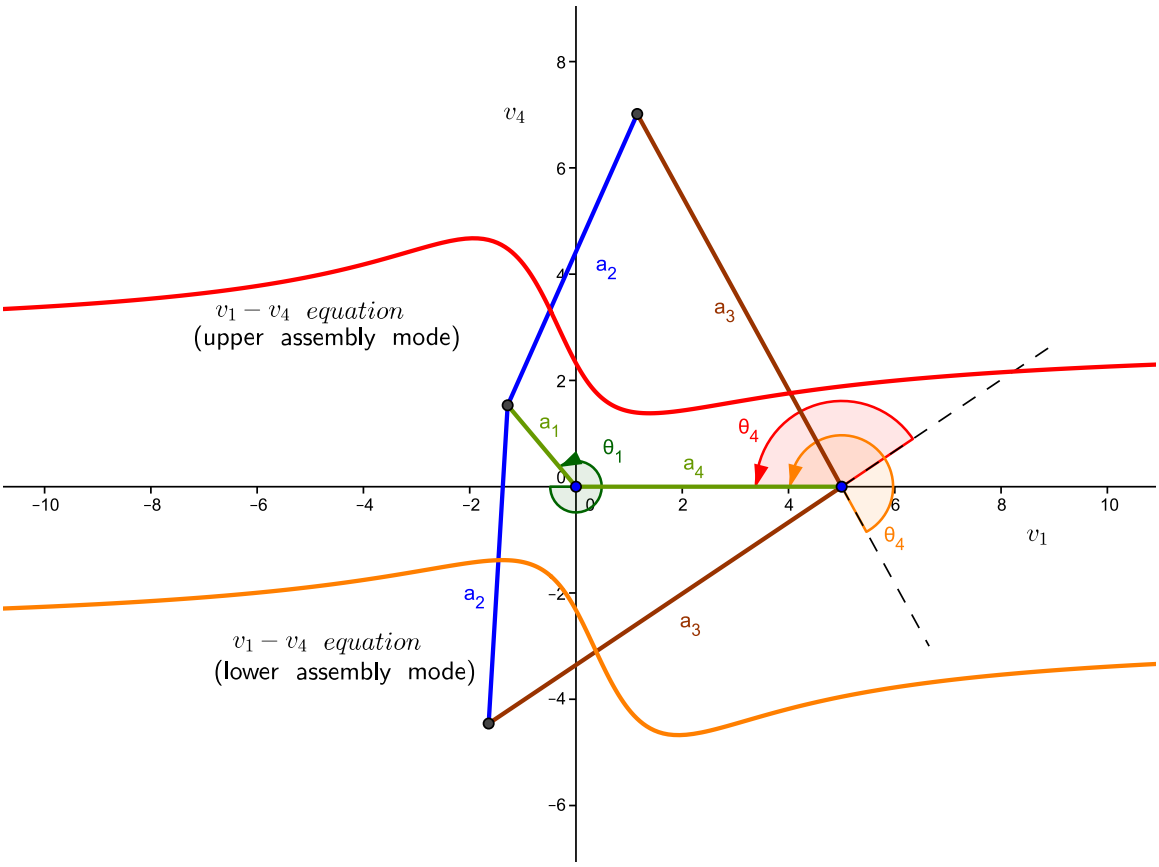

Figure 4.3: v_1-v_4 equation and the corresponding two assembly modes of the linkage where $a_1 = 2$, $a_2 = 6$, $a_3 = 8$ and $a_4 = 5$.

output link a_3 are different which results in two different output angles θ_4. With the tangent half-angle substitution for θ_1 and both θ_4, such that $v_i = \tan(\theta_i/2)$, the locus of the point $P(v_1, v_4)$ can be traced in the v_1-v_4-plane, resulting in the red and orange IO curve as shown in Fig. 4.3. This curve precisely corresponds to Eq. (4.8) with the given design parameters. By simply examining the plot of the v_1-v_4 equation, the following information can be extracted:

- The linkage has two assembly modes: An upper and a lower assembly mode.
- There exists a v_4-value for every v_1. The curve passes through both $v_1 = 0$ and $v_1 = \infty$, corresponding to $\theta_1 = 0$ and $\theta_1 = \pi$, respectively. Thus, both assembly modes have a crank as an input link.

- The output link is restricted by a specific range of bounding values in both assembly modes. The output link neither rocks through $v_4 = 0$ nor through $v_4 = \infty$, corresponding to $\theta_4 = \pi$. Thus, both assembly modes have a regular rocker as an output link.

4.2.2 Slider-crank Linkage

Next, consider the slider-crank linkage that was presented in Section 2.3.2. Following the proposed procedure to derive the IO equation of the RRRP linkage, the first step is to consider the RRRP as an open kinematic chain. The linkage is opened up at the prismatic joint, followed by assigning coordinate frames according to the DH convention which allows to identify the associated DH parameters of the linkage. In exactly the same way as the quadrilteral linkage, the RRRP chain is closed by aligning the base coordinate frame 0 with the end-effector coordinate frame 4. The coordinate frame attachment as well as the identified DH parameters are shown in Fig. 4.4. The P-pair z_3-axis induces the two link twist angles and a link offset listed in Tab. 4.2. Again, it should be noted that the link lengths and the link offset are directed distances with the directions as indicated in the figure.

Moving to the next step, the DH parameters are substituted into Eq. (3.43) for every

Table 4.2: DH parameters for RRRP linkage.

joint axis i	link angle θ_i	link offset d_i	link length a_i	link twist τ_i
1	θ_1	0	a_1	0
2	θ_2	0	a_2	0
3	θ_3	0	0	$-\pi/2$
4	0	d_4	a_4	$+\pi/2$

$i = 1...4$. The four transformation matrices are multiplied according to Eq. (3.44), and the resulting overall transformation ${}^0_4\mathbf{T}$ can be mapped into Study's kinematic image space using Eq. (3.8) and Eq. (3.9), resulting in the eight Study's coordinates that describe a general slider-crank linkage.

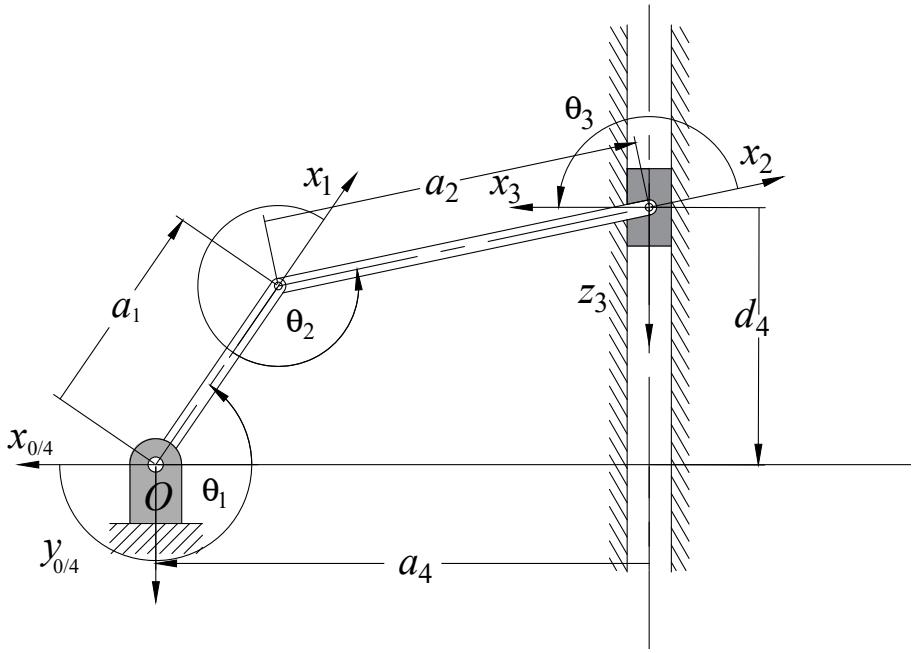

Figure 4.4: DH parameter assignment for the RRRP linkage.

An alternative and more efficient way is to derive the Study soma coordinates directly on Study's quadric by evaluating Eq. (3.53) or Eq. (3.56) with four coordinate tranformations, thus $n = 4$. After substituting the DH parameters of Tab. 4.2, the Study array yields $x_1 = x_2 = y_0 = y_3 = 0$ as the movements of the linkage are all planar, in the $x - y$-plane. The remaining Study parameters yield

$$x_0 = (-2v_2 - 2v_3)v_1 - 2v_2v_3 + 2, \tag{4.15}$$

$$x_3 = -2v_1v_2v_3 + 2v_1 + 2v_2 + 2v_3, \tag{4.16}$$

$$\begin{aligned} y_1 = {} & ((-d_4v_3 - a_1 + a_2 + a_4)v_2 + (-a_1 - a_2 + a_4)v_3 + d_4)v_1 \\ & +((a_1 - a_2 + a_4)v_3 + d_4)v_2 + d_4v_3 - a_1 - a_2 - a_4, \end{aligned} \tag{4.17}$$

$$\begin{aligned} y_2 = {} & (((a_1 - a_2 + a_4)v_3 + d_4)v_2 + d_4v_3 - a_1 - a_2 - a_4)v_1 \\ & +(d_4v_3 + a_1 - a_2 - a_4)v_2 + (a_1 + a_2 - a_4)v_3 - d_4, \end{aligned} \tag{4.18}$$

where $v_i = \tan(\theta_i/2)$.

The Study array is equated to its identity array, $x = [1 : 0 : 0 : 0 : 0 : 0 : 0 : 0]^{\mathsf{T}} \in P^7$, allowing the first and the last coordinate frame in the RRRP linkage to align, as shown in Fig. 4.4. Since the Study coordinates are homogeneous, this leaves a system of three equations, namely, I. $x_3 = 0$; II. $y_1 = 0$; III. $y_2 = 0$. Again similar to the quadrilateral linkage, these three equations define the ideal of a generic slider-crank linkage. The design parameters of this linkage are notably the three link lengths a_1, a_2, and a_4, while the motion parameters correspond to the three link angles θ_1, θ_2, and θ_3 and the link offset d_4. As the motion parameters of the desired IO equation in this linkage are the input angle θ_1 and the output slider distance d_4, the two intermediate motion parameters θ_2 and θ_3 must be eliminated from the generating set describing the ideal. One possibility is to solve the system of equations using resultants. Eliminating the intermediate link angle v_2 from I. and II. yields

$$a_1v_1^2v_3^2+a_2v_1^2v_3^2-a_4v_1^2v_3^2+a_1v_1^2-a_1v_3^2-a_2v_1^2+a_2v_3^2-a_4v_1^2-a_4v_3^2-a_1-a_2-a_4 = 0. \quad (4.19)$$

And eliminating the same intermediate angle v_2 from I. and III. yields

$$-d_4v_1^2v_3^2 - 2a_1v_1v_3^2 + 2a_2v_1^2v_3 - d_4v_1^2 - d_4v_3^2 - 2a_1v_1 + 2a_2v_3 - d_4 = 0. \quad (4.20)$$

Finally, eliminating the intermediate angle v_3 from Eq. (4.19) and Eq. (4.20) reveals the IO equation for RRRP linkages

$$v_1^2d_4^2 + Rv_1^2 + d_4^2 + 4a_1v_1d_4 + S = 0, \quad (4.21)$$

where

$$R = R_1 R_2 = (a_1 + a_2 - a_4)(a_1 - a_2 - a_4),$$

$$S = S_1 S_2 = (a_1 + a_2 + a_4)(a_1 - a_2 + a_4),$$

$$v_1 = \tan \frac{\theta_1}{2}.$$

Using resultants is not the only possibility to solve the system of equations to obtain the IO equation for planar RRRP linkages. For example, applying Gröbner bases on the generating set with a monomial odering of "`lexdeg`", the IO equation, Eq. (4.21), can be computed in one single step.

The four bilinear factors R_1, R_2, S_1, and S_2 can be regarded as four planes intersecting in the faces of a four-sided pyramid in the design parameter space orthogonally spanned by the three lengths a_1, a_2, and a_4, see [22] for a detailed description.

Eq. (4.21) can be verified via the IO equation of the planar 4R linkage, Eq. (4.8), as follows. Since the slider of the RRRP linkage is perpendicular to the fixed ground distance a_4, we can substitute $v_4 = \tan(-90°/2) = -1$ into Eq. (4.8). In addition, the original link length a_3 of the 4R linkage now becomes the slider distance of the RRRP, i.e., a_3 has to be renamed to d_4. After recollecting the equation in its variables v_1 and d_4 it yields Eq. (4.21).

Using the same approach, the five remaining joint variable parameter pairings lead

to the following five additional RRRP algebraic IO equations

$$R_2 v_1^2 v_2^2 + R_1 v_1^2 - S_2 v_2^2 + 4a_2 v_1 v_2 - S_1 = 0; \tag{4.22}$$

$$R_1 v_1^2 v_3^2 + R_2 v_1^2 - S_2 v_3^2 - S_1 = 0; \tag{4.23}$$

$$S_2 v_2^2 v_3^2 - R_2 v_2^2 - R_1 v_3^2 - 4a_1 v_2 v_3 + S_1 = 0; \tag{4.24}$$

$$-v_2^2 d_4^2 + R_2 S_2 v_2^2 - d_4^2 + R_1 S_1 = 0; \tag{4.25}$$

$$-v_3^2 d_4^2 + R_1 S_2 v_3^2 + d_4^2 + 4a_2 v_3 d_4 + R_2 S_1 = 0. \tag{4.26}$$

All six of the RRRP algebraic IO equations are of degree 4, representing quartic curves in the respective joint variable parameter planes. These six IO equations also all possess genus 1 meaning again that there is a maximum number of two assembly modes.

For the RRRP linkages that are rocker-sliders, each distinct circuit of the IO curve also contains two branches, one for each working mode. When the input angle reaches minimum or maximum values the mechanism instantaneously stops moving as the coupler becomes perpendicular to the direction of travel of the P-pair. In this singular configuration, unless mechanical constraints are imposed, the slider may move in one of two directions as the rocker input link begins to move again in the opposite sense. These are defined as the working modes of the particular assembly mode. Each working mode traces a distinct branch in the particular circuit of the IO curve. Together, both branches cover the entire circuit. Detailed examples are covered in [29]. For example, consider the v_1-d_4 equation of the RRRP with the following link lengths: $a_1 = 3$, $a_2 = 2$ and $a_4 = -4$. As illustrated in Fig. 4.5, the linkage has one assembly mode with an input link whose mobility is bounded by v_{1min} and v_{1max}. At these input angles the linkage is in a singular configuration where it can change from one working mode into another.

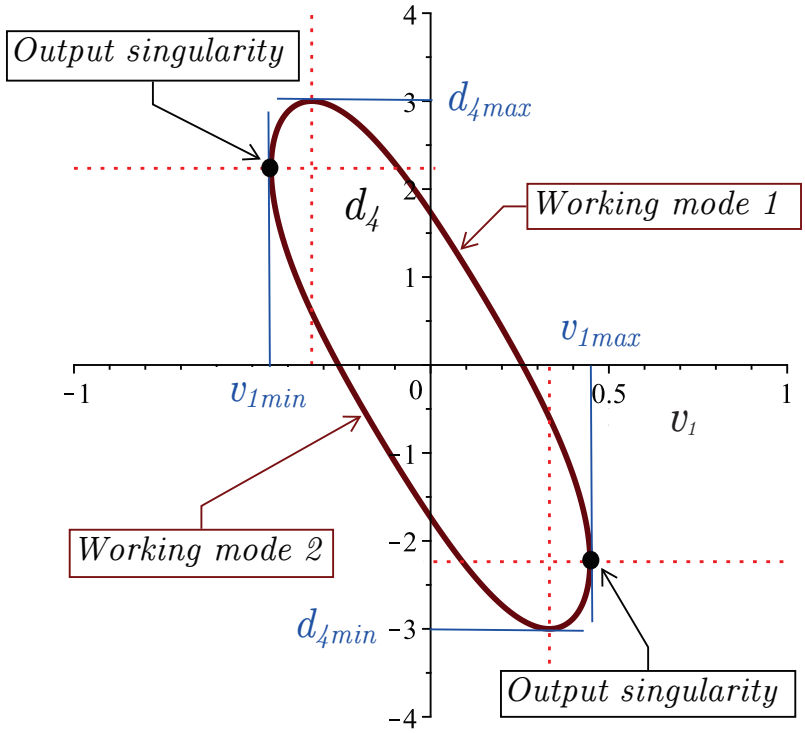

Figure 4.5: v_1-d_4 equation of the RRRP linkage where $a_1 = 3$, $a_2 = 2$ and $a_4 = -4$.

4.2.3 Double Slider Linkage

To complete the IO equation derivation of all planar four-bar linkages of interest, this section shows that the identical approach can be used for the double slider linkage. The usual first step is to open up the linkage. A suitable opening is located, for example, at the intersection of the two slider trajectories. After assigning the coordinate systems according to the DH convention, the DH parameters are determined as shown in Fig. (4.6). The DH parameters are also listed in Tab. (4.3). It can be seen that PRRP elliptical trammel linkages have but two design parameters, namely a_2 and τ_4, the coupler length, and the twist angle between the two P-pairs. The remaining four parameters θ_2, θ_3, d_1 and d_4 are the motion parameters with the latter two being the input and output variables, respectively.

As in the previous cases, the overall displacement of the end-effector frame with respect to the base frame must be mapped onto Study's quadric and expressed in

Table 4.3: DH parameters for PRRP linkage.

joint axis i	link angle θ_i	link offset d_i	link length a_i	link twist τ_i
1	$-\pi/2$	d_1	0	$-\pi/2$
2	θ_2	0	a_2	0
3	θ_3	0	0	$\pi/2$
4	$+\pi/2$	d_4	0	τ_4

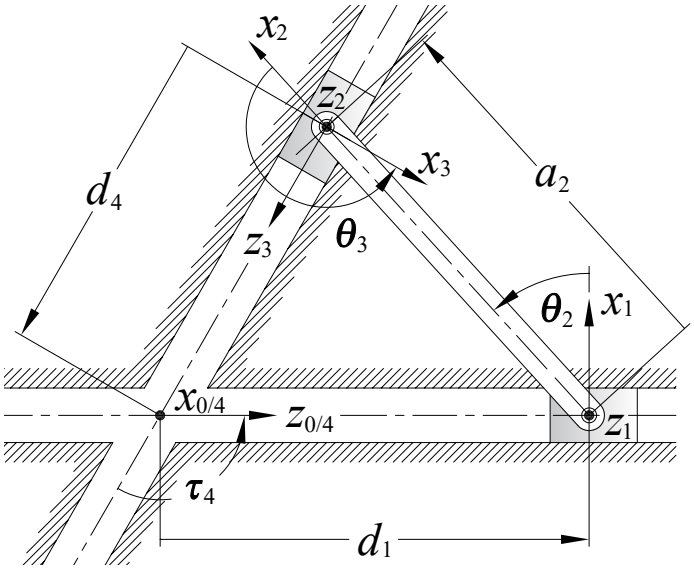

Figure 4.6: DH parameter assignment for the PRRP linkage.

Study parameters. This can either be done by evaluating the displacement with homogeneous transformation matrices and then mapping the displacement in the image space, or the transformations in terms of the DH parameters are directly conducted on the quadric. Again, since there are four coordinate transformations, the general equations, Eq. (3.53) or alternatively Eq. (3.56), leading to the Study parameters describing the overall displacements of a general PRRP linkage are

$$\mathbf{p} = \mathbf{T_b}(M_1)\cdot\mathbf{T_b}(G_1)\cdot\mathbf{T_b}(M_2)\cdot\mathbf{T_b}(G_2)\cdot\mathbf{T_b}(M_3)\cdot\mathbf{T_b}(G_3)\cdot\mathbf{T_b}(M_4)\cdot\mathbf{T_b}(G_4)\cdot\mathbf{id},$$

$$\mathbf{p} = \mathbf{T_m}(G_4)\cdot\mathbf{T_m}(M_4)\cdot\mathbf{T_m}(G_3)\cdot\mathbf{T_m}(M_3)\cdot\mathbf{T_m}(G_2)\cdot\mathbf{T_m}(M_2)\cdot\mathbf{T_m}(G_1)\cdot\mathbf{T_m}(M_1)\cdot\mathbf{id},$$

where the matrices are evaluated with the DH parameters from Tab. (4.3). After

omitting common factors, the resulting non-zero Study parameters yield

$$
\begin{aligned}
x_0 &= (-2v_2 - 2v_3)\,\alpha_4 - 2v_2v_3 + 2, && (4.27)\\
x_1 &= -2\alpha_4 v_2 v_3 + 2\alpha_4 + 2v_2 + 2v_3, && (4.28)\\
y_2 &= (((d_1 + d_4)\,v_3 + a_2)\,v_2 - a_2v_3 - d_1 - d_4)\,\alpha_4 + \\
&\quad (a_2v_3 - d_1 + d_4)\,v_2 + (-d_1 + d_4)\,v_3 + a_2, && (4.29)\\
y_3 &= ((-a_2v_3 + d_1 - d_4)\,v_2 + (d_1 - d_4)\,v_3 - a_2)\,\alpha_4 \\
&\quad + ((d_1 + d_4)\,v_3 + a_2)\,v_2 - a_2v_3 - d_1 - d_4, && (4.30)
\end{aligned}
$$

where $v_i = \tan(\theta_i/2)$.

In the next step, the open chain must be closed which is done applying the closure equation such that

$$[x_0 : x_1 : 0 : 0 : 0 : 0 : y_2 : y_3] = [1 : 0 : 0 : 0 : 0 : 0 : 0 : 0]. \tag{4.31}$$

It follows that the three equations involving the Study parameters x_1, y_2 and y_3 are a generating set, defining an ideal, that describe the constraint variety of the PRRP linkage on the Study quadric. Applying the same elimination step as for the RRRP linkage, such as Gröbner basis with a monomial odering of "`lexdeg`", the IO equation yields

$$(\alpha_4^2 + 1)(d_1^2 + d_4^2) - 2(\alpha_4^2 - 1)d_1d_4 - a_2^2(\alpha_4^2 + 1) = 0. \tag{4.32}$$

The symmetry in the six PRRP IO equations are revealed when we define the following

three coefficients

$$\begin{aligned} T &= a_2^2(\alpha_4^2+1); \\ U &= a_2(\alpha_4^2-1); \\ V &= a_2(\alpha_4^2+1). \end{aligned}$$

Using these coefficients the six algebraic IO equations are

$$(\alpha_4^2+1)(d_1^2+d_4^2) - 2(\alpha_4^2-1)d_1d_4 - T = 0; \tag{4.33}$$

$$2\alpha_4 d_1 v_2^2 + U v_2^2 + 2\alpha_4 d_1 - 4a_2\alpha_4 v_2 - U = 0; \tag{4.34}$$

$$2\alpha_4 d_1 v_3^2 - V v_3^2 + 2\alpha_4 d_1 + V = 0; \tag{4.35}$$

$$\alpha_4 v_2 v_3 - v_2 - v_3 - \alpha_4 = 0; \tag{4.36}$$

$$2\alpha_4 v_2^2 d_4 + V v_2^2 + 2\alpha_4 d_4 - V = 0; \tag{4.37}$$

$$2\alpha_4 v_3^2 d_4 - U v_3^2 + 4a_2\alpha_4 v_3 + 2\alpha_4 d_4 + U = 0. \tag{4.38}$$

It is to be seen that Eqs. (4.34), (4.35), (4.37), and (4.38) are of degree 3, representing cubic curves in their respective joint variable parameter planes, while Eqs. (4.33) and (4.36) are of degree 2, thus, representing two different conics. When the respective quadratic forms are diagonalised it is easy to show that Eq. (4.33) is an ellipse, while Eq. (4.36) is an hyperbola which depends only on the link twist α_4. Moreover, each of the six PRRP algebraic IO equations, Eqs. (4.33-4.38), possess genus 0, unlike the planar 4R and RRRP IO equations. According to Harnack's theorem it can be concluded that the PRRP linkage has at most one assembly mode since each IO equation has a single circuit.

4.3 Spherical Linkage

It will now be demonstrated that the same procedure can be applied to determine the IO equation for spherical linkages. The DH parameters for an open spherical 4R kinematic chain are listed in Tab. 4.4. The assignments of coordinate systems and DH parameters can be seen in Fig. (4.7). Note that in the spherical case, all link lengths, a_i, and offsets, d_i, are zero with strict adherence to the DH conventions for assigning parameters [93]. After evaluating the overall transformation matrix in terms of DH

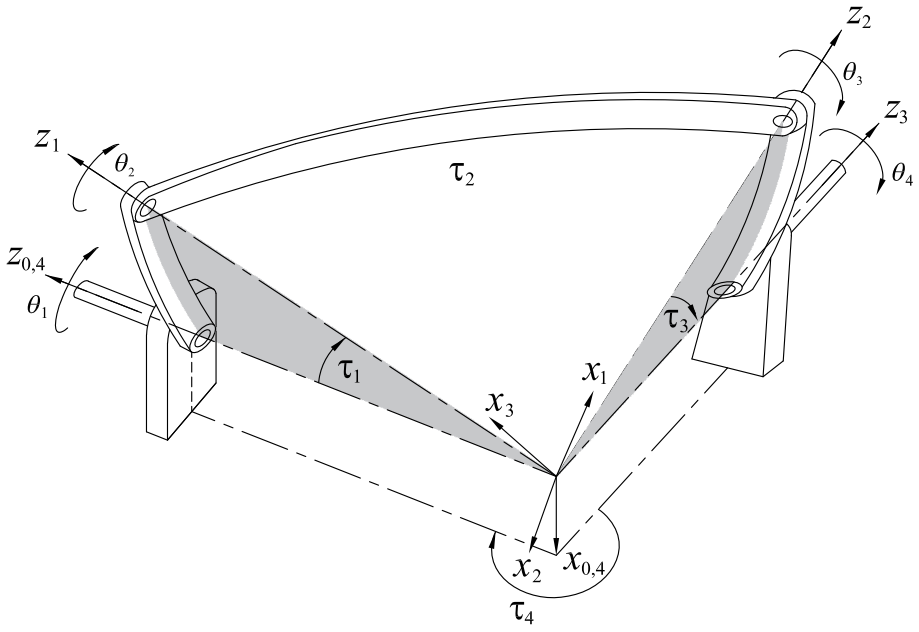

Figure 4.7: DH parameter assignment for the spherical linkage. Note that this is Fig. 2.5 which is reproduced here for easier reference.

parameters by applying Eq. (3.43), the result can be mapped with Equations (3.8, 3.9) onto Study's quadric. Then setting $v_i = \tan(\theta_i/2)$ and $\alpha_i = \tan(\tau_i/2)$ into the result gives a Study array with non-zero entries for x_0, x_1, x_2 and x_3, while the y_i are all

Table 4.4: Open spherical 4R kinematic chain DH parameters.

joint axis i	link length a_i	link angle θ_i	link offset d_i	link twist τ_i
1	0	θ_1	0	τ_1
2	0	θ_2	0	τ_2
3	0	θ_3	0	τ_3
4	0	θ_4	0	τ_4

identically zero, as expected:

$$
\begin{aligned}
x_0 &= ((2\alpha_4((v_2v_3v_4 + v_2 - v_3 + v_4)v_1 + (v_3 - v_4)v_2 + v_3v_4 + 1)\alpha_3 \\
&\quad +(2v_2v_3v_4 - 2v_2 + 2v_3 + 2v_4)v_1 + (-2v_3 - 2v_4)v_2 + 2v_3v_4 - 2)\alpha_2 \\
&\quad +((-2v_2v_3v_4 - 2v_2 - 2v_3 + 2v_4)v_1 + (2v_3 - 2v_4)v_2 - 2v_3v_4 - 2)\alpha_3 \\
&\quad +(2((v_2v_3v_4 - v_2 - v_3 - v_4)v_1 + (v_3 + v_4)v_2 + v_3v_4 - 1))\alpha_4)\alpha_1 \\
&\quad +(((2v_2v_3v_4 + 2v_2 - 2v_3 + 2v_4)v_1 + (-2v_3 + 2v_4)v_2 - 2v_3v_4 - 2)\alpha_3 \\
&\quad -(2((v_2v_3v_4 - v_2 + v_3 + v_4)v_1 + (v_3 + v_4)v_2 - v_3v_4 + 1))\alpha_4)\alpha_2 \\
&\quad +(2((v_2v_3v_4 + v_2 + v_3 - v_4)v_1 + (v_3 - v_4)v_2 - v_3v_4 - 1))\alpha_4\alpha_3 \\
&\quad +(2v_2v_3v_4 - 2v_2 - 2v_3 - 2v_4)v_1 + (-2v_3 - 2v_4)v_2 - 2v_3v_4 + 2; \qquad (4.39) \\
x_1 &= ((((-2v_2v_3v_4 - 2v_2 + 2v_3 - 2v_4)v_1 + (-2v_3 + 2v_4)v_2 - 2v_3v_4 - 2)\alpha_3 \\
&\quad +(2((v_2v_3v_4 - v_2 + v_3 + v_4)v_1 + (-v_3 - v_4)v_2 + v_3v_4 - 1))\alpha_4)\alpha_2 \\
&\quad -2\alpha_4((v_2v_3v_4 + v_2 + v_3 - v_4)v_1 + (-v_3 + v_4)v_2 + v_3v_4 + 1)\alpha_3 \\
&\quad +(-2v_2v_3v_4 + 2v_2 + 2v_3 + 2v_4)v_1 + (-2v_3 - 2v_4)v_2 - 2v_3v_4 + 2)\alpha_1 \\
&\quad +((2((v_2v_3v_4 + v_2 - v_3 + v_4)v_1 + (-v_3 + v_4)v_2 - v_3v_4 - 1))\alpha_4\alpha_3 \\
&\quad +(2v_2v_3v_4 - 2v_2 + 2v_3 + 2v_4)v_1 + (2v_3 + 2v_4)v_2 - 2v_3v_4 + 2)\alpha_2 \\
&\quad +((-2v_2v_3v_4 - 2v_2 - 2v_3 + 2v_4)v_1 + (-2v_3 + 2v_4)v_2 + 2v_3v_4 + 2)\alpha_3 \\
&\quad +(2((v_2v_3v_4 - v_2 - v_3 - v_4)v_1 + (-v_3 - v_4)v_2 - v_3v_4 + 1))\alpha_4; \qquad (4.40) \\
x_2 &= (((((-2v_3 + 2v_4)v_2 - 2v_3v_4 - 2)v_1 + 2v_2v_3v_4 + 2v_2 - 2v_3 + 2v_4)\alpha_3 \\
&\quad -(2(((v_3 + v_4)v_2 - v_3v_4 + 1)v_1 + v_2v_3v_4 - v_2 + v_3 + v_4))\alpha_4)\alpha_2 \\
&\quad +(2(((v_3 - v_4)v_2 - v_3v_4 - 1)v_1 + v_2v_3v_4 + v_2 + v_3 - v_4))\alpha_4\alpha_3 \\
&\quad +((-2v_3 - 2v_4)v_2 - 2v_3v_4 + 2)v_1 + 2v_2v_3v_4 - 2v_2 - 2v_3 - 2v_4)\alpha_1 \\
&\quad +(-(2(((v_3 - v_4)v_2 + v_3v_4 + 1)v_1 + v_2v_3v_4 + v_2 - v_3 + v_4))\alpha_4\alpha_3 \\
&\quad +((2v_3 + 2v_4)v_2 - 2v_3v_4 + 2)v_1 - 2v_2v_3v_4 + 2v_2 - 2v_3 - 2v_4)\alpha_2 \\
&\quad +(((-2v_3 + 2v_4)v_2 + 2v_3v_4 + 2)v_1 + 2v_2v_3v_4 + 2v_2 + 2v_3 - 2v_4)\alpha_3
\end{aligned}
$$

$$-(2(((v_3+v_4)v_2+v_3v_4-1)v_1+v_2v_3v_4-v_2-v_3-v_4))\alpha_4; \tag{4.41}$$

$$\begin{aligned}
x_3 \;=\; & (((2(((v_3-v_4)v_2+v_3v_4+1)v_1-v_2v_3v_4-v_2+v_3-v_4))\alpha_4\alpha_3 \\
& +((-2v_3-2v_4)v_2+2v_3v_4-2)v_1-2v_2v_3v_4+2v_2-2v_3-2v_4)\alpha_2 \\
& +(((2v_3-2v_4)v_2-2v_3v_4-2)v_1+2v_2v_3v_4+2v_2+2v_3-2v_4)\alpha_3 \\
& +2\alpha_4(((v_3+v_4)v_2+v_3v_4-1)v_1-v_2v_3v_4+v_2+v_3+v_4))\alpha_1 \\
& +((((-2v_3+2v_4)v_2-2v_3v_4-2)v_1-2v_2v_3v_4-2v_2+2v_3-2v_4)\alpha_3 \\
& -(2(((v_3+v_4)v_2-v_3v_4+1)v_1-v_2v_3v_4+v_2-v_3-v_4))\alpha_4)\alpha_2 \\
& +2\alpha_4(((v_3-v_4)v_2-v_3v_4-1)v_1-v_2v_3v_4-v_2-v_3+v_4)\alpha_3 \\
& +((-2v_3-2v_4)v_2-2v_3v_4+2)v_1-2v_2v_3v_4+2v_2+2v_3+2v_4.
\end{aligned} \tag{4.42}$$

The same Study parameters result from evaluating Eq. (3.53) or Eq. (3.56) with $n = 4$ and the DH parameters from Tab. 4.4.

Again, the open kinematic chain is closed by equating the Study array to the corresponding identity array in Study coordinates, i.e. setting Equations (4.40-4.42) equal to zero. Subsequently, we use Gröbner bases to eliminate the intermediate angle parameters v_2 and v_3 from Equations (4.40-4.42). The soma coordinates are, however, already too complicated to efficiently use the "`lexdeg`" elimination monomial ordering. To obtain this IO equation from the ideal generated by the three soma coordinates that equate to zero, both v_2 and v_3 are eliminated by first computing the Gröbner bases using the Maple 2021 "`tdeg`" monomial ordering with the list sequence (v_3, v_2, v_4, v_1), meaning that the indeterminate ordering is $v_3 > v_2 > v_4 > v_1$. In this case, 12 bases are computed, all functions of all four v_i. v_2 and v_3 are eliminated by computing the bases of these 12 with the reverse monomial ordering by using "`plex`". This results in 10 new bases, with one that is a function of only v_1 and v_4 and the four α_i, which represents the IO equation. This polynomial splits into three factors. The first two are $(1+v_1^2)(1+v_4^2)$, a product that is always greater than zero, and can

be safely factored out, leaving the desired IO equation

$$Av_1^2v_4^2 + Bv_1^2 + Cv_4^2 + 8\alpha_1\alpha_3\left(\alpha_4^2+1\right)\left(\alpha_2^2+1\right)v_1v_4 + D = 0, \tag{4.43}$$

where

$$\begin{aligned}
A \;=\; A_1A_2 \;&=\; \left(\alpha_1\alpha_2\alpha_3 - \alpha_1\alpha_2\alpha_4 + \alpha_1\alpha_3\alpha_4 - \alpha_2\alpha_3\alpha_4 + \alpha_1 - \alpha_2 + \alpha_3 - \alpha_4\right) \\
&\quad \left(\alpha_1\alpha_2\alpha_3 - \alpha_1\alpha_2\alpha_4 - \alpha_1\alpha_3\alpha_4 - \alpha_2\alpha_3\alpha_4 - \alpha_1 - \alpha_2 - \alpha_3 + \alpha_4\right), \\
B \;=\; B_1B_2 \;&=\; \left(\alpha_1\alpha_2\alpha_3 + \alpha_1\alpha_2\alpha_4 - \alpha_1\alpha_3\alpha_4 - \alpha_2\alpha_3\alpha_4 + \alpha_1 + \alpha_2 - \alpha_3 - \alpha_4\right) \\
&\quad \left(\alpha_1\alpha_2\alpha_3 + \alpha_1\alpha_2\alpha_4 + \alpha_1\alpha_3\alpha_4 - \alpha_2\alpha_3\alpha_4 - \alpha_1 + \alpha_2 + \alpha_3 + \alpha_4\right), \\
C \;=\; C_1C_2 \;&=\; \left(\alpha_1\alpha_2\alpha_3 - \alpha_1\alpha_2\alpha_4 - \alpha_1\alpha_3\alpha_4 + \alpha_2\alpha_3\alpha_4 - \alpha_1 + \alpha_2 + \alpha_3 - \alpha_4\right) \\
&\quad \left(\alpha_1\alpha_2\alpha_3 - \alpha_1\alpha_2\alpha_4 + \alpha_1\alpha_3\alpha_4 + \alpha_2\alpha_3\alpha_4 + \alpha_1 + \alpha_2 - \alpha_3 + \alpha_4\right), \\
D \;=\; D_1D_2 \;&=\; \left(\alpha_1\alpha_2\alpha_3 + \alpha_1\alpha_2\alpha_4 + \alpha_1\alpha_3\alpha_4 + \alpha_2\alpha_3\alpha_4 - \alpha_1 - \alpha_2 - \alpha_3 - \alpha_4\right) \\
&\quad \left(\alpha_1\alpha_2\alpha_3 + \alpha_1\alpha_2\alpha_4 - \alpha_1\alpha_3\alpha_4 + \alpha_2\alpha_3\alpha_4 + \alpha_1 - \alpha_2 + \alpha_3 + \alpha_4\right).
\end{aligned}$$

The coefficients of Eq. (4.43), A, B, C, and D, all have two bicubic factors. While the derivation of this algebraised v_1-v_4 IO equation is novel and far from intuitive, the algebraic form of this fourth degree polynomial in the v_1-v_4 IO angle parameters is not. The earliest derivations of similar equations representing manipulatable octahedra, identical in form, are due to Raoul Bricard in 1897 [104]. This fascinating similarity between movable octahedral and spherical linkage algebraic IO equations is not at all a coincidence, as will be illustrated in Section 5.3.

It can be shown that Eq. (4.43) is identical to the corresponding trigonometric IO equation for spherical four-bar linkages found in [2]. The two algebraic IO equations for planar and spherical 4R linkages already suggest some similarities. As demonstrated in [59], the motion of the planar 4R linkage represents a special case of the spherical 4R linkage. To show that the same relationship is true for the IO equations, we consider the directions of the joint axes. While the joint axes of the spherical 4R

linkage intersect in the centre of the sphere, the joint axes of the planar 4R linkage are all parallel. In Euclidean space $\mathbb{E}^3$ parallel lines never intersect; however, they do meet in a point at infinity in any projective extension of $\mathbb{E}^3$ [60, 61]. This suggests that if the radius of a spherical linkage approaches infinity, the linkage becomes a planar mechanism in the limit [59]. As the link twist parameters α_i of the spherical IO equation are proportional to the ratios of the arc lengths to the sphere radius [31], we can make the following substitution in Eq. (4.43)

$$\alpha_i \quad \propto \quad \frac{a_i}{r}. \tag{4.44}$$

In the resulting equation the first two cubic factors simplify to

$$\begin{aligned} \lim_{r\to\infty} \quad & -\frac{1}{r}\left(\frac{a_1a_2a_3}{r^2} - \frac{a_1a_2a_4}{r^2} + \frac{a_1a_3a_4}{r^2} - \frac{a_2a_3a_4}{r^2} + a_1 - a_2 + a_3 - a_4\right) \\ & \left(-\frac{a_1a_2a_3}{r^2} + \frac{a_1a_2a_4}{r^2} + \frac{a_1a_3a_4}{r^2} + \frac{a_2a_3a_4}{r^2} + a_1 + a_2 + a_3 - a_4\right). \end{aligned} \tag{4.45}$$

In the limit the only terms remaining inside the parentheses in Eq. (4.45) are

$$(a_1 - a_2 + a_3 - a_4)(a_1 + a_2 + a_3 - a_4) \quad = \quad A_1A_2. \tag{4.46}$$

Proceeding with the other cubic factors in the same manner the algebraic IO equation for a spherical 4R mechanism leads directly to that of a planar 4R, Eq. (4.8), in the limit. Hence, the same coefficient names A, B, C, and D are used. As mentioned, this aligns with the results from [59], and further confirms the validity of the derived IO equations as well as the observation in [2] that there exists a connection between the planar and the spherical 4R IO equations via the RSSR linkage.

Using the eight bicubic coefficient definitions from Eq. (4.43), the remaining five v_i-

v_j equations contain all eight of the bicubic coefficients, but in different permutations:

$$A_1B_2v_1^2v_2^2+A_2B_1v_1^2+C_1D_2v_2^2+8\alpha_2\alpha_4(\alpha_1^2+1)(\alpha_3^2+1)v_1v_2+C_2D_1=0; \quad (4.47)$$

$$A_1B_1v_1^2v_3^2+A_2B_2v_1^2+C_2D_2v_3^2+C_1D_1=0; \quad (4.48)$$

$$A_1D_2v_2^2v_3^2+B_2C_1v_2^2+B_1C_2v_3^2-8\alpha_1\alpha_3(\alpha_2^2+1)(\alpha_4^2+1)\,v_2v_3+A_2D_1=0; \quad (4.49)$$

$$A_1C_1v_2^2v_4^2+B_2D_2v_2^2+A_2C_2v_4^2+B_1D_1=0; \quad (4.50)$$

$$A_1C_2v_3^2v_4^2+B_1D_2v_3^2+A_2C_1v_4^2+8\alpha_2\alpha_4(\alpha_1^2+1)(\alpha_3^2+1)\,v_3v_4+B_2D_1=0. \quad (4.51)$$

As for the planar 4R and RRRP linkage algebraic IO equations, we see that Eqs. (4.48) and (4.50) do not contain a bilinear quadratic term because they relate angle parings between the spherical quadrangle edges that intersect in opposite vertices. Each of Eqs. (4.43)-(4.51) has genus 1 from which can be concluded that the spherical linkage can have a maximum of two assembly modes.

The v_1-v_2 IO Equation. The derivation steps are precisely the same as for the v_1-v_4 IO equation. Eliminating v_3 and v_4 from the same three soma coordinates, the resulting v_1-v_2 IO equation splits into three similar factors. The first two, $(1+v_1^2)(1+v_2^2)$, can be safely factored out, leaving Eq. (4.47).

The v_1-v_3 IO Equation. The derivation steps are precisely the same as for the previous two IO equations. But, after the elimination of v_2 and v_4 from the same three soma coordinates, the resulting v_1-v_3 IO equation splits into five factors. The first two are $(1+v_1^2)(1+v_3^2)$, and can be safely factored out. The next two are

$$(\alpha_2^2\alpha_3^2+2\alpha_2\alpha_3+1)v_3^2+\alpha_2^2\alpha_3^2-2\alpha_2\alpha_3+1, \quad (4.52)$$

$$(\alpha_2^2-2\alpha_2\alpha_3+\alpha_3^2)v_3^2+\alpha_2^2+2\alpha_2\alpha_3+\alpha_3^2. \quad (4.53)$$

In order for either, or both, of Eqs. (4.52) or (4.53) to be identically zero the arc

length parameters α_2 and α_3 must be complex. This means these two factors may also be eliminated since we are only interested in real linkages, leaving Eq. (4.48).

The v_2-v_3 IO Equation. To derive this IO equation using elimination methods on the three soma coordinates requires a very different approach. By first applying the *graded reverse lexicographical order*, "`tdeg`", to the three soma coordinates using the list sequence (v_1, v_4, v_2, v_3), then applying *graded lexicographic order* using "`grlex`" to the bases identified with "`tdeg`". This yields 12 bases, all in terms of the four α_i and the four v_i, with the exception of one in the graded lexicographic order set of bases, which is in terms of the four α_i, but only v_1, v_2, and v_3, and is used in the elimination steps. Next, resultants are used to eliminate v_4 first, then v_1. This yields a v_2-v_3 IO equation that splits into nine factors.

The first five of these factors are simple to divide out since they are trivially non-zero: the first is -1; the other four are the squares of a single α_i added to a positive integer. The next three factors are functions of v_2 and v_3, but only α_1, α_2, and α_3:

$$(\alpha_1\alpha_2 - \alpha_1\alpha_3 + \alpha_2\alpha_3 + 1)^2 v_2^2 v_3^2 + (\alpha_1\alpha_2 + \alpha_1\alpha_3 - \alpha_2\alpha_3 + 1)^2 v_2^2 +$$
$$8\alpha_1\alpha_3(\alpha_2^2+1)v_2v_3 + (\alpha_1\alpha_2 - \alpha_1\alpha_3 - \alpha_2\alpha_3 - 1)^2 v_3^2 + (\alpha_1\alpha_2 + \alpha_1\alpha_3 + \alpha_2\alpha_3 - 1)^2; \quad (4.54)$$

$$(\alpha_1\alpha_2\alpha_3 + \alpha_1 - \alpha_2 + \alpha_3)^2 v_2^2 v_3^2 + (\alpha_1\alpha_2\alpha_3 - \alpha_1 + \alpha_2 + \alpha_3)^2 v_2^2 -$$
$$8\alpha_1\alpha_3(\alpha_2^2+1)v_2v_3 + (\alpha_1\alpha_2\alpha_3 + \alpha_1 + \alpha_2 - \alpha_3)^2 v_3^2 + (\alpha_1\alpha_2\alpha_3 - \alpha_1 - \alpha_2 - \alpha_3)^2; \quad (4.55)$$

$$\alpha_3(\alpha_1\alpha_2+1)(\alpha_1-\alpha_2)v_2^2 + 2\alpha_1\alpha_3(\alpha_2^2+1)v_2v_3 - \alpha_1(\alpha_2\alpha_3+1)(\alpha_2-\alpha_3)v_3^2 +$$
$$\alpha_2(\alpha_1+\alpha_3)(\alpha_1\alpha_3 - 1). \quad (4.56)$$

In order for Eqs. (4.54), (4.55), and/or (4.56) to be identically zero the arc length

parameters α_1, α_2, and/or α_3 must be complex numbers, so these three factors can safely be divided out, leaving only Eq. (4.49) as the desired IO equation.

The v_2-v_4 IO Equation. The derivation steps for the v_2-v_4 IO equation are the same as those for the v_1-v_4, v_1-v_2, and v_1-v_3 IO equations. The second set of Gröbner bases computed using the pure lexicographic order with list sequence (v_3, v_1, v_2, v_4) lead to an IO equation that splits into five factors, of which the first two are trivial. The next two are

$$(\alpha_1^2\alpha_2^2 + 2\alpha_1\alpha_2 + 1)v_2^2 + \alpha_1^2\alpha_2^2 - 2\alpha_1\alpha_2 + 1, \tag{4.57}$$

$$(\alpha_1^2 - 2\alpha_1\alpha_2 + \alpha_2^2)v_2^2 + \alpha_1^2 + 2\alpha_1\alpha_2 + \alpha_2^2. \tag{4.58}$$

For either, or both of Eqs. (4.57) and (4.58) to equate to zero, it requires both α_1 and α_2 to be complex. Therefore, both of these can be factored out, leaving only the desired v_2-v_4 IO, Eq. (4.50).

The v_3-v_4 IO Equation. Finally, the derivation steps for the v_3-v_4 IO equation are precisely the same as for the v_2-v_4 IO equation. After the elimination of v_1 and v_2 from the same three soma coordinates, the resulting v_3-v_4 IO equation splits into three factors. The first two are safely divided out, leaving Eq. (4.51).

4.4 Spatial Four-bar Linkages

4.4.1 Bennett Linkage

The IO equation for the Bennett linkage is derived following the same procedure. First, as illustrated in Fig. (2.6) the coordinate frames are attached to the linkage according to the DH convention. The DH coordinate frame assignment allows to

define the DH parameters for the linkage. It turns out that the Bennett linkage does not contain any link offsets d_i. However, it contains four motion parameters, the variable joint angles of the R joints, θ_i, and the design parameters a_i and τ_i. The DH parameters for the Bennett linkage are given in Tab. 4.5.

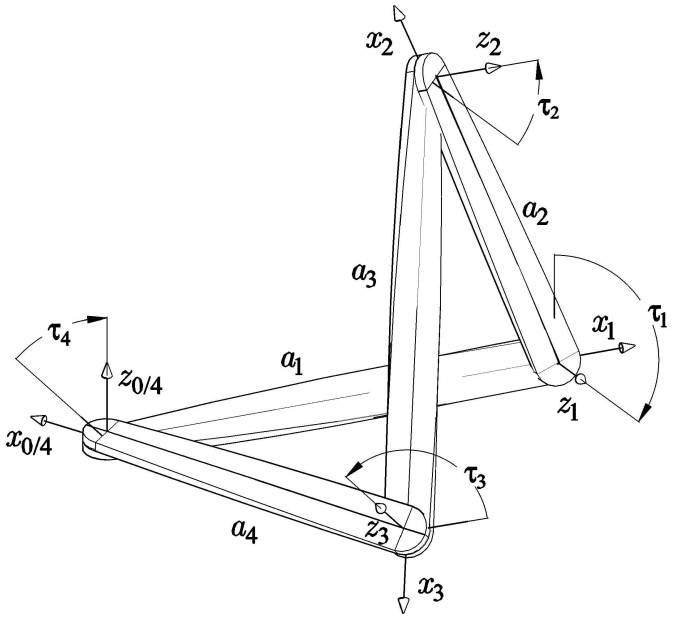

Figure 4.8: DH parameter assignment for the Bennett linkage. Note that this is Fig. 2.6 which is reproduced here for easier reference.

Table 4.5: DH parameters for the Bennett linkage.

joint axis i	link angle θ_i	link offset d_i	link length a_i	link twist τ_i
1	θ_1	0	a_1	τ_1
2	θ_2	0	a_2	τ_2
3	θ_3	0	a_3	τ_3
4	θ_4	0	a_4	τ_4

To evaluate the overall transformation of the position and orientation of the last joint with respect to the base coordinate system, the DH parameters from Tab. 4.5 are substituted into Eq. (3.43), and multiplied according to Eq. (3.44). This transformation matrix can then be mapped onto Study's quadric and expressed in Study parameters. The other method, leading to the same result, requires setting up Eq. (3.53)

or Eq. (3.56) as in the previous four linkages. Subsequent substitution of the DH parameters from Tab. 4.5 then also reveals the eight Study parameters.

Since the Bennett linkage is subjected to a set of special conditions, they can be used to further simplify the Study array. The Bennett conditions from Eq. (2.7) are reformulated with Weierstraß substitution, i.e., the tangent half-angle substitution [47]. This implies that

$$\cos\tau_i = \frac{1-\alpha_i^2}{1+\alpha_i^2}, \quad \sin\tau_i = \frac{2\alpha_i}{1+\alpha_i^2}. \tag{4.59}$$

Hence, the Bennett conditions can be expressed algebraically as

$$\begin{aligned} a_2 &= \frac{a_1\alpha_2(\alpha_1^2+1)}{\alpha_1(\alpha_2^2+1)}; \\ a_4 &= \frac{a_1\alpha_2(\alpha_1^2+1)}{\alpha_1(\alpha_2^2+1)}; \\ a_3 &= a_1; \\ \alpha_3 &= \alpha_1; \\ \alpha_4 &= \alpha_2; \end{aligned} \tag{4.60}$$

where $\alpha_i = \tan(\tau_i/2)$. Eq. (4.60) is substituted into the Study array which reduces the number of unknown parameters, and yields

$$\begin{aligned} x_0 &= \alpha_1^3\alpha_2^4v_1v_2v_3v_4 + \alpha_1^3\alpha_2^4v_1v_2 - \alpha_1^3\alpha_2^4v_1v_3 + \alpha_1^3\alpha_2^4v_1v_4 + \alpha_1^3\alpha_2^4v_2v_3 - \alpha_1^3\alpha_2^4v_2v_4 \\ &\quad +\alpha_1^3\alpha_2^4v_3v_4 + 4\alpha_1^2\alpha_2^3v_1v_2v_3v_4 - \alpha_1\alpha_2^4v_1v_2v_3v_4 + \alpha_1^3\alpha_2^4 - 2\alpha_1^3\alpha_2^2v_1v_3 \\ &\quad +2\alpha_1^3\alpha_2^2v_1v_4 + 2\alpha_1^3\alpha_2^2v_2v_3 - 2\alpha_1^3\alpha_2^2v_2v_4 - \alpha_1^3v_1v_2v_3v_4 + 4\alpha_1^2\alpha_2v_1v_2v_3v_4 \\ &\quad +\alpha_1\alpha_2^4v_1v_2 - \alpha_1\alpha_2^4v_1v_3 - \alpha_1\alpha_2^4v_1v_4 - \alpha_1\alpha_2^4v_2v_3 - \alpha_1\alpha_2^4v_2v_4 + \alpha_1\alpha_2^4v_3v_4 \\ &\quad -\alpha_1^3v_1v_2 - \alpha_1^3v_1v_3 + \alpha_1^3v_1v_4 + \alpha_1^3v_2v_3 - \alpha_1^3v_2v_4 - \alpha_1^3v_3v_4 - 4\alpha_1^2\alpha_2^3 - \alpha_1\alpha_2^4 \\ &\quad -2\alpha_1\alpha_2^2v_1v_3 - 2\alpha_1\alpha_2^2v_1v_4 - 2\alpha_1\alpha_2^2v_2v_3 - 2\alpha_1\alpha_2^2v_2v_4 + \alpha_1v_1v_2v_3v_4 - \alpha_1^3 \\ &\quad -4\alpha_1^2\alpha_2 - \alpha_1v_1v_2 - \alpha_1v_1v_3 - \alpha_1v_1v_4 - \alpha_1v_2v_3 - \alpha_1v_2v_4 - \alpha_1v_3v_4 + \alpha_1, \end{aligned} \tag{4.61}$$

$$x_1 = -2\alpha_1^3\alpha_2^3v_1v_2v_3v_4 + 2\alpha_1^2\alpha_2^4v_1v_2v_3v_4 - 2\alpha_1^3\alpha_2^3v_1v_2 - 2\alpha_1^3\alpha_2^3v_3v_4 - 2\alpha_1^3\alpha_2v_1v_2v_3v_4$$

$$
\begin{aligned}
&+2\alpha_1^2\alpha_2^4v_1v_4 - 2\alpha_1^2\alpha_2^4v_2v_3 + 2\alpha_1\alpha_2^3v_1v_2v_3v_4 - 2\alpha_1^3\alpha_2^3 - 2\alpha_1^3\alpha_2v_1v_2 - 2\alpha_1^3\alpha_2v_3v_4\\
&-2\alpha_1^2\alpha_2^4 + 4\alpha_1^2\alpha_2^2v_1v_4 - 4\alpha_1^2\alpha_2^2v_2v_3 - 2\alpha_1^2v_1v_2v_3v_4 - 2\alpha_1\alpha_2^3v_1v_2 - 2\alpha_1\alpha_2^3v_3v_4\\
&+2\alpha_1\alpha_2v_1v_2v_3v_4 - 2\alpha_1^3\alpha_2 + 2\alpha_1^2v_1v_4 - 2\alpha_1^2v_2v_3 + 2\alpha_1\alpha_2^3 - 2\alpha_1\alpha_2v_1v_2\\
&-2\alpha_1\alpha_2v_3v_4 + 2\alpha_1^2 + 2\alpha_1\alpha_2, \qquad (4.62)\\
x_2 \;=\;& -2\alpha_1^3\alpha_2^3v_1v_3v_4 + 2\alpha_1^3\alpha_2^3v_2v_3v_4 - 2\alpha_1^2\alpha_2^4v_1v_2v_3 - 2\alpha_1^2\alpha_2^4v_2v_3v_4 - 2\alpha_1^3\alpha_2^3v_1\\
&+2\alpha_1^3\alpha_2^3v_2 - 2\alpha_1^3\alpha_2v_1v_3v_4 + 2\alpha_1^3\alpha_2v_2v_3v_4 - 2\alpha_1^2\alpha_2^4v_1 - 2\alpha_1^2\alpha_2^4v_4 - 4\alpha_1^2\alpha_2^2v_1v_2v_3\\
&-2\alpha_1\alpha_2^3v_1v_3v_4 - 2\alpha_1\alpha_2^3v_2v_3v_4 - 2\alpha_1^3\alpha_2v_1 + 2\alpha_1^3\alpha_2v_2 - 4\alpha_1^2\alpha_2^2v_4 - 2\alpha_1^2v_1v_2v_3\\
&+2\alpha_1^2v_2v_3v_4 + 2\alpha_1\alpha_2^3v_1 + 2\alpha_1\alpha_2^3v_2 - 2\alpha_1\alpha_2v_1v_3v_4 - 2\alpha_1\alpha_2v_2v_3v_4\\
&+2\alpha_1^2v_1 - 2\alpha_1^2v_4 + 2\alpha_1\alpha_2v_1 + 2\alpha_1\alpha_2v_2, \qquad (4.63)\\
x_3 \;=\;& \alpha_1^3\alpha_2^4v_1v_2v_3 - \alpha_1^3\alpha_2^4v_1v_2v_4 + \alpha_1^3\alpha_2^4v_1v_3v_4 - \alpha_1^3\alpha_2^4v_2v_3v_4 + \alpha_1^3\alpha_2^4v_1 - \alpha_1^3\alpha_2^4v_2\\
&+\alpha_1^3\alpha_2^4v_3 - \alpha_1^3\alpha_2^4v_4 + 2\alpha_1^3\alpha_2^2v_1v_2v_3 - 2\alpha_1^3\alpha_2^2v_1v_2v_4 - 4\alpha_1^2\alpha_2^3v_2v_3v_4 - \alpha_1\alpha_2^4v_1v_2v_3\\
&-\alpha_1\alpha_2^4v_1v_2v_4 + \alpha_1\alpha_2^4v_1v_3v_4 + \alpha_1\alpha_2^4v_2v_3v_4 + 2\alpha_1^3\alpha_2^2v_3 - 2\alpha_1^3\alpha_2^2v_4 + \alpha_1^3v_1v_2v_3\\
&-\alpha_1^3v_1v_2v_4 - \alpha_1^3v_1v_3v_4 + \alpha_1^3v_2v_3v_4 - 4\alpha_1^2\alpha_2^3v_1 - 4\alpha_1^2\alpha_2v_2v_3v_4 - \alpha_1\alpha_2^4v_1\\
&-\alpha_1\alpha_2^4v_2 + \alpha_1\alpha_2^4v_3 + \alpha_1\alpha_2^4v_4 - 2\alpha_1\alpha_2^2v_1v_2v_3 - 2\alpha_1\alpha_2^2v_1v_2v_4 - \alpha_1^3v_1 + \alpha_1^3v_2\\
&+\alpha_1^3v_3 - \alpha_1^3v_4 - 4\alpha_1^2\alpha_2v_1 + 2\alpha_1\alpha_2^2v_3 + 2\alpha_1\alpha_2^2v_4 - \alpha_1v_1v_2v_3 - \alpha_1v_1v_2v_4\\
&-\alpha_1v_1v_3v_4 - \alpha_1v_2v_3v_4 + \alpha_1v_1 + \alpha_1v_2 + \alpha_1v_3 + \alpha_1v_4, \qquad (4.64)\\
y_0 \;=\;& -2a_1\alpha_1^4\alpha_2^2v_1v_2v_3v_4 + 4a_1\alpha_1^3\alpha_2^3v_1v_2v_3v_4 - 2a_1\alpha_1^2\alpha_2^4v_1v_2v_3v_4 - 2a_1\alpha_1^4\alpha_2^2v_1v_2\\
&-2a_1\alpha_1^4\alpha_2^2v_3v_4 - 2a_1\alpha_1^2\alpha_2^4v_1v_4 - 2a_1\alpha_1^2\alpha_2^4v_2v_3 - 2a_1\alpha_1^4\alpha_2^2 - 4a_1\alpha_1^3\alpha_2^3 - 2a_1\alpha_1^2\alpha_2^4\\
&-4a_1\alpha_1^2\alpha_2^2v_1v_2 - 4a_1\alpha_1^2\alpha_2^2v_1v_4 - 4a_1\alpha_1^2\alpha_2^2v_2v_3 - 4a_1\alpha_1^2\alpha_2^2v_3v_4 + 2a_1\alpha_1^2v_1v_2v_3v_4\\
&-4a_1\alpha_1\alpha_2v_1v_2v_3v_4 + 2a_1\alpha_2^2v_1v_2v_3v_4 - 2a_1\alpha_1^2v_1v_4 - 2a_1\alpha_1^2v_2v_3\\
&-2a_1\alpha_2^2v_1v_2 - 2a_1\alpha_2^2v_3v_4 + 2a_1\alpha_1^2 + 4a_1\alpha_1\alpha_2 + 2a_1\alpha_2^2, \qquad (4.65)\\
y_1 \;=\;& -a_1\alpha_1^4\alpha_2^3v_1v_2v_3v_4 + a_1\alpha_1^3\alpha_2^4v_1v_2v_3v_4 - a_1\alpha_1^4\alpha_2^3v_1v_2 - a_1\alpha_1^4\alpha_2^3v_3v_4\\
&+a_1\alpha_1^4\alpha_2v_1v_2v_3v_4 + a_1\alpha_1^3\alpha_2^4v_1v_4 - a_1\alpha_1^3\alpha_2^4v_2v_3 - 4a_1\alpha_1^3\alpha_2^2v_1v_2v_3v_4\\
&+4a_1\alpha_1^2\alpha_2^3v_1v_2v_3v_4 - a_1\alpha_1\alpha_2^4v_1v_2v_3v_4 - a_1\alpha_1^4\alpha_2^3 + a_1\alpha_1^4\alpha_2v_1v_2 + a_1\alpha_1^4\alpha_2v_3v_4
\end{aligned}
$$

$$
\begin{aligned}
& -a_1\alpha_1^3\alpha_2^4 + 2a_1\alpha_1^3\alpha_2^2 v_1 v_4 - 2a_1\alpha_1^3\alpha_2^2 v_2 v_3 - a_1\alpha_1^3 v_1 v_2 v_3 v_4 - 2a_1\alpha_1^2\alpha_2^3 v_1 v_2 \\
& -2a_1\alpha_1^2\alpha_2^3 v_3 v_4 + 4a_1\alpha_1^2\alpha_2 v_1 v_2 v_3 v_4 - a_1\alpha_1\alpha_2^4 v_1 v_4 + a_1\alpha_1\alpha_2^4 v_2 v_3 \\
& -4a_1\alpha_1\alpha_2^2 v_1 v_2 v_3 v_4 + a_1\alpha_2^3 v_1 v_2 v_3 v_4 + a_1\alpha_1^4\alpha_2 + 4a_1\alpha_1^3\alpha_2^2 + a_1\alpha_1^3 v_1 v_4 \\
& -a_1\alpha_1^3 v_2 v_3 + 4a_1\alpha_1^2\alpha_2^3 + 2a_1\alpha_1^2\alpha_2 v_1 v_2 + 2a_1\alpha_1^2\alpha_2 v_3 v_4 + a_1\alpha_1\alpha_2^4 - 2a_1\alpha_1\alpha_2^2 v_1 v_4 \\
& +2a_1\alpha_1\alpha_2^2 v_2 v_3 + a_1\alpha_1 v_1 v_2 v_3 v_4 - a_1\alpha_2^3 v_1 v_2 - a_1\alpha_2^3 v_3 v_4 - a_1\alpha_2 v_1 v_2 v_3 v_4 + a_1\alpha_1^3 \\
& +4a_1\alpha_1^2\alpha_2 + 4a_1\alpha_1\alpha_2^2 - a_1\alpha_1 v_1 v_4 + a_1\alpha_1 v_2 v_3 + a_1\alpha_2^3 + a_1\alpha_2 v_1 v_2 + a_1\alpha_2 v_3 v_4 \\
& -a_1\alpha_1 - a_1\alpha_2, \qquad (4.66)
\end{aligned}
$$

$$
\begin{aligned}
y_2 \;=\; & -a_1\alpha_1^4\alpha_2^3 v_1 v_3 v_4 + a_1\alpha_1^4\alpha_2^3 v_2 v_3 v_4 - a_1\alpha_1^3\alpha_2^4 v_1 v_2 v_3 - a_1\alpha_1^3\alpha_2^4 v_2 v_3 v_4 - a_1\alpha_1^4\alpha_2^3 v_1 \\
& +a_1\alpha_1^4\alpha_2^3 v_2 + a_1\alpha_1^4\alpha_2 v_1 v_3 v_4 - a_1\alpha_1^4\alpha_2 v_2 v_3 v_4 - a_1\alpha_1^3\alpha_2^4 v_1 - a_1\alpha_1^3\alpha_2^4 v_4 \\
& -2a_1\alpha_1^3\alpha_2^2 v_1 v_2 v_3 + 4a_1\alpha_1^3\alpha_2^2 v_2 v_3 v_4 - 2a_1\alpha_1^2\alpha_2^3 v_1 v_3 v_4 - 4a_1\alpha_1^2\alpha_2^3 v_2 v_3 v_4 \\
& +a_1\alpha_1\alpha_2^4 v_1 v_2 v_3 + a_1\alpha_1\alpha_2^4 v_2 v_3 v_4 + a_1\alpha_1^4\alpha_2 v_1 - a_1\alpha_1^4\alpha_2 v_2 + 4a_1\alpha_1^3\alpha_2^2 v_1 \\
& -2a_1\alpha_1^3\alpha_2^2 v_4 - a_1\alpha_1^3 v_1 v_2 v_3 + a_1\alpha_1^3 v_2 v_3 v_4 + 4a_1\alpha_1^2\alpha_2^3 v_1 + 2a_1\alpha_1^2\alpha_2^3 v_2 \\
& +2a_1\alpha_1^2\alpha_2 v_1 v_3 v_4 - 4a_1\alpha_1^2\alpha_2 v_2 v_3 v_4 + a_1\alpha_1\alpha_2^4 v_1 + a_1\alpha_1\alpha_2^4 v_4 + 2a_1\alpha_1\alpha_2^2 v_1 v_2 v_3 \\
& +4a_1\alpha_1\alpha_2^2 v_2 v_3 v_4 - a_1\alpha_2^3 v_1 v_3 v_4 - a_1\alpha_2^3 v_2 v_3 v_4 + a_1\alpha_1^3 v_1 - a_1\alpha_1^3 v_4 + 4a_1\alpha_1^2\alpha_2 v_1 \\
& -2a_1\alpha_1^2\alpha_2 v_2 + 4a_1\alpha_1\alpha_2^2 v_1 + 2a_1\alpha_1\alpha_2^2 v_4 + a_1\alpha_1 v_1 v_2 v_3 - a_1\alpha_1 v_2 v_3 v_4 + a_1\alpha_2^3 v_1 \\
& +a_1\alpha_2^3 v_2 + a_1\alpha_2 v_1 v_3 v_4 + a_1\alpha_2 v_2 v_3 v_4 - a_1\alpha_1 v_1 + a_1\alpha_1 v_4 - a_1\alpha_2 v_1 \\
& -a_1\alpha_2 v_2, \qquad (4.67)
\end{aligned}
$$

$$
\begin{aligned}
y_3 \;=\; & -2a_1\alpha_1^4\alpha_2^2 v_1 v_3 v_4 + 2a_1\alpha_1^4\alpha_2^2 v_2 v_3 v_4 - 4a_1\alpha_1^3\alpha_2^3 v_2 v_3 v_4 - 2a_1\alpha_1^2\alpha_2^4 v_1 v_2 v_3 \\
& +2a_1\alpha_1^2\alpha_2^4 v_2 v_3 v_4 - 2a_1\alpha_1^4\alpha_2^2 v_1 + 2a_1\alpha_1^4\alpha_2^2 v_2 - 4a_1\alpha_1^3\alpha_2^3 v_1 - 2a_1\alpha_1^2\alpha_2^4 v_1 \\
& +2a_1\alpha_1^2\alpha_2^4 v_4 - 4a_1\alpha_1^2\alpha_2^2 v_1 v_2 v_3 - 4a_1\alpha_1^2\alpha_2^2 v_1 v_3 v_4 + 4a_1\alpha_1^2\alpha_2^2 v_2 + 4a_1\alpha_1^2\alpha_2^2 v_4 \\
& -2a_1\alpha_1^2 v_1 v_2 v_3 - 2a_1\alpha_1^2 v_2 v_3 v_4 + 4a_1\alpha_1\alpha_2 v_2 v_3 v_4 - 2a_1\alpha_2^2 v_1 v_3 v_4 - 2a_1\alpha_2^2 v_2 v_3 v_4 \\
& +2a_1\alpha_1^2 v_1 + 2a_1\alpha_1^2 v_4 + 4a_1\alpha_1\alpha_2 v_1 + 2a_1\alpha_2^2 v_1 + 2a_1\alpha_2^2 v_2. \qquad (4.68)
\end{aligned}
$$

Again, to form a closed-loop chain, it requires that the base and the fourth coordinate

frames align. Hence, the Study array is equated to the identity array,

$$[x_0 : x_1 : x_2 : x_3 : y_0 : y_1 : y_2 : y_3] = [1 : 0 : 0 : 0 : 0 : 0 : 0 : 0]. \tag{4.69}$$

As the Study coordinates are homogeneous, i.e., a point represented by these coordinates remains unchanged if every entry is multiplied by the same factor, the system of equations which has to be solved consists of seven equations. These seven polynomials, Eq. (4.62-4.68), that equate to zero, generate the ideal containing all geometric information about a general Bennett mechanism.

The last step is to extract the IO equation from the ideal by eliminating the intermediate link angles using Gröbner bases. Using the Maple 2021 "`tdeg`" monomial ordering and with list sequence $(x_1 > ... > x_n) \rightarrow (v_2 > v_3 > v_4 > v_1)$ followed by "`plex`" with the same list sequence reveals one polynomial that no longer contains v_2 and v_3. Similar to the planar linkages a single application of the ordering "`lexdeg`" leads to the same result

$$(v_4^2 + 1)(v_1^2 + 1)((\alpha_1 - \alpha_2)v_1v_4 - \alpha_1 - \alpha_2) = 0. \tag{4.70}$$

Since the expressions $(v_4^2 + 1)$ and $(v_1^2 + 1)$ can never be zero, we can safely divide Eq. (4.70) by these two terms. This yields the IO equation for the Bennett linkage

$$(\alpha_1 - \alpha_2)v_1v_4 - \alpha_1 - \alpha_2 = 0, \tag{4.71}$$

where $\alpha_i = \tan(\tau_i/2)$ and $v_i = \tan(\theta_i/2)$. Eq. (4.71) is identical to the IO relation of the Bennett linkage obtained in [67] after algebraisation with tangent half-angle substitutions. With the "`lexdeg`" monomial ordering the remaining five algebraic IO equations yield

$$(\alpha_1 - \alpha_2)v_1v_2 + \alpha_1 + \alpha_2 = 0; \tag{4.72}$$

$$v_1 + v_3 = 0; \tag{4.73}$$

$$(\alpha_1 - \alpha_2)v_2v_3 - \alpha_1 - \alpha_2 = 0; \tag{4.74}$$

$$v_2 + v_4 = 0; \tag{4.75}$$

$$(\alpha_1 - \alpha_2)v_3v_4 + \alpha_1 + \alpha_2 = 0. \tag{4.76}$$

4.4.2 RSSR Linkage

The final four-bar linkage whose IO equation is being derived with the presented algorithm is the RSSR linkage. In contrast to the previous linkages, this type of linkage does not only contain R pairs that provide 1 dof, but also two S pairs that each provide 3 dof. Each of the two S joints of the RSSR can be modelled as three R joints whose rotation axes are mutually orthogonal and intersect at the sphere centre. Hence, eight coordinate frames are attached to the linkage. The chosen coordinate systems are illustrated in Fig. 4.9 and the corresponding DH parameters are found in Tab. 4.6. Note that the only link twist that is a design parameter is τ_8. The twists between the three mutually orthogonal R joint axes comprising the S joints are $\pm\pi$. We arbitrarily use the positive value, as the sign has no impact on the resulting algebraic IO equation, relating the two link angles of the R joints, θ_1 and θ_8, to one another.

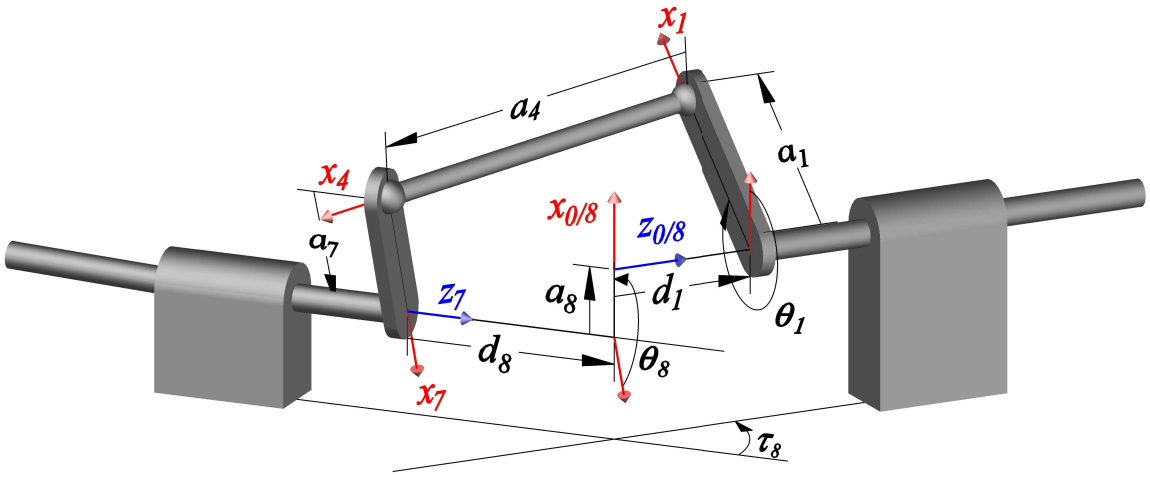

Figure 4.9: RSSR function generator.

We begin with a serial RSSR kinematic chain and determine the forward kine-

Table 4.6: DH parameters for the RSSR linkage.

joint axis i	link angle θ_i	link offset d_i	link length a_i	link twist τ_i
1	θ_1	d_1	a_1	0
2	θ_2	0	0	$\pi/2$
3	θ_3	0	0	$\pi/2$
4	θ_4	0	a_4	0
5	θ_5	0	0	$\pi/2$
6	θ_6	0	0	$\pi/2$
7	θ_7	0	a_7	0
8	θ_8	d_8	a_8	τ_8

matics. The required multiplication of the individual DH transformations matrices from one coordinate frame to another yields the overall homogeneous transformation matrix that describes the relationship between the first and last coordinate frames. To close the kinematic chain, we want the first and last coordinate systems to align in both their orientation and position. Algebraically, this is again specified using the kinematic closure equation, where the overall transformation equates to the identity [93]

$$\prod_{i=1}^{8} {}_{i}^{i-1}\mathbf{T} = \mathbf{I}. \tag{4.77}$$

The elements of this algebraic DH transformation matrix are then directly mapped into Study's kinematic image space where the constraint manifold could be analysed as it was successfully demonstrated for the planar 4R, spherical 4R, and Bennett linkages earlier. However, applying Gröbner bases or other elimination methods to symbolically obtain the IO equation for the RSSR linkage is computationally too demanding using algebraic geometry and computer algebra software, such as Maple 2021. To solve the polynomial equation this linkage requires a different approach.

A very efficient and elegant algebraic geometry approach, which, for example, has already been successfully applied in [9], is to split the closure equation in two by multiplying both sides by the inverses of half of the DH transformations. In the case

of the RSSR, the closure equation becomes

$$ {}^{0}_{1}\mathbf{T}\,{}^{1}_{2}\mathbf{T}\,{}^{2}_{3}\mathbf{T}\,{}^{3}_{4}\mathbf{T} = \mathbf{I}\,{}^{7}_{8}\mathbf{T}^{-1}\,{}^{6}_{7}\mathbf{T}^{-1}\,{}^{5}_{6}\mathbf{T}^{-1}\,{}^{4}_{5}\mathbf{T}^{-1}. \tag{4.78} $$

This step essentially divides the linkage into two serial chains joined at the 4th coordinate frame located in the second S joint., i.e., one chain between the coordinate frame 0 and 4, and one chain between the coordinate frame 4 and 8, which correspond to the expressions on the left and right sides of the equation, respectively, which we call the left RS and right RS dyads. In this way, mapping the left hand side of Eq. (4.78) into Study's kinematic image space yields eight polynomials describing the left RS dyad

$$
\begin{aligned}
x_0 &= 4v_1v_2v_3v_4 - 4v_1v_3 - 4v_2v_3 - 4v_3v_4,\\
x_1 &= -4v_1v_2 + 4v_1v_4 + 4v_2v_4 + 4,\\
x_2 &= 4v_1v_2v_4 + 4v_1 + 4v_2 - 4v_4,\\
x_3 &= -4v_1v_2v_3 - 4v_1v_3v_4 - 4v_2v_3v_4 + 4v_3,\\
y_0 &= -2d_1v_1v_2v_3 - 2d_1v_1v_3v_4 - 2d_1v_2v_3v_4 + 2a_1v_1v_2 - 2a_4v_1v_2 - 2a_1v_1v_4\\
&\quad + 2a_4v_1v_4 + 2a_1v_2v_4 + 2a_4v_2v_4 + 2d_1v_3 + 2a_1 + 2a_4,\\
y_1 &= 2a_1v_1v_2v_3v_4 - 2a_4v_1v_2v_3v_4 + 2d_1v_1v_2v_4 - 2a_1v_1v_3 + 2a_4v_1v_3 + 2a_1v_2v_3\\
&\quad + 2a_4v_2v_3 + 2a_1v_3v_4 + 2a_4v_3v_4 + 2d_1v_1 + 2d_1v_2 - 2d_1v_4,\\
y_2 &= 2a_1v_1v_2v_3 + 2a_4v_1v_2v_3 + 2a_1v_1v_3v_4 + 2a_4v_1v_3v_4 - 2a_1v_2v_3v_4 + 2a_4v_2v_3v_4\\
&\quad + 2d_1v_1v_2 - 2d_1v_1v_4 - 2d_1v_2v_4 + 2a_1v_3 - 2a_4v_3 - 2d_1,\\
y_3 &= -2d_1v_1v_2v_3v_4 + 2a_1v_1v_2v_4 + 2a_4v_1v_2v_4 + 2d_1v_1v_3 + 2d_1v_2v_3 + 2d_1v_3v_4\\
&\quad + 2a_1v_1 + 2a_4v_1 - 2a_1v_2 + 2a_4v_2 + 2a_1v_4 - 2a_4v_4.
\end{aligned} \tag{4.79}
$$

And finally, mapping the right hand side of Eq. (4.78) into Study's kinematic image space yields eight additional polynomials describing the right RS dyad

$$ x_0 = 4v_5v_6v_7v_8 - 4v_5v_6 - 4\alpha_8v_5v_7 - 4\alpha_8v_5v_8 - 4v_6v_7 - 4v_6v_8 + 4\alpha_8v_7v_8 - 4\alpha_8, $$

$$
\begin{aligned}
x_1 =& -4\alpha_8 v_5 v_6 v_7 v_8 + 4\alpha_8 v_5 v_6 - 4v_5 v_7 - 4v_5 v_8 + 4\alpha_8 v_6 v_7 + 4\alpha_8 v_6 v_8 + 4v_7 v_8 - 4,\\
x_2 =& \, 4\alpha_8 v_5 v_6 v_7 + 4\alpha_8 v_5 v_6 v_8 + 4v_5 v_7 v_8 + 4\alpha_8 v_6 v_7 v_8 - 4v_5 - 4\alpha_8 v_6 + 4v_7 + 4v_8,\\
x_3 =& \, 4v_5 v_6 v_7 + 4v_5 v_6 v_8 - 4\alpha_8 v_5 v_7 v_8 + 4v_6 v_7 v_8 + 4\alpha_8 v_5 - 4v_6 - 4\alpha_8 v_7 - 4\alpha_8 v_8,\\
y_0 =& -2a_7\alpha_8 v_5 v_6 v_7 v_8 + 2a_8\alpha_8 v_5 v_6 v_7 v_8 - 2d_8 v_5 v_6 v_7 - 2d_8 v_5 v_6 v_8 - 2\alpha_8 d_8 v_5 v_7 v_8\\
& - 2d_8 v_6 v_7 v_8 - 2a_7\alpha_8 v_5 v_6 - 2a_8\alpha_8 v_5 v_6 + 2a_7 v_5 v_7 + 2a_8 v_5 v_7 - 2a_7 v_5 v_8\\
& + 2a_8 v_5 v_8 - 2a_7\alpha_8 v_6 v_7 - 2a_8\alpha_8 v_6 v_7 + 2a_7\alpha_8 v_6 v_8 - 2a_8\alpha_8 v_6 v_8 + 2a_7 v_7 v_8\\
& - 2a_8 v_7 v_8 + 2\alpha_8 d_8 v_5 + 2d_8 v_6 - 2\alpha_8 d_8 v_7 - 2\alpha_8 d_8 v_8 + 2a_7 + 2a_8, \qquad (4.80)\\
y_1 =& -2a_7 v_5 v_6 v_7 v_8 + 2a_8 v_5 v_6 v_7 v_8 + 2\alpha_8 d_8 v_5 v_6 v_7 + 2\alpha_8 d_8 v_5 v_6 v_8 - 2d_8 v_5 v_7 v_8\\
& + 2\alpha_8 d_8 v_6 v_7 v_8 - 2a_7 v_5 v_6 - 2a_8 v_5 v_6 - 2a_7\alpha_8 v_5 v_7 - 2a_8\alpha_8 v_5 v_7 + 2a_7\alpha_8 v_5 v_8\\
& - 2a_8\alpha_8 v_5 v_8 - 2a_7 v_6 v_7 - 2a_8 v_6 v_7 + 2a_7 v_6 v_8 - 2a_8 v_6 v_8 - 2a_7\alpha_8 v_7 v_8\\
& + 2a_8\alpha_8 v_7 v_8 + 2d_8 v_5 - 2\alpha_8 d_8 v_6 - 2d_8 v_7 - 2d_8 v_8 - 2a_7\alpha_8 - 2a_8\alpha_8,\\
y_2 =& \, 2\alpha_8 d_8 v_5 v_6 v_7 v_8 - 2a_7 v_5 v_6 v_7 - 2a_8 v_5 v_6 v_7 + 2a_7 v_5 v_6 v_8 - 2a_8 v_5 v_6 v_8\\
& - 2a_7\alpha_8 v_5 v_7 v_8 + 2a_8\alpha_8 v_5 v_7 v_8 + 2a_7 v_6 v_7 v_8 - 2a_8 v_6 v_7 v_8 - 2\alpha_8 d_8 v_5 v_6\\
& - 2d_8 v_5 v_7 - 2d_8 v_5 v_8 - 2\alpha_8 d_8 v_6 v_7 - 2\alpha_8 d_8 v_6 v_8 + 2d_8 v_7 v_8 - 2a_7\alpha_8 v_5\\
& - 2a_8\alpha_8 v_5 + 2a_7 v_6 + 2a_8 v_6 + 2a_7\alpha_8 v_7 + 2a_8\alpha_8 v_7 - 2a_7\alpha_8 v_8 + 2a_8\alpha_8 v_8 - 2d_8,\\
y_3 =& \, 2d_8 v_5 v_6 v_7 v_8 + 2a_7\alpha_8 v_5 v_6 v_7 + 2a_8\alpha_8 v_5 v_6 v_7 - 2a_7\alpha_8 v_5 v_6 v_8 + 2a_8\alpha_8 v_5 v_6 v_8\\
& - 2a_7 v_5 v_7 v_8 + 2a_8 v_5 v_7 v_8 - 2a_7\alpha_8 v_6 v_7 v_8 + 2a_8\alpha_8 v_6 v_7 v_8 - 2d_8 v_5 v_6\\
& + 2\alpha_8 d_8 v_5 v_7 + 2\alpha_8 d_8 v_5 v_8 - 2d_8 v_6 v_7 - 2d_8 v_6 v_8 - 2\alpha_8 d_8 v_7 v_8 - 2a_7 v_5 - 2a_8 v_5\\
& - 2a_7\alpha_8 v_6 - 2a_8\alpha_8 v_6 + 2a_7 v_7 + 2a_8 v_7 - 2a_7 v_8 + 2a_8 v_8 + 2\alpha_8 d_8.
\end{aligned}
$$

To obtain the RSSR algebraic IO equation, the parametric equations of the Study coordinates of Eqs. (4.79) and (4.80) need to be expressed implicitly as a polynomial equation in the desired motion parameters v_1 and v_8 in the seven-dimensional kinematic mapping image space. This requires an algorithm that eliminates the unwanted motion parameters v_i where $i \in \{2, \ldots, 7\}$. One implicitisation algorithm that allows

for the transformation from the explicit parametric Study representation into a set of implicit polynomial equations was presented in Section 3.5.3, the linear implicitisation algorithm. The resulting constraint equations are implicit polynomials that form an algebraic variety in $\mathbb{P}^7$ and can be manipulated with different tools to obtain the IO equation.

The two serial RS chains of the RSSR linkage consist of one revolute and one spherical joint each. Clearly, the S joint spherical displacements, $SO(3)$, are completely contained on sub-spaces of the Study quadric as there is no translation involved and thus, all four y_i Study coordinates are identically zero. In other words, the displacements constrained by the S joints form special A-planes on the Study quadric. Further, the R joint in the serial RS chain rotates the S joint in a planar displacement thereby moving this special A-plane on S_6^2. It is well known that a 3-space can be represented by the intersection of four hyperplanes in the kinematic image space. To determine the RSSR algebraic IO equation we must identify these hyperplanes, one set for each serial RS chain. To obtain their implicit equations the linear implicitisation algorithm will be employed. The main goal of the linear implicitisation algorithm is to find the minimal number of implicit equations that describe the mechanical constraints in the image space. It allows for the elimination of motion parameters which, in the case of the RSSR, correspond to the variables $v_2, v_3, \ldots, v_7$. On the other hand, the design parameters a_i, d_i and α_i are fixed values that depend on the chosen linkage. However, to obtain the implicit polynomials for the spherical special 3-spaces v_1 and v_8 are temporarily also considered as design parameter constants.

To begin, we assume that the resulting variety is defined by linear constraint equations, and hence a general linear *ansatz polynomial* can be written, using the

graded reverse lexicographic monomial ordering [100], as

$$C_1y_3 + C_2y_2 + C_3y_1 + C_4y_0 + C_5x_3 + C_6x_2 + C_7x_1 + C_8x_0 = 0. \tag{4.81}$$

This linear ansatz polynomial has eight unknown coefficients C_i, $i \in \{1, \cdots, 8\}$. In the case of the left hand side of the RSSR chain, Eq. (4.79) is substituted into Eq. (4.81) and after reorganising such that the variable angle parameters of the spherical displacement are collected, yields

$$\begin{aligned}
&(-2C_1d_1v_1 + 2C_3a_1v_1 - 2C_3a_4v_1 + 4C_8v_1 - 2C_4d_1 - 2C_2a_1 + 2C_2a_4 - 4C_5)v_2v_3v_4 \\
&+ (2C_2a_1v_1 + 2C_2a_4v_1 - 2C_4d_1v_1 - 4C_5v_1 + 2C_1d_1 + 2C_3a_1 + 2C_3a_4 - 4C_8)v_2v_3 \\
&+ (2C_1a_1v_1 + 2C_1a_4v_1 + 2C_3d_1v_1 + 4C_6v_1 - 2C_2d_1 + 2C_4a_1 + 2C_4a_4 + 4C_7)v_2v_4 \\
&+ (2C_2d_1v_1 + 2C_4a_1v_1 - 2C_4a_4v_1 - 4C_7v_1 - 2C_1a_1 + 2C_1a_4 + 2C_3d_1 + 4C_6)v_2 \\
&+ (2C_2a_1v_1 + 2C_2a_4v_1 - 2C_4d_1v_1 - 4C_5v_1 + 2C_1d_1 + 2C_3a_1 + 2C_3a_4 - 4C_8)v_3v_4 \\
&+ (2C_1d_1v_1 - 2C_3a_1v_1 + 2C_3a_4v_1 - 4C_8v_1 + 2C_2a_1 - 2C_2a_4 + 2C_4d_1 + 4C_5)v_3 \\
&+ (-2C_2d_1v_1 - 2C_4a_1v_1 + 2C_4a_4v_1 + 4C_7v_1 + 2C_1a_1 - 2C_1a_4 - 2C_3d_1 - 4C_6)v_4 \\
&+ (2C_1a_1v_1 + 2C_1a_4v_1 + 2C_3d_1v_1 + 4C_6v_1 - 2C_2d_1 + 2C_4a_1 + 2C_4a_4 + 4C_7) = 0.
\end{aligned} \tag{4.82}$$

To fulfil this equation, the coefficients of the motion parameters in Eq. (4.82) must vanish since the v_2, v_3, and v_4 orientation angle parameters are, in general, non-zero. In matrix form, this can be expressed as

$$\begin{bmatrix}
2a_1v_1 + 2a_4v_1 & -2d_1 & 2d_1v_1 & 2a_1 + 2a_4 & 0 & 4v_1 & 4 & 0 \\
-2d_1v_1 & -2a_1 + 2a_4 & 2a_1v_1 - 2a_4v_1 & -2d_1 & -4 & 0 & 0 & 4v_1 \\
-2a_1 + 2a_4 & 2d_1v_1 & 2d_1 & 2a_1v_1 - 2a_4v_1 & 0 & 4 & -4v_1 & 0 \\
2a_1v_1 + 2a_4v_1 & -2d_1 & 2d_1v_1 & 2a_1 + 2a_4 & 0 & 4v_1 & 4 & 0 \\
2d_1 & 2a_1v_1 + 2a_4v_1 & 2a_1 + 2a_4 & -2d_1v_1 & -4v_1 & 0 & 0 & -4 \\
2d_1 & 2a_1v_1 + 2a_4v_1 & 2a_1 + 2a_4 & -2d_1v_1 & -4v_1 & 0 & 0 & -4 \\
2d_1v_1 & 2a_1 - 2a_4 & -2a_1v_1 + 2a_4v_1 & 2d_1 & 4 & 0 & 0 & -4v_1 \\
2a_1 - 2a_4 & -2d_1v_1 & -2d_1 & -2a_1v_1 + 2a_4v_1 & 0 & -4 & 4v_1 & 0
\end{bmatrix}
\begin{bmatrix} C_1 \\ C_2 \\ C_3 \\ C_4 \\ C_5 \\ C_6 \\ C_7 \\ C_8 \end{bmatrix}
=
\begin{bmatrix} 0 \\ 0 \\ 0 \\ 0 \\ 0 \\ 0 \\ 0 \\ 0 \end{bmatrix}.$$

Solving for the unknown C_i and back-substituting their solutions into the general

linear ansatz polynomial Eq. (4.81) reveals all four hyperplanes that satisfy the variety in $\mathbb{P}^7$. The solution shows that C_1, C_3, C_4, and C_8 are all free parameters with arbitrary values while C_2, C_5, C_6, and C_7 are expressions containing the design parameters and, after simplifying, are each linear in four of the Study parameters, and therefore hyperplanes. These four hyperplanes collected in terms of the Study parameters are

$$\begin{aligned}
0 &= (a_1^2v_1^2 - a_4^2v_1^2 + d_1^2v_1^2 + a_1^2 - a_4^2 + d_1^2)x_3 + (-2d_1v_1^2 - 2d_1)y_0 \\
&\quad + 4a_1v_1y_1 + (2a_1v_1^2 - 2a_4v_1^2 - 2a_1 - 2a_4)y_2, \qquad (4.83)\\
0 &= (a_1^2v_1^2 - a_4^2v_1^2 + d_1^2v_1^2 + a_1^2 - a_4^2 + d_1^2)x_2 - 4a_1v_1y_0 + (-2d_1v_1^2 - 2d_1)y_1 \\
&\quad + (-2a_1v_1^2 + 2a_4v_1^2 + 2a_1 + 2a_4)y_3, \qquad (4.84)\\
0 &= (a_1^2v_1^2 - a_4^2v_1^2 + d_1^2v_1^2 + a_1^2 - a_4^2 + d_1^2)x_1 + (2a_1v_1^2 + 2a_4v_1^2 - 2a_1 + 2a_4)y_0 \\
&\quad + (2d_1v_1^2 + 2d_1)y_2 - 4a_1v_1y_3, \qquad (4.85)\\
0 &= (a_1^2v_1^2 - a_4^2v_1^2 + d_1^2v_1^2 + a_1^2 - a_4^2 + d_1^2)x_0 + (-2a_1v_1^2 - 2a_4v_1^2 + 2a_1 - 2a_4)y_1 \\
&\quad + 4a_1v_1y_2 + (2d_1v_1^2 + 2d_1)y_3. \qquad (4.86)
\end{aligned}$$

The same procedure can be performed with the right-hand side of the RSSR by substituting Eq. (4.80) in the general linear ansatz polynomial, Eq. (4.81). In this case, the motion parameters to be eliminated are v_5, v_6 and v_7. Solving the resulting homogeneous matrix equation for the new unknown C_i yields the following four hyperplanes in a similar way. They are

$$\begin{aligned}
0 &= (a_7^2\alpha_8^2v_8^2 - 2a_7a_8\alpha_8^2v_8^2 + a_8^2\alpha_8^2v_8^2 + \alpha_8^2d_8^2v_8^2 + a_7^2v_8^2 - 2a_8a_7v_8^2 \\
&\quad + a_8^2v_8^2 + d_8^2v_8^2 + \alpha_8^2a_7^2 + 2a_7a_8\alpha_8^2 + a_8^2\alpha_8^2 + \alpha_8^2d_8^2 + a_7^2 + 2a_7a_8 + a_8^2 + d_8^2)x_3 \\
&\quad + (-2\alpha_8^2d_8v_8^2 + 2d_8v_8^2 + 8a_7\alpha_8v_8 - 2\alpha_8^2d_8 + 2d_8)y_0 \\
&\quad + (-4d_8\alpha_8v_8^2 - 4\alpha_8^2a_7v_8 + 4a_7v_8 - 4d_8\alpha_8)y_1 \\
&\quad + (-2a_7\alpha_8^2v_8^2 + 2\alpha_8^2a_8v_8^2 - 2a_7v_8^2 + 2a_8v_8^2 + 2a_7\alpha_8^2 + 2\alpha_8^2a_8 + 2a_7 + 2a_8)y_2, \qquad (4.87)
\end{aligned}$$

$$
\begin{aligned}
0 = &(a_7^2\alpha_8^2v_8^2 - 2a_7a_8\alpha_8^2v_8^2 + a_8^2\alpha_8^2v_8^2 + \alpha_8^2d_8^2v_8^2 + a_7^2v_8^2 - 2a_8a_7v_8^2 \\
&+ a_8^2v_8^2 + d_8^2v_8^2 + \alpha_8^2a_7^2 + 2a_7a_8\alpha_8^2 + a_8^2\alpha_8^2 + \alpha_8^2d_8^2 + a_7^2 + 2a_7a_8 + a_8^2 + d_8^2)x_2 \\
&+ (4d_8\alpha_8v_8^2 + 4\alpha_8^2a_7v_8 - 4a_7v_8 + 4d_8\alpha_8)y_0 \\
&+ (-2\alpha_8^2d_8v_8^2 + 2d_8v_8^2 + 8a_7\alpha_8v_8 - 2\alpha_8^2d_8 + 2d_8)y_1 \\
&+ (2a_7\alpha_8^2v_8^2 - 2\alpha_8^2a_8v_8^2 + 2a_7v_8^2 - 2a_8v_8^2 - 2a_7\alpha_8^2 - 2\alpha_8^2a_8 - 2a_7 - 2a_8)y_3, \quad (4.88) \\
0 = &(a_7^2\alpha_8^2v_8^2 - 2a_7a_8\alpha_8^2v_8^2 + a_8^2\alpha_8^2v_8^2 + \alpha_8^2d_8^2v_8^2 + a_7^2v_8^2 - 2a_8a_7v_8^2 \\
&+ a_8^2v_8^2 + d_8^2v_8^2 + \alpha_8^2a_7^2 + 2a_7a_8\alpha_8^2 + a_8^2\alpha_8^2 + \alpha_8^2d_8^2 + a_7^2 + 2a_7a_8 + a_8^2 + d_8^2)x_1 \\
&+ (-2a_7\alpha_8^2v_8^2 + 2\alpha_8^2a_8v_8^2 - 2a_7v_8^2 + 2a_8v_8^2 + 2a_7\alpha_8^2 + 2\alpha_8^2a_8 + 2a_7 + 2a_8)y_0 \\
&+ (2\alpha_8^2d_8v_8^2 - 2d_8v_8^2 - 8a_7\alpha_8v_8 + 2\alpha_8^2d_8 - 2d_8)y_2 \\
&+ (4d_8\alpha_8v_8^2 + 4\alpha_8^2a_7v_8 - 4a_7v_8 + 4d_8\alpha_8)y_3, \quad (4.89) \\
0 = &(a_7^2\alpha_8^2v_8^2 - 2a_7a_8\alpha_8^2v_8^2 + a_8^2\alpha_8^2v_8^2 + \alpha_8^2d_8^2v_8^2 + a_7^2v_8^2 - 2a_8a_7v_8^2 \\
&+ a_8^2v_8^2 + d_8^2v_8^2 + \alpha_8^2a_7^2 + 2a_7a_8\alpha_8^2 + a_8^2\alpha_8^2 + \alpha_8^2d_8^2 + a_7^2 + 2a_7a_8 + a_8^2 + d_8^2)x_0 \\
&+ (2a_7\alpha_8^2v_8^2 - 2\alpha_8^2a_8v_8^2 + 2a_7v_8^2 - 2a_8v_8^2 - 2a_7\alpha_8^2 - 2\alpha_8^2a_8 - 2a_7 - 2a_8)y_1 \\
&+ (-4d_8\alpha_8v_8^2 - 4\alpha_8^2a_7v_8 + 4a_7v_8 - 4d_8\alpha_8)y_2 \\
&+ (2\alpha_8^2d_8v_8^2 - 2d_8v_8^2 - 8a_7\alpha_8v_8 + 2\alpha_8^2d_8 - 2d_8)y_3. \quad (4.90)
\end{aligned}
$$

Solving Eqs. (4.83), ..., (4.86) for the four y_i and substituting these expressions into Eqs. (4.87), ..., (4.90) leaves four equations in the four unknown Study parameters x_i. This suggests solving the system of four equations for the four unknown x_i. However, doing so leads only to the trivial solution $x_i = y_i = 0$, $i \in \{0, 1, 2, 3\}$, which we call the null point. This result can be explained geometrically in $\mathbb{P}^7$ as follows: the two special 3-spaces representing the displacements of the S joints are two $SO(3)$ A-planes that are moved around on S_6^2 under the action of the two R joints, and only ever intersect in the null point.

But, there is a solution. Further inspection of the four equations shows that the

equations form a homogeneous system of linear equations. Expressing this linear homogeneous system in matrix-vector form $\mathbf{Ax} = \mathbf{0}$, we know that this system only has a nontrivial solution when the determinant of the 4×4 coefficient matrix $\mathbf{A}$ with respect to the x_i vanishes [105]. Thus, after computing the determinant of the Jacobian and omitting the factors that can never vanish, the general algebraic IO equation of the RSSR linkage arises directly from the determinant as

$$\begin{aligned} &Av_1^2v_8^2 + 8d_1\alpha_8a_7v_1^2v_8 + 8d_8\alpha_8a_1v_1v_8^2 + Bv_1^2 \\ &+8a_1a_7(\alpha_8 - 1)(\alpha_8 + 1)v_1v_8 + Cv_8^2 + 8d_8\alpha_8a_1v_1 + 8d_1\alpha_8a_7v_8 + D = 0, \end{aligned} \tag{4.91}$$

where

$$\begin{aligned} A &= (\alpha_8^2 + 1)A_1A_2 + E, \\ B &= (\alpha_8^2 + 1)B_1B_2 + E, \\ C &= (\alpha_8^2 + 1)C_1C_2 + E, \\ D &= (\alpha_8^2 + 1)D_1D_2 + E, \end{aligned}$$

and

$$\begin{aligned} A_1 &= (a_1 - a_4 + a_7 - a_8), & A_2 &= (a_1 + a_4 + a_7 - a_8), \\ B_1 &= (a_1 + a_4 - a_7 - a_8), & B_2 &= (a_1 - a_4 - a_7 - a_8), \\ C_1 &= (a_1 - a_4 - a_7 + a_8), & C_2 &= (a_1 + a_4 - a_7 + a_8), \\ D_1 &= (a_1 + a_4 + a_7 + a_8), & D_2 &= (a_1 - a_4 + a_7 + a_8), \end{aligned}$$

$$E = (d_1 - d_8)^2\alpha_8^2 + (d_1 + d_8)^2.$$

Eq. (4.91) is an implicit biquadratic algebraic curve of degree 4 in the joint angle parameters v_1 and v_8, as one would expect.

To verify this result, the IO equation of an arbitrary linkage was animated in GeoGebra. The model enabled measurement of the output angle for any given input angle. Tracing the locus of each input-output pair results in a curve which is compared

with the herein derived IO equation, Eq. (4.91). The chosen design parameters for the example linkage are $a_1 = 3$, $a_4 = 5$, $a_7 = 9$, $d_8 = 3$, $a_8 = 11$ and $\tau_8 = 60°$. While

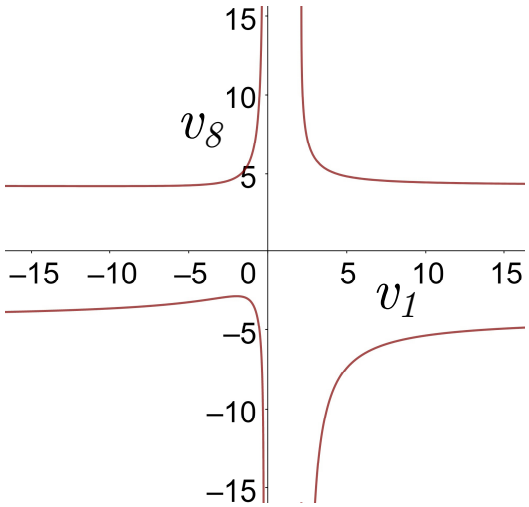

(a) IO equation geometrically generated in GeoGebra.

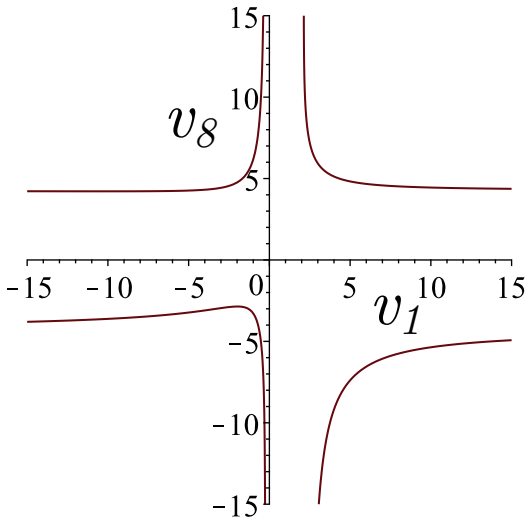

(b) Derived IO equation according to Eq. (4.91).

Figure 4.10: Example RSSR function generator with $a_1 = 3$, $a_4 = 5$, $a_7 = 9$, $d_8 = 3$, $a_8 = 11$ and $\tau_8 = 60°$.

the result of the GeoGebra file is displayed in Fig. (4.10a), substituting the same design parameters into Eq. (4.91) yields the curve in Fig. (4.10b). As can be seen, the curves are congruent which further suggests that Eq. (4.91) is indeed correct.

Following [2, Sec. 11.4] the IO equation of the RSSR linkage can be directly transformed into the IO equation of the planar 4R linkage since the planar 4R is a special case of the RSSR. This requires substituting $\alpha_8 = d_1 = d_8 = 0$ into Eq. (4.91). After renaming the link lengths and the output angle such that the coupler becomes a_2, the output link a_3, the base link a_4, and the angle of the output v_4 instead of the notation from Fig. (4.9), i.e., a_4, a_7, a_8, and v_8, respectively, the RSSR IO equation reduces to the IO equation, Eq. (4.8), as derived in Section 4.2.1 for planar 4R linkages.

Chapter 5

Applications

Thanks to the algebraic nature of the IO equations derived earlier, it is a simple task to get extensive information on the linkage. While it must be acknowledged that the IO equations themselves are not all new, the algebraic forms lead to computationally efficient and mathematically elegant tools for synthesis and analysis for four-bar linkages that are entirely new. To demonstrate the simplicity of these calculations, some applications will be discussed in the following chapter which will include the mobility, velocity and acceleration analysis. While the algebraic IO equations also provide serious advantages in terms of processing time to synthesis problems, the application chapter will be restricted to analysis applications. The reader interested in kinematic synthesis using algebraic IO equations is referred to [17, 24]. All computations and results presented can be obtained trigonometry-free using basic calculus knowledge which may, e.g., benefit robotic real-time operations. Consider a serial 6R robotic arm that must compute its own joint angles to enable the end effector to move a tool through a desired sequence of motions. If any one of the required transformation matrices contain a representational singularity, causing its determinant to vanish, then the particular joint will need to provide an infinite amount of torque. To avoid

causing damage to the motor drive, the controller will stop the motion of the arm. If the robot kinematics were free of representational singularities this scenario would not exist.

In particular, the mobility analysis will focus on analysing the singularities of a linkage as well as specifying a general mobility classification. It can be shown that the mobility classification of some linkages is closely linked to the linkage design parameter space which will be discussed in the second part of this chapter.

It should be noted that in general the singularity analysis and the mobility classification follow the same steps for every linkage. For that reason this thesis will limit itself to a few examples. The singular analysis and the mobility classification will be demonstrated on the example of the slider-crank and quadrilateral linkage, respectively. In addition, the design parameter space of the quadrilateral, slider-crank and spherical linkage will be outlined.

In the last part of this chapter, the utility of the algebraic IO equations will be emphasized by discussing the differential kinematics of two linkages, the planar four-bar as well as an example of the RSSR.

5.1 Singularity Analysis

The study of singular configurations is not trivial and fills numerous articles, books, and also leads to many discussions among kinematicians. They all agree though that if a mechanism approaches a singular configuration, the mechanism becomes uncontrollable because the dof of the mechanism instantaneously changes. A mechanical singularity, if it exists, is defined to be a configuration of a mechanism where the subsequent behaviour of the mechanism as it exits the singularity, if it can, is not predictable, or the forces or torques required to leave the singularity become either

infinite or nondeterministic.

Singularities can be obtained by examining the tangent space of the IO equation. Since the IO equation is, in general, an n-dimensional implicit function of the input and the output variables, the tangent space can be evaluated by taking the derivative of the IO equation with respect to time [36]. Given the input and output variable are denoted as x and y, respectively, then the tangent space is defined as

$$\mathbf{J_O}\dot{x} + \mathbf{J_I}\dot{y} = 0, \tag{5.1}$$

where

$$\mathbf{J_O} = \frac{\partial IO}{\partial x}, \quad \text{and} \quad \mathbf{J_I} = \frac{\partial IO}{\partial y}.$$

The determinants of the input Jacobian $\mathbf{J_I}$ and the output Jacobian $\mathbf{J_O}$ can be used to classify the linkage's singular configurations. There are three different singularity groups.

1. If $\det(\mathbf{J_I}) = 0$ the linkage is in an input singularity, also referred to an inverse-kinematics singularity. For a serial robot arm this occurs at the workspace boundary where the arm is completely stretched out. In the example of the RRRP, it can be used to determine the maximal slider distance $d_{4min/max}$. In this position the linkage loses one, or more, dof and is said to be locked.

2. If $\det(\mathbf{J_O}) = 0$ the linkage is in an output singularity, also referred to direct-kinematics singularity. This configuration occurs when the input link is at a dead-point where the rotation of the input link must change direction. Thus, in the example of the RRRP, it can be used to determine the upper and lower limits of the input rotation, $v_{1min/max}$. In this configuration the linkage gains a dof.

3. If both $\det(\mathbf{J_I}) = 0$ and $\det(\mathbf{J_O}) = 0$ the linkage is in a combined singularity. This typically requires special link lengths.

Consider the four different examples of the slider-crank linkage in Fig. (5.1). These figures display the algebraic IO curves of four scenarios where the input corresponds to a a) crank, b) π-rocker, c) 0-rocker, and d) rocker. Clearly, the algebraic curves are considered in two dimensions, the input and output motion parameters, which reduces the tangent space to tangent lines. The location of these tangent lines on the curve can be computed using simple calculus. The idea to find the values for $d_{4min/max}$ and $v_{1min/max}$ remains always the same: First, reformulate the equation such that it is considered as a function of one motion parameter, i.e., $f(v_1)$ and $f(d_4)$, respectively. Second, find the extrema by taking the derivative with respect to the other motion parameter, set the resulting equation to zero and solve for the extreme value.

Specifically, to find the input and output singularities using the algebraic IO equation of the slider crank, Eq. (4.21) must first be solved for d_4 and v_1, respectively which yields

$$\begin{aligned} d_4 = & \frac{-2a_1v_1 \pm \sqrt{-\left(a_1v_1^2 + a_2v_1^2 - a_4v_1^2 - a_1 + a_2 - a_4\right)\left(a_1v_1^2 - a_2v_1^2 - a_4v_1^2 - a_1 - a_2 - a_4\right)}}{v_1^2 + 1}; \\ v_1 = & \frac{-2a_1d_4 \pm \sqrt{-\left(a_1^2 + 2a_1a_2 + a_2^2 - a_4^2 - d_4^2\right)\left(a_1^2 - 2a_1a_2 + a_2^2 - a_4^2 - d_4^2\right)}}{a_1^2 - 2a_1a_4 - a_2^2 + a_4^2 + d_4^2}. \end{aligned} \tag{5.2}$$

Differentiating with respect to the motion parameters v_1 and d_4, respectively, equating the results to zero and solving for the same motion parameter yields the expressions containing information on the singularity locations. The input singularity, corresponding to the maximal slider positions $d_{4min/max}$, are located at

$$\begin{aligned} v_{1crit} &= \pm\frac{\sqrt{(a_1 + a_2 - a_4)(a_1 + a_2 + a_4)}}{a_1 + a_2 - a_4}; \\ v_{1crit} &= \pm\frac{\sqrt{(a_1 - a_2 - a_4)(a_1 - a_2 + a_4)}}{a_1 - a_2 - a_4}. \end{aligned} \tag{5.3}$$

With the bilinear factors defined in the original IO equation, Eq. (4.21), this expres-

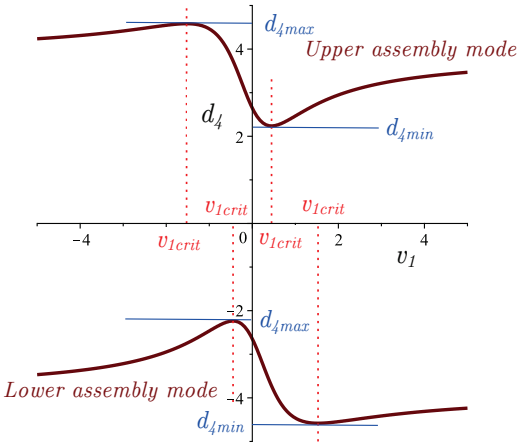

(a) Crank: $a_1 = 1$, $a_2 = 4$ and $a_4 = 2$.

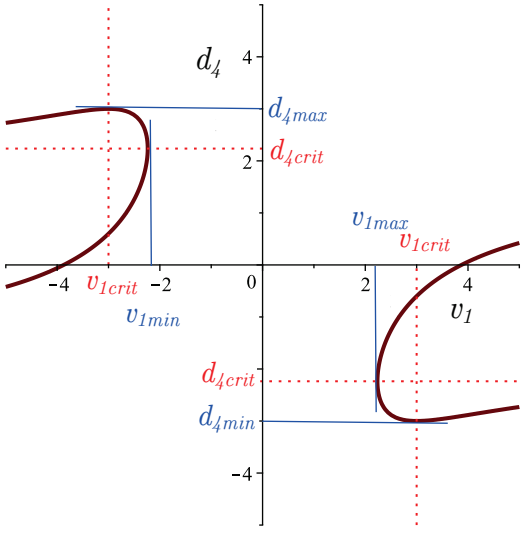

(b) π-rocker: $a_1 = 3$, $a_2 = 2$ and $a_4 = 4$.

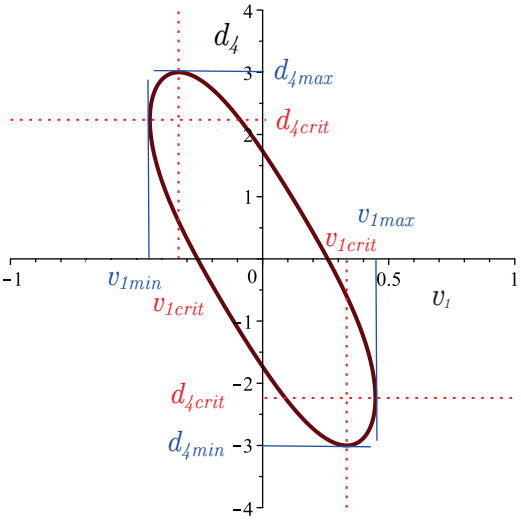

(c) 0-rocker: $a_1 = 3$, $a_2 = 2$ and $a_4 = -4$.

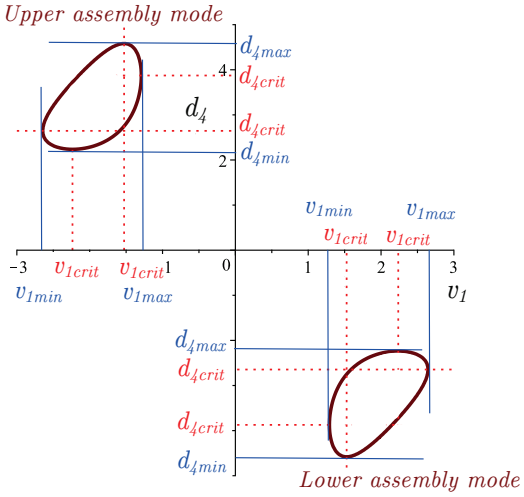

(d) Rocker: $a_1 = 4$, $a_2 = 1$ and $a_4 = 2$.

Figure 5.1: RRRP example with maximal slider positions $d_{4min/max}$ and boundaries of the input rotation angles $v_{1min/max}$.

sion reduces to

$$\begin{aligned} v_{1crit} &= \pm\frac{\sqrt{R_1 S_1}}{R_1}; \\ v_{1crit} &= \pm\frac{\sqrt{R_2 S_2}}{R_2}. \end{aligned} \tag{5.4}$$

The output singularities, corresponding to the boundaries of the input rotation angles $v_{1min/max}$, if they exist, are located at

$$\begin{aligned} d_{4crit} &= \pm\sqrt{(a_1 + a_2 + a_4)(a_1 - a_2 - a4)} = \pm\sqrt{S_1 R_2}; \\ d_{4crit} &= \sqrt{(a_1 + a_2 - a_4)(a_1 - a_2 + a4)} = \pm\sqrt{R_1 S_2}. \end{aligned} \tag{5.5}$$

This example clearly demonstrates that singularity analysis calculations of algebraic IO equations are simple and intuitive. The same concept can be applied to any other algebraic IO equation derived earlier, but including additional examples is deemed to be unnecessary.

5.2 Mobility Classification

While the singularity analysis focuses on examining the possible range and limits of a linkage, the following mobility classification is aiming to identify under which conditions a link becomes a crank, 0-rocker, π-rocker or rocker. Clearly, this type of discussion is only suitable if an R joint, i.e., the motion parameter v_i, is involved. As mentioned in the introduction of this chapter, the mobility classification will be conducted on the example of the quadrilateral linkage.

The mobility of the links in the quadrilateral linkage is established through whether the link is able to reach the two extreme positions where:

1. The link aligns with and extends the previous link. This corresponds to a link angle of $\theta_i = 0°$, or $v_i = 0$. A simple verification whether there exists real solutions for $v_i = 0$ in the IO equation is sufficient to determine whether the

link can physically reach this position.

2. The link aligns and overlaps with the previous link. This corresponds to a link angle of $\theta_i = 180°$, or $v_i = \infty$. Since each IO equation in the plane spanned by the coordinate axes v_i and v_j contains double points at infinity on each of the v_i and v_j axes, the type of double point determines whether the link can physically reach this position.

Hence, the examination of these two points is sufficient to determine whether a particular joint enables a crank, a rocker, a π-rocker, or a 0-rocker link motion [52, 27]. The conditions are shown in Tab. 5.1 which requires some additional explanation on double points. The maximum number of double points, DP_{max}, for an arbitrary

Table 5.1: Mobility Conditions for an R joint.

solution for $v_i = 0$	double point at $v_i = \infty$	link mobility
$\mathbb{R}$	crunode/cusp	crank
$\mathbb{R}$	acnode	0-rocker
$\mathbb{C}$	crunode/cusp	π-rocker
$\mathbb{C}$	acnode	rocker

algebraic curve of degree n can be determined by [66]

$$DP_{max} = \frac{(n-1)(n-2)}{2}. \tag{5.6}$$

For a planar algebraic curve to possess a double point, its degree must be $n > 3$. Hence, this analysis does not apply to PRRP linkages, but it does apply to the R-pairs in an RRRP linkage.

To determine the type of double point, it requires homogenising the algebraic curve, and subsequently, evaluating the discriminant of the resulting equation at the double point. This reveals whether the double point has a pair of real or complex conjugate tangents [74, 106] in turn yielding information about the topology of the mechanism [48, 106]. Let v_0 be the homogenising coordinate of the homogenised algebraic IO equation IO_h, then the following discriminant yields information on the

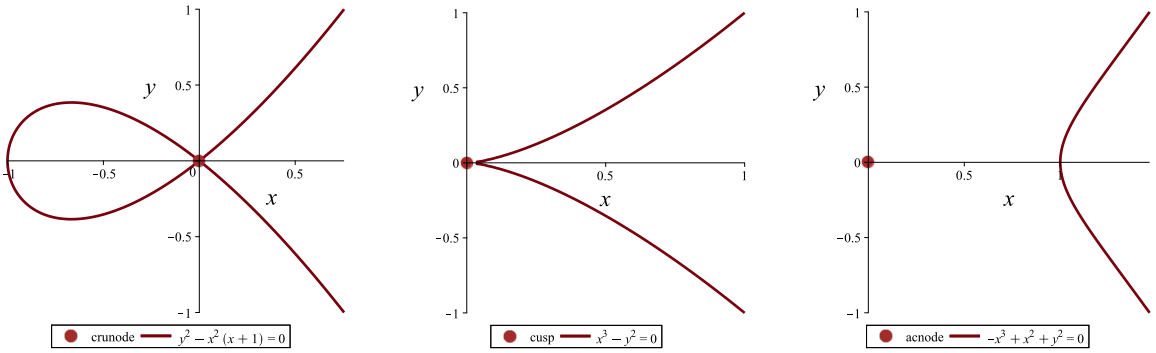

(a) crunode (b) cusp (c) acnode

Figure 5.2: Different types of double points.

double point at infinity on the v_j axis:

$$\Delta := \left(\frac{\partial^2 IO_h}{\partial v_i \partial v_0}\right)^2 - \frac{\partial^2 IO_h}{\partial v_i^2}\frac{\partial^2 IO_h}{\partial v_0^2} \begin{cases} > 0 \Rightarrow \text{crunode;} \\ = 0 \Rightarrow \text{cusp;} \\ < 0 \Rightarrow \text{acnode.} \end{cases} \tag{5.7}$$

If the tangents are complex conjugates the double point is an acnode: a *hermit* point that satisfies the equation of the curve but is isolated from all other points on the curve. If the double point has two real distinct tangents, it is a crunode, also known as an *ordinary double point*. In this case, the algebraic curve is intersecting itself. Finally, if the double point has two real coincident tangents, it is a cusp. In this point, the algebraic curve changes direction which creates a sharp point [74, 107]. Typical examples of the different types of double points are shown in Fig. (5.2). Clearly, if a double point is identified as an acnode, the point is isolated from the rest of the curve. This implies that the link length is unable to reach $\theta_i = 180°$. For example, a double point analysis of the v_1-d_4 equation of the RRRP at infinity on the d_4 axis yields that it is always an acnode, independent of the lengths of the links and offsets, which is reassuring as this means the travel of the prismatic slider is always finite. Let us determine the double points for the v_1-v_4 IO curve for a planar 4R. First homogenise Eq. (4.8) using the homogenising coordinate v_0, then redefine the

IO equation as

$$IO_h := Av_1^2v_4^2 + Bv_0^2v_1^2 + Cv_0^2v_4^2 - 8a_1a_3v_0^2v_1v_4 + Dv_0^4 = 0. \quad (5.8)$$

Computing the partial derivatives of IO_h with respect to the three homogeneous coordinates gives

$$\frac{\partial IO_h}{\partial v_0} := 2Bv_0v_1^2 + 2Cv_0v_4^2 - 16a_1a_3v_0v_1v_4 + 4Dv_0^3 = 0, \quad (5.9)$$

$$\frac{\partial IO_h}{\partial v_1} := 2Av_1v_4^2 + 2Bv_0^2v_1 - 8a_1a_3v_0^2v_4 = 0, \quad (5.10)$$

$$\frac{\partial IO_h}{\partial v_4} := 2Av_1^2v_4 + 2Cv_0^2v_4 - 8a_1a_3v_0^2v_1 = 0. \quad (5.11)$$

Finally solve the system of four equations (5.8)-(5.11) for v_0, v_1, and v_4. In this case, similar for all the IO equations, there are two solutions which are independent of the design parameters a_1, a_2, a_3, and a_4. These two solutions are double points at infinity on the v_1 and v_4 axes, named DP_1 and DP_2:

$$DP_1 = \{v_0 = 0, v_1 = v_1, v_4 = 0\}; \quad (5.12)$$

$$DP_2 = \{v_0 = 0, v_1 = 0, v_4 = v_4\}. \quad (5.13)$$

Proceeding with the double point analysis of all six v_i-v_j equations, the points at infinity on each axis result in 12 discriminants. However, as the v_i-v_j equations are all dependent on each other, only four are distinct. Each one describes the nature of the double point at infinity of each v_i for $i \in \{1...4\}$:

$$\Delta_{v_1} = -4(a_1 + a_2 - a_3 - a_4)(a_1 + a_2 + a_3 - a_4)$$
$$(a_1 - a_2 + a_3 - a_4)(a_1 - a_2 - a_3 - a_4);$$

$$\Delta_{v_2} = -4(a_1 - a_2 - a_3 + a_4)(a_1 - a_2 + a_3 + a_4)$$
$$(a_1 - a_2 + a_3 - a_4)(a_1 - a_2 - a_3 - a_4);$$

$$\begin{aligned}\Delta_{v_3} &= -4(a_1 - a_2 + a_3 + a_4)(a_1 + a_2 - a_3 + a_4) \\ &\quad (a_1 + a_2 - a_3 - a_4)(a_1 - a_2 + a_3 - a_4);\end{aligned}$$

$$\begin{aligned}\Delta_{v_4} &= -4(a_1 + a_2 - a_3 + a_4)(a_1 - a_2 - a_3 + a_4) \\ &\quad (a_1 - a_2 + a_3 - a_4)(a_1 + a_2 + a_3 - a_4).\end{aligned}$$

Using the bilinear factors defined by Eq. (4.8) these discriminants can be rewritten compactly as

$$\Delta_{v_1} = -4\ A_1A_2B_1B_2, \tag{5.14}$$

$$\Delta_{v_2} = -4\ A_1B_2C_1D_2, \tag{5.15}$$

$$\Delta_{v_3} = -4\ A_1B_1C_2D_2, \tag{5.16}$$

$$\Delta_{v_4} = -4\ A_1A_2C_1C_2. \tag{5.17}$$

From these conditions we can extract the following information. If $\Delta_{v_1} \geq 0$, then the double point at infinity on the v_1 axis is either a crunode or a cusp. Knowing that $v_1 = \infty$ corresponds to $\theta_1 = 180^\circ$ this implies that the link a_1 can physically reach the extreme position where a_1 aligns with and overlays the previous link a_4. Similarly, if $\Delta_{v_1} < 0$, then the double point at $v_1 = \infty$ is an acnode which in turn indicates that a_1 cannot physically reach the extreme position where a_1 aligns with and overlays a_4. Analogous conclusions can be drawn from Equations (5.15), (5.16), and (5.17).

As previously mentioned, to fully understand the mobility of every link, it equally requires the analysis of whether the other extremes where the link under investigation aligns with, but does not overlay, the previous link. We need to investigate whether the linkage is assemblable at $v_i = 0$. Clearly, one possibility to obtain a condition with this information can be derived using the six v_i-v_j equations by substituting $v_i = 0$ and solving for v_j. Again, due to the equations' dependencies, we obtain four

distinct conditions, one for each v_i:

$$\begin{aligned}
\Omega_{v_1} &= [-(a_1 - a_2 - a_3 + a_4)(a_1 - a_2 + a_3 + a_4) \\
&\quad (a_1 + a_2 - a_3 + a_4)(a_1 + a_2 + a_3 + a_4)]^{\frac{1}{2}}; \\
\Omega_{v_2} &= [-(a_1 + a_2 - a_3 - a_4)(a_1 + a_2 + a_3 - a_4) \\
&\quad (a_1 + a_2 - a_3 + a_4)(a_1 + a_2 + a_3 + a_4)]^{\frac{1}{2}}; \\
\Omega_{v_3} &= [-(a_1 + a_2 + a_3 - a_4)(a_1 - a_2 - a_3 - a_4) \\
&\quad (a_1 - a_2 - a_3 + a_4)(a_1 + a_2 + a_3 + a_4)]^{\frac{1}{2}}; \\
\Omega_{v_4} &= [-(a_1 - a_2 - a_3 - a_4)(a_1 + a_2 - a_3 - a_4) \\
&\quad (a_1 - a_2 + a_3 + a_4)(a_1 + a_2 + a_3 + a_4)]^{\frac{1}{2}}.
\end{aligned}$$

Using the bilinear factors from Eq. (4.8) these expressions can be rewritten compactly as:

$$\Omega_{v_1} = \sqrt{-C_1 C_2 D_1 D_2}; \tag{5.18}$$

$$\Omega_{v_2} = \sqrt{-A_2 B_1 C_2 D_1}; \tag{5.19}$$

$$\Omega_{v_3} = \sqrt{-A_2 B_2 C_1 D_1}; \tag{5.20}$$

$$\Omega_{v_4} = \sqrt{-B_1 B_2 D_1 D_2}. \tag{5.21}$$

With this information we can establish a completely generic classification scheme to determine the relative mobilities of every link in the simple closed kinematic chain. Using the bilinear factors the classification can be constructed according to Tab. 5.2-5.5. The beauty of this classification scheme lies in its completely generic nature, covering both positive and negative values for the a_i. This result requires the a_i to be considered as directed line segments. For example $a_1 > 0$ means that it is directed from the joint with a_4 to a_2, $a_1 < 0$ means a_1 points in the opposite direction. Moreover, the classification scheme is directly linked to the algebraic IO equations.

These results allow to explain the different spatial sections that are spanned by the linear factors in the design parameter space which will be discussed in the next section.

Table 5.2: Mobility of a_1 relative to a_4.

$A_1A_2B_1B_2$	$C_1C_2D_1D_2$	mobility of a_1
≤ 0	≤ 0	crank
≤ 0	> 0	π-rocker
> 0	≤ 0	0-rocker
> 0	> 0	rocker

Table 5.3: Mobility of a_2 relative to a_1.

$A_1B_2C_1D_2$	$A_2B_1C_2D_1$	mobility of a_2
≤ 0	≤ 0	crank
≤ 0	> 0	π-rocker
> 0	≤ 0	0-rocker
> 0	> 0	rocker

Table 5.4: Mobility of a_3 relative to a_2.

$A_1B_1C_2D_2$	$A_2B_2C_1D_1$	mobility of a_3
≤ 0	≤ 0	crank
≤ 0	> 0	π-rocker
> 0	≤ 0	0-rocker
> 0	> 0	rocker

Table 5.5: Mobility of a_4 relative to a_3.

$A_1A_2C_1C_2$	$B_1B_2D_1D_2$	mobility of a_4
≤ 0	≤ 0	crank
≤ 0	> 0	π-rocker
> 0	≤ 0	0-rocker
> 0	> 0	rocker

It is straightforward to use this same analysis applied to the spherical 4R as well as the planar RRRP linkages to determine the relative mobility conditions for each link in the chain. However, in the interest of brevity, it will not be listed here.

5.3 Design Parameter Spaces

The first graphical representation of the design parameter space of planar and spherical 4R linkages can be found in [108, 109, 110]. In the case of the planar 4R it reveals plane bound regions in a three-space having the Freudenstein parameters as mutually orthogonal basis vectors. However, the full symmetry of the group of planar 4R linkages is obscured by the trigonometric description of the IO equation. In addition, it is not possible to represent all v_i-v_j equations of one type of linkage in the same design parameter space. For example, the trigonometric Freudenstein equation relating the v_i input of the quadrilateral linkage to the corresponding v_j output angle contains different Freudenstein parameters than the trigonometric equation relating the input to the transmission angle. As a result the design parameter space where the axes are spanned by the Freudenstein parameters differs for every equation.

This is different with the algebraic IO equations. The symmetries of the algebraic IO equations for the spherical and planar 4R and the planar RRRP and PRRP linkages are fully revealed graphically when one considers the link lengths a_i, link offsets d_i, and link twist angle parameters α_i as design parameters, see [22, 25, 27]. For planar and spherical 4R function generators the scale of the linkage is irrelevant. This allows to consider these four a_i and four α_i design parameters as homogeneous coordinates, and to assign a_4 and α_4 which normalises the four coordinates, thereby setting $a_4 = 1$ for the planar and $\alpha_4 = 1$ as the spherical design space parameter coordinates and treat the remaining three lengths or twist angles as mutually orthogonal basis vectors.

In the planar 4R design parameter three-space, each of the distinct eight bilinear factors in Eqs. (4.8)-(4.13) represent eight distinct planes. These eight planes intersect in 12 lines which are the edges of a stellated octahedron having order 48 octahedral symmetry [111]. Johannes Kepler named this topology "stella octangula", which is

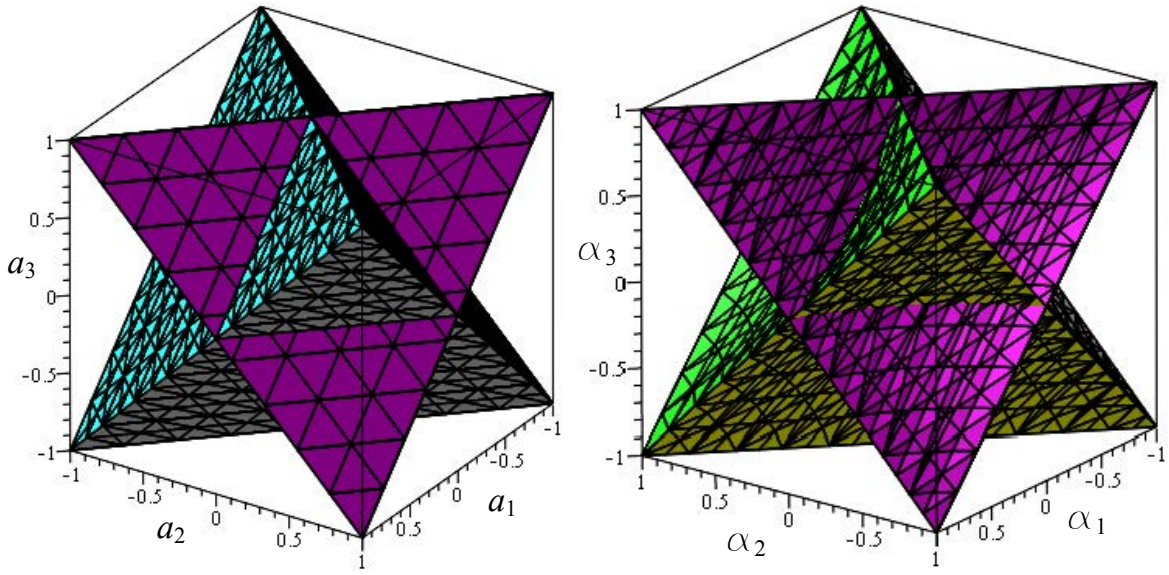

(a) Planar 4R stellated octahedron. (b) Spherical 4R degenerate bicubic surfaces.

Figure 5.5: Planar and spherical 4R design parameter spaces.

Latin for "eight-pointed star", referring to the eight vertices, see Fig. 5.5a. In the entire universe of polytopes, it is the only regular compound of two tetrahedra [111]: two tetrahedra which intersect in an octahedron. Each distinct point in the design parameter space represents a distinct planar 4R linkage. The eight planes segment the design parameter space into regions that represent the mobility of the linkages contained in that region [27, 19].

For the spherical 4R, the eight bicubic factors in the four coefficients A, B, C, and D in Eq. (4.43) are symmetric singular cubic surfaces, see Fig. 5.5b, which each possess three distinct finite lines and three common lines at infinity [25]. Note that a cubic surface can contain as many as 27 lines [112]; those that contain less than 27 are called *singular*, while those that contain exactly 27 are *non-singular*. Each of these cubic surfaces possess three ordinary double points [25]. It is also shown in [112] that a cubic surface possessing three ordinary double points can have, at most, 12 lines, which is the case for these eight cubic surfaces. Of these 12 lines on each surface, six are complex and six are real. Of the six real lines three are at infinity. The remaining

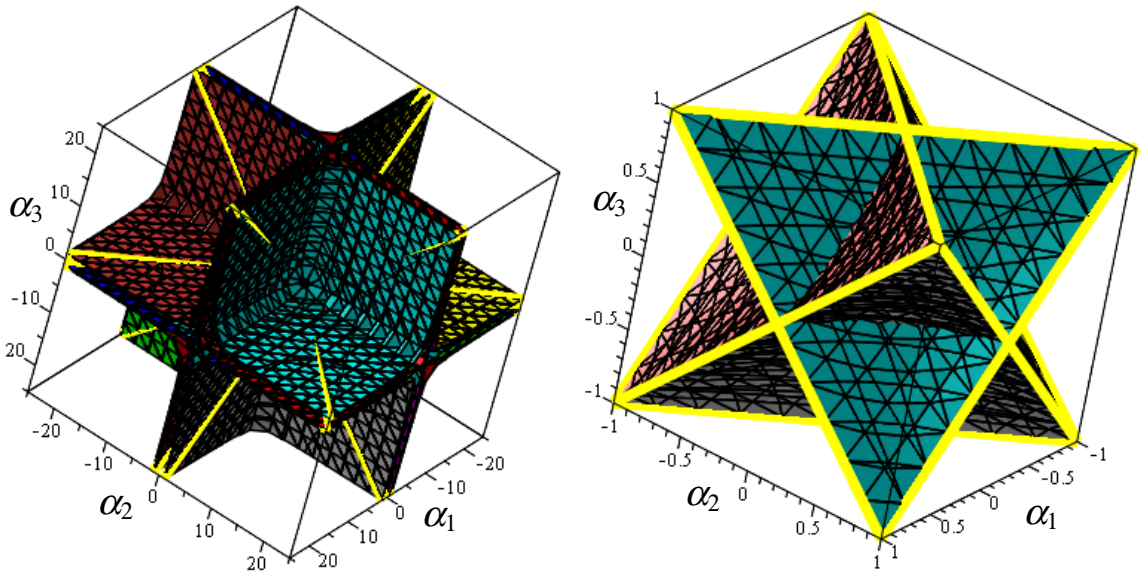

(a) In the range $-25 \leq \alpha_i \leq 25$.

(b) In the range $-1 \leq \alpha_i \leq 1$.

Figure 5.6: Eight cubic surfaces in the spherical 4R design parameter space.

three lines on each surface intersect each other in an equilateral triangle.

Different pairs of the eight cubic surfaces have one finite line in common, meaning there are 12 distinct finite lines among the eight surfaces. The finite lines contain the twelve edges of another stellated octahedron. The faces of the same stellated octahedron are also found in the design parameter space of planar 4R linkages. The edges of this regular double tetrahedron can be regarded as the intersection of the bilinear factors of the coefficients of the planar 4R and the singular cubic surfaces formed by the coefficients of the spherical 4R IO equations in the design parameter spaces. This is as remarkable as it is fascinating! Fig. 5.6 illustrates the eight cubic surfaces and the three finite lines on each. This illustrates the connection between Bricard's movable octahedra mentioned in Section 4.3 and the intersection of the spherical 4R and planar 4R design parameter spaces.

With the six algebraic v_i-v_j equations, and the previously identified mobility classification using double points and discriminants in Section 5.2, it becomes evident that the planes spanning the faces of the stellated octahedron contain complete in-

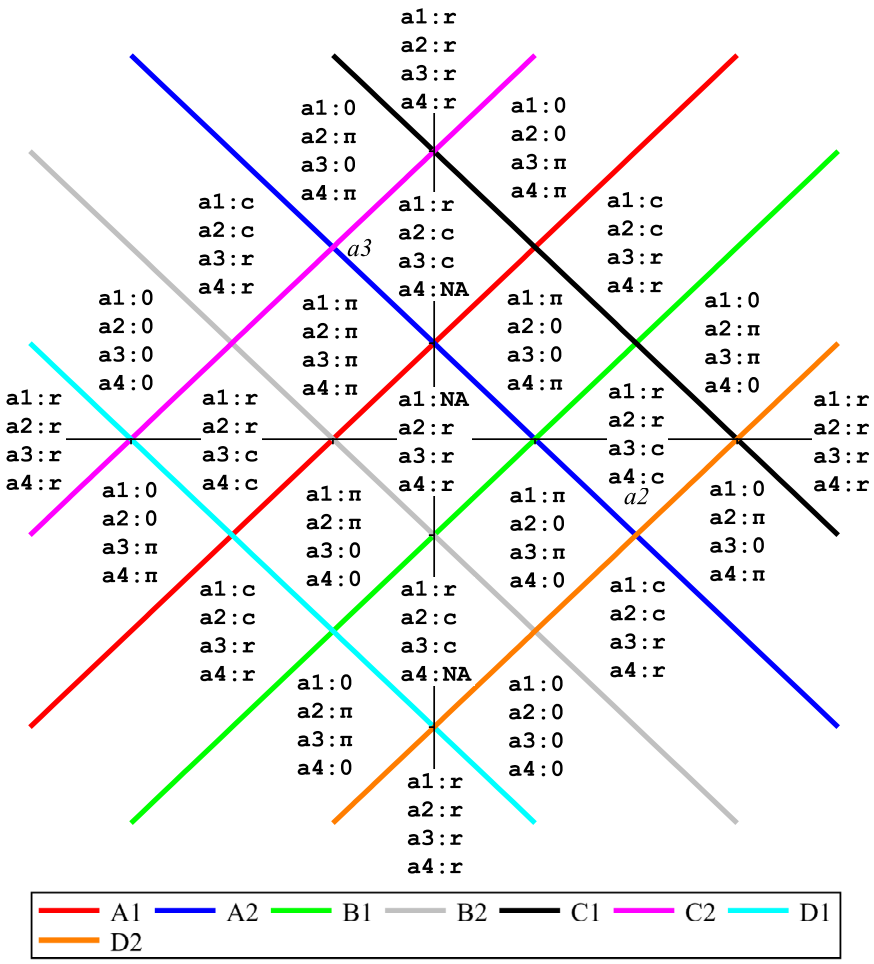

Figure 5.7: Intersection of the planar 4R stellated octahedron in the design parameter space with the plane $a_1 = 0.5$.

formation on the relative mobility of every link in the chain! In fact, the stellated octahedron face planes segment the design parameter space into distinct regions which each describes the relative mobility of a_1, a_2, a_3 and a_4. For a better understanding of this concept, let us have a look at the following example.

Consider the intersection traces of the bilinear factors in the parameter plane $a_1 = 0.5$ spanned by a_2 and a_3 in the design parameter space where a_2 and a_3 are the horizontal and vertical axes, respectively. Here the bilinear factors are parallel and orthogonal plane trace lines. Together with Tabs. 5.2-5.5, the mobility of all link lengths of the quadrilateral linkage can now be identified, resulting in Fig. 5.7 where

r indicates that the corresponding link is a rocker, **c** a crank, π a π-rocker, and **0** a 0-rocker, while NA indicates the linkage is not assemblable. This analysis can be conducted for every area separated by the bilinear factors in the design parameter space, resulting in a complete geometric mobility classification of planar four-bar linkages which is directly linked to the six algebraic v_i-v_j IO equations.

Another interesting design parameter space is revealed by the algebraic IO equations of the slider-crank linkage, Eq. (4.21)-(4.26). The four bilinear coefficient factors R_1, R_2, S_1, and S_2 each contain one of the four possible permutations of addition to, and subtraction from, a_1 of the remaining link lengths a_2 and a_4. These bilinear factors can be thought of as four distinct planes in a space spanned by three mutually orthogonal basis direction vectors for each one of the link lengths a_1, a_2, and a_4, constituting the design parameter space. Each distinct point in the space represents the three directed link lengths of a distinct planar RRRP linkage. These four planes each contain a triangular face of a regular square pyramid whose axis is perpendicular to the plane $a_4 = 0$, illustrated in Fig. 5.8c. The four planes bound four distinct regions in planes parallel to $a_4 = 0$, where each bounded region contains points representing linkages with different relative link mobility characteristics. Let us consider the intersections of a_1 and a_2 with planes where a_4 is greater than, less than, and identically equal to zero. Different non-zero values for a_4 simply scale the amplitude of a desired slider position as a function of the input angle parameter: $d_4 = a_4 f(v_1)$. Fig. 5.8c shows intersections of the design parameter pyramid with the three planes $a_4 = \pm 1$ and $a_4 = 3$ illustrating the scaling effect for different values of a_4. Fig. 5.8a illustrates the intersection of the regular square pyramid with the plane $a_4 = 1$ while Fig. 5.8b illustrates the intersection of the regular square pyramid with the plane $a_4 = -1$.

In each intersection of a_1 and a_2 with planes where $a_4 > 0$ the four parameter planes of the algebraic IO equations intersect in the four plane traces illustrated in

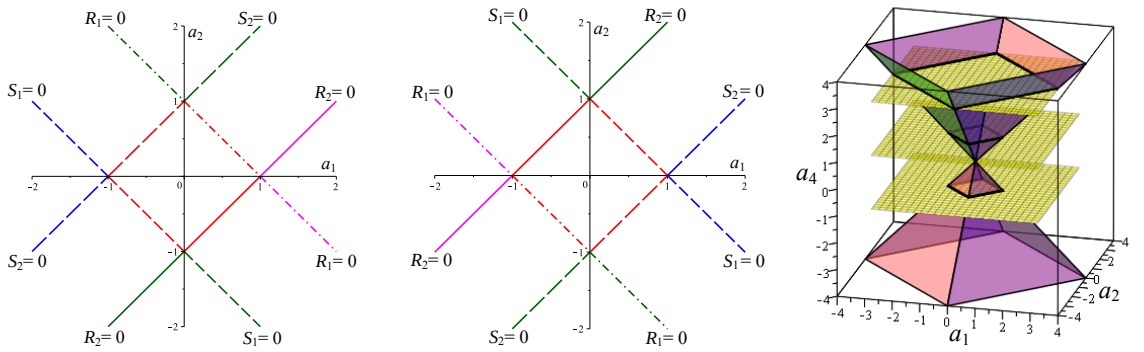

(a) Intersection with the plane $a_4 = 1$.

(b) Intersection with the plane $a_4 = -1$.

(c) Pyramid-plane intersections.

Figure 5.8: RRRP design parameter space.

Fig. 5.8a. These traces have the equations $R_1 = 0$, $R_2 = 0$, $S_1 = 0$, and $S_2 = 0$. Linkages consisting of points on these plane traces represent either folding linkages or non-movable structures. Points in the regions separated by the plane traces represent linkages with very specific displacement capabilities, while points on the interior of the square that has vertices $(a_1, a_2) = (\pm 1, 0), (0, \pm 1)$ represent non-assemblable linkages. To determine which linkage types occupy the eight distinct trace-bound regions on the exterior of the unit squares, the procedure is analogous to the quadrilateral linkage as outlined in Section 5.2. For brevity, let us limit the discussion to the relative mobility of the input link. Using Eq. (4.21) the double point analysis and the condition whether the input link is assemblable at $v_1 = 0$ yields

$$\begin{aligned} \Delta_{v_1} &= -4\, R_1 R_2\ ; \\ \Omega_{v_1} &= \pm\sqrt{-S_1 S_2}. \end{aligned}$$

With the decision Tab. 5.1, this results in the relative mobility classification of the input link, i.e., a_1 with respect to a_4, as provided in Tab. 5.6. As the conditions solely depend on the four bilinear coefficient factors R_1, R_2, S_1, and S_2 from the algebraic IO equations, each region in the design parameter space contains linkages with different relative input mobility as illustrated in Fig. (5.9). Locations of unique points in this space define unique planar RRRP mechanisms with relative mobility limits implied by

Table 5.6: Relative mobility classification of the input link of the slider-crank.

R_1R_2	S_2S_2	mobility of a_1
≤ 0	≤ 0	crank
≤ 0	> 0	π-rocker
> 0	≤ 0	0-rocker
> 0	> 0	rocker

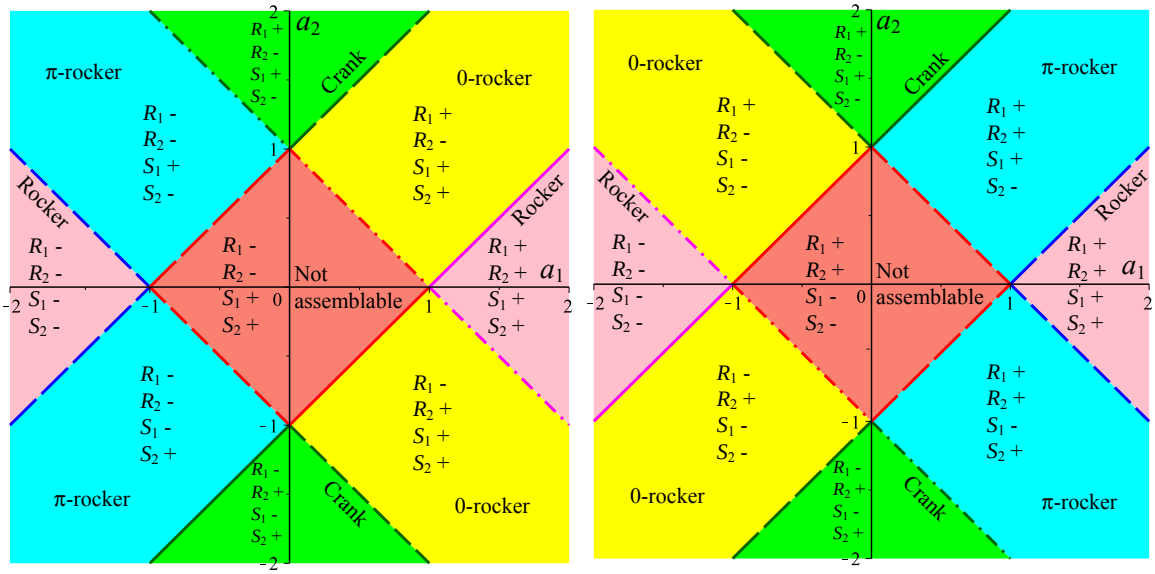

(a) Linkage type regions of the input link in the plane $a_4 = 1$.

(b) Linkage type regions of the input link in the plane $a_4 = -1$.

Figure 5.9: Feasible linkage type regions of the input link within the design parameter space in the planes $a_4 = \pm 1$.

the location of the individual points. These results provide a comprehensive numerical classification scheme based on algebraic parameters, but it also provides an elegant and straightforward graphical method to design planar RRRP linkages with desired mobility characteristics.

5.4 Differential Kinematics

While IO equations can help mechanism designers with position analysis and synthesis, e.g., by finding the most appropriate link lengths for a desired output path, velocity and acceleration values provide information that can be used to evaluate

e.g., the mechanical advantage of the linkage, or the magnitude of the forces acting on the mechanism. Using the algebraic IO equations, the velocity and acceleration loop equations can be directly computed by differentiating with respect to time. For brevity, the velocity and acceleration loop equations are computed for the quadrilateral and the RSSR linkage. However, the approach is general and also applies to any other algebraic IO equation presented in this thesis.

5.4.1 Quadrilateral: $\dot{v}_i$-$\dot{v}_j$ Equations

For the velocity level kinematics, let us consider again the quadrilateral linkage. This example is ideal to demonstrate how the algebraic IO equations fill the gap of today's research. After the works from Kraus [113] and Rosenauers [114] on extreme values in the quadrilateral, Freudenstein published a graphical method using instant centres of velocity (ICV) for determining an extreme of the output to input angular velocity ratio $\dot{\theta}_4/\dot{\theta}_1$ [115, 116]. In his first theorem, he states that this ratio can be expressed by the ratio of the values of the relative directed distances between the three ICVs located on the x_0-axis in the following way:

$$\frac{\dot{\theta}_4}{\dot{\theta}_1} = \frac{d_{P_{13}P_{14}}}{d_{P_{13}P_{14}} + d_{P_{14}P_{34}}}, \tag{5.22}$$

where P indicate the ICVs, as shown in Fig. (5.10). The directed distances $d_{P_{14}P_{34}}$ and $d_{P_{13}P_{14}}$ can be positive or negative depending on their relative directions. Taking this concept one step further, Freudenstein's first theorem also applies to the ICVs on each of the three other Aronhold-Kennedy lines of three collinear ICVs with respect to a number line coincident with the line of three ICVs having its origin on the central ICV. This fact has never been discussed in the literature. The six ICVs are known as *velocity poles* and the curves they move along are described as *polodes*, see [33, 117, 3, 2] for example. However, it seems that the following three velocity ratios expressed as ratios of the absolute values of the relative locations of the three

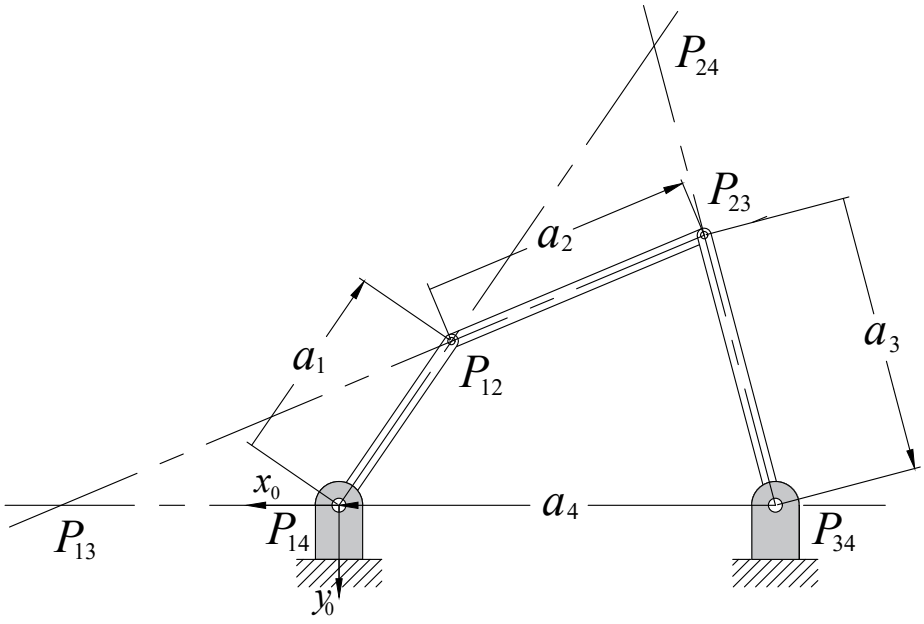

Figure 5.10: The six instantaneous centres of velocity.

ICVs on the three other Aronhold-Kennedy lines, see Figure 5.10, have never been stated explicitly as:

$$\frac{\dot{\theta}_1}{\dot{\theta}_2} = \frac{d_{P_{24}P_{12}}}{d_{P_{24}P_{12}} + d_{P_{12}P_{14}}}; \tag{5.23}$$

$$\frac{\dot{\theta}_3}{\dot{\theta}_2} = \frac{d_{P_{13}P_{12}}}{d_{P_{13}P_{12}} + d_{P_{12}P_{23}}}; \tag{5.24}$$

$$\frac{\dot{\theta}_4}{\dot{\theta}_3} = \frac{d_{P_{24}P_{23}}}{d_{P_{24}P_{23}} + d_{P_{23}P_{34}}}. \tag{5.25}$$

Clearly, in addition to theses four ratios, Eq. (5.22)-(5.25), there must be two other velocity ratios of interest, namely $\dot{\theta}_3/\dot{\theta}_1$ and $\dot{\theta}_4/\dot{\theta}_2$. To obtain expressions for all velocity ratios, the algebraic IO equations can be used as follows.

The equation relating the time rates of change of the joint angle parameters v_1 and v_4 can be determined as the first time derivative of Eq. (4.8):

$$\left((Av_4^2 + B)v_1 - 4a_1a_3v_4\right)\dot{v}_1 + \left((Av_1^2 + C)v_4 - 4a_1a_3v_1\right)\dot{v}_4. \tag{5.26}$$

Because Eq. (5.26) equates to zero, the velocity parameter ratio can be expressed as

$$\frac{\dot{v}_4}{\dot{v}_1} = -\frac{(Av_4^2 + B)v_1 - 4a_1a_3v_4}{(Av_1^2 + C)v_4 - 4a_1a_3v_1}, \tag{5.27}$$

which can also be directly obtained as the implicit derivatives of Eq. (4.8) with respect to v_1 and v_4. It is important to note that for the ith link, $\dot{v}_i \neq \dot{\theta}_i$ since $v_i = \tan(\theta_i/2)$. But it is a simple matter to show that

$$\dot{v}_i = \frac{\dot{\theta}_i(1 + v_i^2)}{2}, \tag{5.28}$$

and that

$$\dot{\theta}_i = \frac{2\dot{v}_i}{(1 + v_i^2)}. \tag{5.29}$$

Hence, the reciprocal of the mechanical advantage is

$$\frac{\dot{\theta}_4}{\dot{\theta}_1} = -\frac{((Av_4^2 + B)v_1 - 4a_1a_3v_4)(1 + v_1^2)}{((Av_1^2 + C)v_4 - 4a_1a_3v_1)(1 + v_4^2)}. \tag{5.30}$$

Using the remaining v_i-v_j equations the remaining velocity parameter equations are expressed as the following ratios

$$\frac{\dot{v}_2}{\dot{v}_1} = -\frac{(A_1B_2v_2^2 + A_2B_1)v_1 - 4a_2a_4v_2}{(A_1B_2v_1^2 + C_1D_2)v_2 - 4a_2a_4v_1}, \tag{5.31}$$

$$\frac{\dot{v}_3}{\dot{v}_1} = -\frac{(A_1B_1v_3^2 + A_2B_2)v_1}{(A_1B_1v_1^2 + C_2D_2)v_3}, \tag{5.32}$$

$$\frac{\dot{v}_3}{\dot{v}_2} = -\frac{(A_1D_2v_3^2 + B_2C_1)v_2 - 4a_1a_3v_3}{(A_1D_2v_2^2 + B_1C_2)v_3 - 4a_1a_3v_2}, \tag{5.33}$$

$$\frac{\dot{v}_4}{\dot{v}_2} = -\frac{(A_1C_1v_4^2 + B_2D_2)v_2}{(A_1C_1v_2^2 + A_2C_2)v_4}, \tag{5.34}$$

$$\frac{\dot{v}_4}{\dot{v}_3} = -\frac{(A_1C_2v_4^2 + B_1D_2)v_3 + 4a_2a_4v_4}{(A_1C_2v_3^2 + A_2C_1)v_4 + 4a_2a_4v_3}. \tag{5.35}$$

Following Freudenstein's geometrical method only four of the ratios could be established. However, it is an easy task to differentiate all six algebraic v_i-v_j IO equations to obtain all velocity ratios. With these velocity profiles, extrema for all joints can be calculated. Moreover, these velocity profiles also lay the foundation to calculate the

acceleration profiles which are crucial to examine the forces acting on the mechanism which will be discussed next.

5.4.2 Quadrilateral: $\ddot{v}_i$-$\ddot{v}_j$ Equations

The acceleration level IO equations, also known as acceleration loop equations, express the angular acceleration parameter generated by joint angle parameter v_i in terms of v_j. The $\ddot{v}_1$-$\ddot{v}_4$ IO equation expresses $\ddot{v}_4$ in terms of $\ddot{v}_1$ at any instant in time as a function of the configuration at that time. That is, if a set of numerical values for four constant link lengths a_1-a_4 are given in a feasible state of numerical values for v_1, v_4, $\dot{v}_1$, $\dot{v}_4$, and $\ddot{v}_1$, then $\ddot{v}_4$ is determined. This in turn means that if the mass centres and distributions are known, the extreme values for $\ddot{v}_1$, and $\ddot{v}_4$ can be used to identify the extreme values of the bearing reaction forces generated by the motion.

According to Freudenstein in [115], the maximum output angular acceleration, assuming constant input angular velocity is computed first for a crank-rocker then drag-link as

$$\ddot{\theta}_{4_{\max}} = \frac{\dot{\theta}_1^2 a_1}{a_2 a_3}(a_1 + a_2) \quad \text{and} \quad \frac{\dot{\theta}_1^2 a_4}{a_2 a_3}(a_2 + a_4). \tag{5.36}$$

But the configuration conditions he lists in the paper are incorrect, and the crank-rocker and drag-link he uses in an example are actually both non-Grashof double-rockers. A reliable way to calculate the extrema of the link's accelerations can, however, be obtained using the velocity loop equations from the previous section.

The time derivative of Eq. (5.26) is

$$\begin{aligned}((Av_4^2 + B)v_1 - 4a_1a_3v_4)\ddot{v}_1 + ((Av_1^2 + C)v_4 - 4a_1a_3v_1)\ddot{v}_4 \\ + (Av_4^2 + B)\dot{v}_1^2 + (Av_1^2 + C)\dot{v}_4^2 + (4Av_1v_4 - 8a_1a_3)\dot{v}_1\dot{v}_4.\end{aligned} \tag{5.37}$$

The angular acceleration parameters, $\ddot{v}_i$, are related to the angular accelerations,

$\ddot{\theta}_i$, as

$$\ddot{v}_i = \frac{1}{2}(\ddot{\theta}_i + \dot{\theta}_i{}^2 v_i)(1 + v_i^2), \tag{5.38}$$

and

$$\ddot{\theta}_i = \frac{2\ddot{v}_i}{(1 + v_i^2)} - \dot{\theta}_i^2 v_i. \tag{5.39}$$

The five other angular acceleration parameter equations are

$$\begin{aligned}((A_1B_2v_2^2 + A_2B_1)v_1 - 4a_2a_4v_2)\ddot{v}_1 + ((A_1B_2v_1^2 + C_1D_2)v_2 - 4a_2a_4v_1)\ddot{v}_2 \\ + (A_1B_2v_2^2 + A_2B_1)\dot{v}_1^2 + (A_1B_2v_1^2 + C_1D_2)\dot{v}_2^2 + (4A_1B_2v_1v_2 - 8a_2a_4)\dot{v}_1\dot{v}_2,\end{aligned} \tag{5.40}$$

$$\begin{aligned}(A_1B_1v_3^2 + A_2B_2)v_1\ddot{v}_1 + (A_1B_1v_1^2 + C_2D_2)v_3\ddot{v}_3 \\ + (A_1B_1v_3^2 + A_2B_2)\dot{v}_1^2 + (A_1B_1v_1^2 + C_2D_2)\dot{v}_3^2 + 4A_1B_1v_1v_3\dot{v}_1\dot{v}_3,\end{aligned} \tag{5.41}$$

$$\begin{aligned}((A_1D_2v_3^2 + B_2C_1)v_2 - 4a_1a_3v_3)\ddot{v}_2 + ((A_1D_2v_2^2 + B_1C_2)v_3 - 4a_1a_3v_2)\ddot{v}_3 \\ + (A_1D_2v_3^2 + B_2C_1)\dot{v}_2^2 + (A_1D_2v_2^2 + B_1C_2)\dot{v}_3^2 + (4A_1D_2v_2v_3 - 8a_1a_3)\dot{v}_2\dot{v}_3,\end{aligned} \tag{5.42}$$

$$\begin{aligned}(A_1C_1v_4^2 + B_2D_2)v_2\ddot{v}_2 + (A_1C_1v_2^2 + A_2C_2)v_4\ddot{v}_4 \\ + (A_1C_1v_4^2 + B_2D_2)\dot{v}_2^2 + (A_1C_1v_2^2 + A_2C_2)\dot{v}_4^2 + 4A_1C_1v_2v_4\dot{v}_2\dot{v}_4,\end{aligned} \tag{5.43}$$

$$\begin{aligned}((A_1C_2v_4^2 + B_1D_2)v_3 + 4a_2a_4v_4)\ddot{v}_3 + ((A_1C_2v_3^2 + A_2C_1)v_4 + 4a_2a_4v_3)\ddot{v}_4 \\ + (A_1C_2v_4^2 + B_1D_2)\dot{v}_3^2 + (A_1C_2v_3^2 + A_2C_1)\dot{v}_4^2 + (4A_1C_2v_3v_4 + 8a_2a_4)\dot{v}_3\dot{v}_4.\end{aligned} \tag{5.44}$$

These equations allow to evaluate extreme angular accelerations which in return can be used to determine the inertial reaction forces in the frame-attached bearings of the mechanism. Since the velocities and accelerations are obtained directly, calculating the extrema is made significantly easier compared to traditional vector methods.

An example of determining the velocity and acceleration extrema of the quadrilateral is provided in [20], and an example of the RSSR will follow hereinafter.

5.4.3 RSSR: Extreme Angular Velocity and Acceleration Example

Finally, let us consider an example to determine the extreme output angular velocities and accelerations for a constant input angular velocity. These are important for bearing sizing, among other design considerations that are vital to robust mechanical design of linkages. While there have been some investigations in the literature examining these extreme values for the RSSR, and the configurations in which they occur, there are no straightforward methods to be found that give explicit algebraic equations for computing the extremes for the RSSR, see [118] for an example. In contrast, following the procedure as outlined for the quadrilateral in the previous chapter, the velocity and acceleration IO equations resulting from Eq. (4.91) can be computed in two steps. To identify extreme angular velocity and acceleration outputs for a constant input angular velocity requires that the angle parameters be transformed back into angles. While $\dot{\theta}_1$ may be constant the corresponding parameter $\dot{v}_1$ is not since it is configuration dependent. That is

$$\dot{v}_1 = \frac{\dot{\theta}_1(v_1^2+1)}{2}. \tag{5.45}$$

The next step is to take the first two time derivatives of Eq. (4.91), which will not be listed here in the interest of brevity. The extreme angular velocities and accelerations, along with the configurations in which they occur in both assembly modes can be easily obtained computationally with the following two algorithms.

Extreme RSSR angular velocity algorithm.

If values for a_1, a_4, a_7, a_8, d_1, d_8, and α_8 are specified and the input angular velocity

is a constant specified value, we wish to determine the critical values $\theta_{1_{\text{crit}}}$ that result in $\dot{\theta}_{8_{\text{max/min}}}$, so we need to eliminate θ_8 from both the position and angular velocity IO equations.

1. Convert v_1 and v_8 in the IO equation to angles as $v_i = \tan(\theta_i/2)$ and solve for θ_8.

2. Substitute the expression for θ_8 from Step 1 into the $\dot{\theta}_1$-$\dot{\theta}_8$ equation and solve for $\dot{\theta}_8$, which gives $\dot{\theta}_8 = f(\theta_1)$ since $\dot{\theta}_1$ is a specified constant.

3. Solve $\dfrac{d\dot{\theta}_8}{d\theta_1} = 0$ for $\theta_{1_{\text{crit}}}$ and determine the values of $\dot{\theta}_{8_{\text{max/min}}}$ corresponding to each distinct value of $\theta_{1_{\text{crit}}}$.

Extreme RSSR angular acceleration algorithm.

If values for a_1, a_4, a_7, a_8, d_1, d_8, and α_8 are specified and the input angular velocity is a constant specified value, we wish to determine the critical values $\theta_{1_{\text{crit}}}$ that result in $\ddot{\theta}_{8_{\text{max/min}}}$, so we need to eliminate θ_8 and $\dot{\theta}_8$ from the position, angular velocity and acceleration IO equations.

1. Convert v_1 and v_8 in the IO equation to angles as $v_i = \tan(\theta_i/2)$ and solve for θ_8.

2. Substitute the expression for θ_8 from Step 1 into the $\dot{\theta}_1$-$\dot{\theta}_8$ equation and solve for $\dot{\theta}_8$, which gives $\dot{\theta}_8 = f(\theta_1)$ since $\dot{\theta}_1$ is a specified constant.

3. Substitute the expressions for θ_8 and $\dot{\theta}_8$ into the $\ddot{\theta}_1$-$\ddot{\theta}_8$ equation.

4. Solve the resulting equation for $\ddot{\theta}_8$, which gives $\ddot{\theta}_8 = f(\theta_1)$ since $\ddot{\theta}_1 = 0$.

5. Solve $\dfrac{d\ddot{\theta}_8}{d\theta_1} = 0$ for $\theta_{1_{\text{crit}}}$ and determine the values of $\ddot{\theta}_{8_{\text{max/min}}}$ corresponding to each distinct value of $\theta_{1_{\text{crit}}}$.

For an example, let the DH parameters be $a_1 = 1/8$, $a_4 = 4$, $a_7 = 1$, $a_8 = 1/8$,

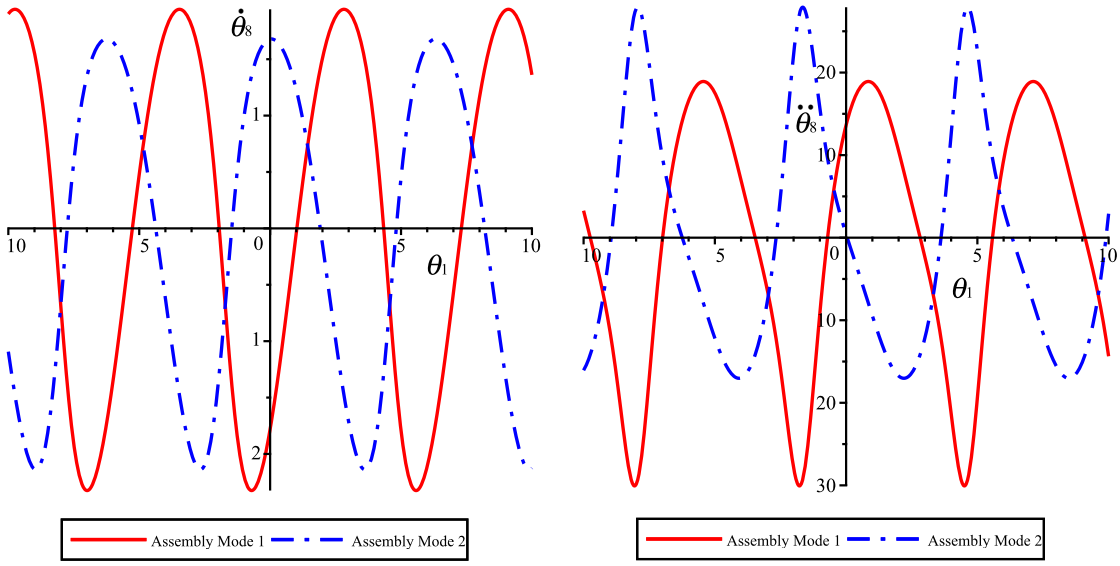

(a) RSSR angular velocity profile.

(b) RSSR angular acceleration profile.

Figure 5.11: RSSR angular velocity and acceleration profiles for $a_1 = 1/8$, $a_4 = 4$, $a_7 = 1$, $a_8 = 1/8$, $\alpha_8 = \tan((60\pi/180)/2)$, $d_1 = 2$, $d_8 = 2$, $\dot{\theta}_1 = 10$ rad/s.

$\alpha_8 = \tan((60\pi/180)/2)$, $d_1 = 2$, $d_8 = 2$ and the constant input angular velocity be $\dot{\theta}_1 = 10$ rad/s. Using the two algorithms above the output angular velocity and acceleration are expressed in terms of the input angle, see Figs. 5.11. The extreme angular accelerations for an RSSR linkage have not been reported in the literature until now. Even if this is not precisely so, it is clear that the algebraic form of the RSSR equation in the form presented herein has distinct advantages for computation compared to any other representation. The extreme angular accelerations $\ddot{\theta}_{8_{\text{max/min}}}$ and critical input angles are computed and listed in Tab. 5.7.

Table 5.7: $\ddot{\theta}_{8_{\text{max/min}}}$ and $\theta_{1_{\text{crit}}}$ for $\dot{\theta}_1 = 10$ rad/s.

Assembly Mode	$\ddot{\theta}_{8_{\text{max/min}}}$ rad/s^2	$\theta_{1_{\text{crit}}}$ rad
1	18.91834314	0.8463167974
	-30.06554948	4.506090280
2	-17.03055542	2.201742476
	27.91274981	4.631288097

To the best of the author's knowledge, computational examples determining the extreme output angular accelerations, and corresponding configurations cannot be found in the body of archival literature.

Chapter 6

Conclusion

In this chapter, the key findings are summarised by answering the research questions provided in the introduction of this thesis and by discussing the main contribution to the field. This chapter will also examine the limitations and propose opportunities for further research.

This thesis aimed to generalise the procedure for determining one single method to obtain the algebraic IO equations for any kinematic architecture of a four-bar linkage using only algebraic means. The proposed method consisted of considering the linkages as an open kinematic chain which is described using the standard DH parameters. Subsequently, the overall displacement of the end-effector of the chain is mapped into Study's kinematic image space and the linkage is conceptually closed by equating the resulting set of polynomials to the identity which results in a complete and general description of the linkage. Finally, the polynomial equations are manipulated using elimination techniques from algebraic geometry to obtain the desired algebraic IO equations.

The algebraic IO equations of all planar linkages discussed in this thesis, namely the quadrilateral, slider-crank and double slider linkages, are derived following the

exact same procedure. Clearly, the DH parameters differ with each linkage in the initial problem statement. However, due to the simplicity of the linkages and the constraint to move in a plane, the overall displacements map to four Study parameters each. Equating these four polynomials to the identity in Study's kinematic image space, leaves only three equations that define the ideal which contains all information on each of the planar linkages. Applying Gröbner bases with elimination ordering "`lexdeg`" in Maple 2021 to eliminate two DH link variables reveals six algebraic IO equations for each planar four-bar linkage. Each of these six equations is relating two link variables and share the same coefficients.

Similar to the planar linkages, the IO equation of the spherical linkage was derived by establishing the DH parameters, and mapping the displacement of the four-bar chain on Study's quadric. As expected, the last four Study parameters have zero entries since there are no translational movements. After equating the overall displacement to its identity, the ideal describing the linkage also consists of three polynomial equations. Interestingly, the Gröbner basis elimination ordering "`lexdeg`" is computationally very demanding. Instead, the monomial orderings "`tdeg`" followed by "`plex`" lead, with one exception, to the desired algebraic IO equations. Eliminating the first and last link variables to obtain the IO equation relating the two intermediate joint variables, the v_3-v_3 equation, required a different sequence of monomial orderings: "`tdeg`" followed by "`grlex`".

The derivation of the algebraic IO equation of the Bennett linkage follows the same steps as for the planar linkages. First, the linkage is described using DH parameters. As this linkage involves spatial movements, the overall displacement of the end-effector with respect to the base frame maps to eight Study parameters which simplify by substituting the well-known Bennett conditions. Thus, after equating the set of polynomials to the identity, the ideal describing the linkage consists of

seven polynomial equations. Joint variables are eliminated using Gröbner bases with elimination ordering "`lexdeg`" that yields all six algebraic IO equations.

In contrast to all previous discussed IO equation derivations, the second spatial linkage, the RSSR, requires a different elimination procedure. While describing the linkage with standard DH parameters and establishing the closure equation by equating the overall displacement to its identity remains the same, the linkage is separated into two dyads which are both expressed explicitly using Study parameters. Applying the linear implicitisation algorithm yields four hyperplanes in terms of the Study parameters for each dyad which can be solved to obtain the algebraic IO equation of the RSSR linkage.

Taken together, these results suggest that the procedure described herein is a sophisticated method for obtaining algebraic IO equations of four-bar linkages. There are no geometric insights of the linkage required except in the initial statement when the DH parameters are defined. Moreover, there are no trigonometric expressions involved which facilitates computing IO equations with modern algebra software.

The most important limitation, however, lies in manipulating the ideal that results from equating the Study parameters to the identity. The more complex the kinematic chain, such as spatial chains with lower pairs containing more than one dof, the larger the polynomials, and the more motion and design parameters are involved in the ideal. As the example of the RSSR has shown, it was not possible to apply Gröbner bases in order to eliminate the intermediate joint angles. While computing a Gröbner basis would in theory lead to a solution, the algorithm does not necessarily finish in practice with the processing power available for this thesis. Nonetheless, this work has shown that Gröbner bases constitute a great elimination tool for all planar and spherical four-bar linkages.

Although this thesis was limited to a selection of linkages, the results indicate that

it is feasible to use the suggested procedure to obtain algebraic IO equations for other less investigated linkages. Clearly, having access to additional IO equations opens up new perspectives in terms of finding a linkage that approximates a desired function with minimal error. This could ultimately lead mechanical designers to choose from a wider variety of linkages that "best" approximate the desired task.

In addition, Chapter 5 illustrated some concrete applications of the derived algebraic IO equations. One promising application of the algebraic IO equations is the evaluation of singular positions of the linkage using simple calculus. In addition, this work has also revealed that the algebraic IO equations can easily be analysed to examine the linkages' relative mobility by determining the nature of its double points and whether a link is assemblable at $v_i = 0$. One interesting aspect that emerged from the mobility analysis of the quadrilateral linkage is its representation in the newly interpreted design parameter space which is spanned by the different link length parameters. Every point in this space symbolises a proper linkage that lies in a region with particular mobility information. Thus, mechanical designers can use this tool for quickly analysing a given linkage on the link's relative mobility. Finally, the algebraic IO equations can be beneficial in determining the velocity and acceleration kinematics. As an example has shown, the algebraic IO equations can be efficiently differentiated and used to find extreme velocities and accelerations.

Overall, the results presented in this thesis are encouraging and should be validated by applying the algebraic IO equation derivation technique to other linkages, such as the Bricard orthogonal 6R linkage. Furthermore, this study provides a backbone for continuous approximate synthesis as the optimisers of computer algebra software require less processing time for integrating algebraic over trigonometric terms. Not only does this thesis provide the algebraic IO equations, but it also revealed algebraic velocity and acceleration equations that can be used for kinematic synthesis.

Research into using these algebraic IO equations for kinematic synthesis is already underway.

Bibliography

[1] R.L. Norton. *Design of Machinery,* 5^{th} Edition. McGraw-Hill, New York, NY, U.S.A., 2012.

[2] J.M. McCarthy and G.S. Soh. *Geometric Design of Linkages,* , 2^{nd} Edition Interdisciplinary Applied Mathematics. Springer, New York, N.Y., 2011.

[3] R.S. Hartenberg and J. Denavit. *Kinematic synthesis of linkages*. McGraw-Hill, Book Co., New York, N.Y., U.S.A., 1964.

[4] J. Denavit. *Description and Displacement Analysis of Mechanisms Based on* (2×2) *Dual Matrices*. PhD thesis, Northwestern University, 1956.

[5] A. Guigue and M.J.D. Hayes. Continuous Approximate Synthesis of Planar Function-generators Minimising the Design Error. *Mechanism and Machine Theory*, 101:158–167, 2016.

[6] M. Rotzoll, M.H. Regan, M.J.D. Hayes, and M.L. Husty. Kinematic Geometry of Spatial RSSR Mechanisms. *Mechanism and Machine Theory*, 185(105335), 2023.

[7] M.J.D. Hayes, M.L. Husty, and M. Pfurner. Input-output Equation for Planar Four-bar Linkages. In J. Lenarčič and V. Parenti-Castelli, editors, *Advances in Robot Kinematics 2018*, pages 12–19, Cham, Switzerland, 2018. Springer

International Publishing.

[8] O. Bottema and B. Roth. *Theoretical Kinematics*. Dover Publications, Inc., New York, NY, U.S.A., 1990.

[9] M. Pfurner, T. Stigger, and M.L. Husty. Algebraic analysis of overconstrained single loop four link mechanisms with revolute and prismatic joints. *Mechanism and Machine Theory*, 114:11–19, 2017.

[10] E. Study. *Geometrie der Dynamen*. Teubner Verlag, Leipzig, Germany, 1903.

[11] M.L. Husty and H.-P. Schröcker. Kinematics and Algebraic Geometry. In *21st Century Kinematics*, pages 85–123. Springer London Heidelberg New York Dordrecht, 2013.

[12] M.L. Husty and D.R. Walter. *Mechanism Constraints and Singularities - the Algebraic Formulation*, pages 101–180. CISM International Centre for Mechanical Sciences 589. Springer International Publishing, Cham, Switzerland, 2019.

[13] K. Brunnthaler. *Synthesis of 4R Linkages Using Kinematic Mapping*. PhD thesis, University of Innsbruck, Innsbruck, Austria, 2006.

[14] M. Pfurner. *Analysis of spatial serial manipulators using kinematic mapping*. PhD thesis, University of Innsbruck, Innsbruck, Austria, 2006.

[15] B. Buchberger. *Ein Algorithmus zum Auffinden der Basiselemente des Restklassenringes nach einem nulldimensionalen Polynomideal*. PhD thesis, University of Innsbruck, Innsbruck, Austria, 1965.

[16] D.R. Walter and M.L. Husty. On Implicitization of Kinematic Constraint Equations. *Machine Design & Research (CCMMS 2010)*, 26:218–226, 2010.

[17] Z.A. Copeland and M.J.D. Hayes. Multi-modal Continuous Approximate Synthesis of Planar Four-bar Function Generators. *International Journal of Mech-*

anisms and Robotic Systems, 2022. Accepted for publication October 6, 2022.

[18] M.J.D. Hayes, M. Rotzoll, Q. Bucciol, and Z.A. Copeland. Planar and Spherical Four-bar Linkage v_i-v_j Algebraic Input-output Equations. *Mechanism and Machine Theory*, 182(105222), 2023.

[19] M. Rotzoll, Q. Bucciol, and M.J.D. Hayes. Algebraic Input-output Angle Equation Derivation Algorithm for the Six Distinct Angle Pairings in Arbitrary Planar 4R Linkages. In *20th International Conference on Advanced Robotics, ICAR 2021,* Ljubljana, Slovenia, 2021.

[20] M.J.D. Hayes, M. Rotzoll, A. Iraei, A. Nichol, and Q. Bucciol. Algebraic Differential Kinematics of Planar 4R Linkages. 20th International Conference on Advanced Robotics, ICAR 2021, Ljubljana, Slovenia, 2021.

[21] M. Rotzoll and M.J.D. Hayes. A General Method for Determining Algebraic Input-output Equations for the Slider-crank and the Bennett Linkage. *11^{th} CCToMM Symposium on Mechanisms, Machines, and Mechatronics*, Ontario Tech University, Oshawa, ON, Canada, June 3-4, 2021.

[22] A. Nichol, M. Rotzoll, and M.J.D. Hayes. Planar RRRP Mechanism Design Parameter Space. *11^{th} CCToMM Symposium on Mechanisms, Machines, and Mechatronics*, Ontario Tech University, Oshawa, ON, Canada, June 3-4, 2021.

[23] M.J.D. Hayes and M. Rotzoll. Mobility Classification in the Design Parameter Space of Spherical 4R Linkages. *11^{th} CCToMM Symposium on Mechanisms, Machines, and Mechatronics*, Ontario Tech University, Oshawa, ON, Canada, June 3-4, 2021.

[24] Z.A. Copeland, M. Rotzoll, and M.J.D. Hayes. Continuous Type and Dimensional Continuous Approximate Function Generator Synthesis for All Planar Four-bar Mechanisms. *11^{th} CCToMM Symposium on Mechanisms, Machines,*

and Mechatronics, Ontario Tech University, Oshawa, ON, Canada, June 3-4, 2021.

[25] M.J.D. Hayes, M. Rotzoll, C. Ingalls, and M. Pfurner. Design Parameter Space of Spherical Four-bar Linkages. In D. Pisla, B. Corves, and C. Vaida, editors, *New Trends in Mechanism and Machine Science: EuCoMeS 2020,* Volume 89, pages 19–27, Cham, Switzerland, 2020. Springer International Publishing.

[26] M. Rotzoll, M.J.D. Hayes, M.L. Husty, and M. Pfurner. A General Method for Determining Algebraic Input-output Equations for Planar and Spherical 4R Linkages. In J. Lenarčič and B. Siciliano, editors, *Advances in Robot Kinematics 2020,* Volume 15, pages 90–97, Cham, Switzerland, 2021. Springer International Publishing.

[27] M.J.D. Hayes, M. Rotzoll, M.L. Husty, and M. Pfurner. Design Parameter Space of Planar Four-bar Linkages. Proceedings of the 15^{th} IFToMM World Congress, June 30-July 4, 2019.

[28] M. Rotzoll, M.J.D. Hayes, and M.L. Husty. An Algebraic Input–output Equation for Planar RRRP and PRRP Linkages. *Transactions of the Canadian Society for Mechanical Engineering*, 44(4):520–529, 2020.

[29] M. Rotzoll, M.J.D. Hayes, and M.L. Husty. An Algebraic Input-Output Equation for Planar RRRP and PRRP Linkages. *Proceedings of the 10^{th} CCToMM Symposium on Mechanisms, Machines, and Mechatronics*, École de technologie supérieure, Montréal, QC, Canada, May 16-17, 2019.

[30] T.W. Wright. *Elements of mechanics including kinematics, kinetics and statics, with applications.* D. Van Nostrand Company, 1898.

[31] J.J. Uicker, Pennock. G.R., and J.E. Shigley. *Theory of Machines and Mechanisms,* 5^{th} Edition. Oxford University Press, New York, N.Y., 2017.

[32] J. Angeles. *Fundamentals of Robotic Mechanical Systems,* 4^{th} Edition. Springer International Publishing Switzerland, 2014.

[33] F. Reuleaux and A.B.W. Kennedy. *The Kinematics of Machinery: Outlines of a Theory of Machines.* Kessinger Publishing, 1876.

[34] J.E. Shigley and J.J. Uicker. *Theory of Machines and Mechanisms.* McGraw-Hill, New York, 1980.

[35] X.-J. Liu and J. Wang. *Parallel Kinematics.* Springer-Verlag Berlin Heidelberg, 2014.

[36] C.M. Gosselin and J. Angeles. Singularity Analysis of Closed-Loop Kinematic Chains. *IEEE Transactions on Robotics and Automation*, 6(3):281–290, 1990.

[37] A. Müller and D. Zlatanov. *Singular Configurations of Mechanisms and Manipulators.* Springer, Cham, Switzerland, 2019.

[38] D. Zlatanov, R.G. Fenton, and B. Benhabib. Singularity analysis of mechanisms and robots via a motion-space model of the instantaneous kinematics. In *Proceedings of the 1994 IEEE International Conference on Robotics and Automation,* Volume 2, pages 980–985, San Diego, CA, USA, 1994. IEEE.

[39] J. Angeles. Kinematic Synthesis. Lecture Notes MECH451, Department of Mechanical Engineering and McGill Centre for Intelligent Machines, January 2016.

[40] M.J.D. Hayes. *Kinematics of General Planar Stewart-Gough Platforms.* PhD thesis, McGill University, Montréal, Qué, Canada, 1999.

[41] F. Freudenstein. *Design of Four-link Mechanisms.* PhD thesis, Columbia University, New York, N.Y., USA, 1954.

[42] S. De Sa. *Classification and Properties of Planar Motion using Kinematic Map-*

ping. PhD thesis, Stanford University, 1979.

[43] B. Ravani and B. Roth. Mappings of Spatial Kinematics. *ASME, J. of Mechanisms, Transmissions, & Automation in Design*, 106:341–347, 1984.

[44] J. Angeles. *Rational Kinematics*. Springer Verlag New York, 1988.

[45] J. Yao and J. Angeles. The Kinematic Synthesis of Steering Mechanisms. *Transactions of the Canadian Society for Mechanical Engineering*, 24(3-4):453–476, 2000.

[46] M. Choubey and A.C. Rao. Synthesizing linkages with minimal structural and mechanical error based upon tolerance allocation. *Mechanism and Machine Theory*, 17(2):91–97, 1982.

[47] G.L. Bradley and K.J. Smith. *Calculus*. Prentice Hall, Englewood Cliffs, NJ, U.S.A., 1995.

[48] M.L. Husty and M. Pfurner. An Algebraic Version of the Input-output Equation of Planar Four-bar Mechanisms. pages 746–757. *International Conference on Geometry and Graphics*, Milan, Italy, 2018.

[49] J.K. Pickard, J.A. Carretero, and J.-P. Merlet. Appropriate analysis of the four-bar linkage. *Mechanism and Machine Theory*, 139:237–250, 2019.

[50] M. Muller. A novel classification of planar four-bar linkages and its application to the mechanical analysis of animal systems. *Philosophical Transactions of the Royal Society of London. Series B: Biological Sciences*, 351(1340):689–720, 1996.

[51] C.R. Barker. A complete classification of planar four-bar linkages. *Mechanism and Machine Theory*, 20(6):535–554, 1985.

[52] A.P. Murray and P.M. Larochelle. A Classification Scheme for Planar $4R$, Spher-

ical $4R$, and Spatial $RCCR$ Linkages to Facilitate Computer Animation. *Proceedings of 1998 ASME Design Engineering Technical Conferences (DETC'98)*, Atlanta, Georgia, U.S.A., September 13-16, 1998.

[53] F.W. Merchant and C.A. Chant. *The Ontario High School Physics*. Copp, Clark Co. Ltd., 1917.

[54] W. Wunderlich. *Ebene Kinematik*. Hochschultaschenbücher-Verlag, Mannheim, Wien, Zürich, 1970.

[55] F. van Schooten. *Mathematische Oeffeningen*. Gerrit van Goedesbergh, 1646.

[56] C.M. Gosselin and J.-F. Hamel. The agile eye: a high-performance three-degree-of-freedom camera-orienting device. In *Proceedings of the 1994 IEEE international conference on robotics and automation*, pages 781–786. IEEE, 1994.

[57] N. Sancisi, D. Zannoli, V. Parenti-Castelli, C. Belvedere, and A. Leardini. A one-degree-of-freedom spherical mechanism for human knee joint modelling. *Proceedings of the Institution of Mechanical Engineers, Part H: Journal of Engineering in Medicine*, 225(8):725–735, 2011.

[58] C.H. Chiang. Spherical kinematics in contrast to planar kinematics. *Mechanism and machine theory*, 27(3):243–250, 1992.

[59] J. M. McCarthy. Planar and Spatial Rigid Motion as Special Cases of Spherical and 3-Spherical Motion. *Journal of Mechanisms, Transmissions, and Automation in Design*, 105(3):569–575, 1983.

[60] H.S.M. Coxeter. *Non-Euclidean Geometry,* 5^{th} Edition. University of Toronto Press, Toronto, On., Canada, 1965.

[61] W.T. Fishback. *Projective and Euclidean Geometry,* 2^{nd} Edition. John Wiley & Sons, Inc., New York, N.Y., U.S.A., 1969.

[62] An Tzu Yang. *Application of quaternion algebra and dual numbers to the analysis of spatial mechanisms*. PhD thesis, Columbia University Morningside Heights, New York, 1963.

[63] W. Pin, L. Hong, and W. Shi'en. New method for input-output equation of spherical four-bar mechanism. In *2011 International Conference on Multimedia Technology*, pages 4986–4989, Hangzhou, China, 2011. IEEE.

[64] E.L. Harrisberger. *Gross motions of a space mechanism*. PhD thesis, Purdue University, 1963.

[65] G.T. Bennett. A New Mechanism. *Engineering*, 76:777, 1903.

[66] K.H. Hunt. *Kinematic Geometry of Mechanisms*. Clarendon Press, Oxford, England, 1978.

[67] J.E. Baker. Kinematic Investigation of the Deployable Bennett Loop. *Journal of Mechanical Design*, 129(6):602–610, 2006.

[68] M. Skreiner. Methods to identify the mobility regions of a spatial four-link mechanism. *Journal of Mechanisms*, 2(4):415–427, 1967.

[69] H. Nolle. Ranges of motion transfer by the R-G-G-R linkage. *Journal of Mechanisms*, 4(2):145–157, 1969.

[70] E.L. Harrisberger. Space crank mechanisms. *Machine Design*, 36(10):170–175, 1964.

[71] O. Bottema. The motion of the skew four-bar. *Journal of Mechanisms*, 6(1):69–79, 1971.

[72] F. Freudenstein and E.J.F. Primrose. On the Criteria for the Rotatability of the Cranks of a Skew Four-bar Linkage. *ASME Journal of Engineering for Industry*, 98(4):1285–1288, 1976.

[73] N.M. Abbasi. Review of the geometry of screw axes. Retrieved December 6, 2022, from *https://www.12000.org/my_notes/screw_axis/index.htm*, 2006.

[74] M.L. Husty, A. Karger, H. Sachs, and W. Steinhilper. *Kinematik und Robotik*. Springer-Verlag Berlin Heidelberg New York, 1997.

[75] J. Grünwald. Ein Abbildungsprinzip, welches die ebene Geometrie und Kinematik mit der räumlichen Geometrie verknüpft. *Sitzber. Ak. Wiss. Wien*, 120:677–741, 1911.

[76] W. Blaschke. *Kinematik und Quaternionen,* Volume 4. Deutscher Verlag der Wissenschaften, Berlin, 1960.

[77] H.R. Müller. *Sphärische Kinematik,* Volume 6. Deutscher Verlag der Wissenschaften, 1962.

[78] J.M. Selig. *Geometric Fundamentals of Robotics,* 2^{nd} Edition. Springer Science + Business Media Inc, New York, NY, U.S.A., 2005.

[79] D.F. Scharler. Characterization of lines in the extended kinematic image space. Master's thesis, University of Innsbruck, Innsbruck, Austria, 2017.

[80] B.O. Rodriguez. Des lois géométriques qui régissent les déplacements d'un système solide dans l'espace: et de la variation des cordonnées provenant de ces déplacements considérés indépendamment des causes qui peuvent les produire. *Journal Mathématiques Pures Appliquées*, 5:380–440, 1840.

[81] W.R. Hamilton. On quaternions, or on a new system of imaginaries in algebra: Copy of a letter from Sir William R. Hamilton to John T. Graves, esq. on quaternions. *The London, Edinburgh, and Dublin Philosophical Magazine and Journal of Science*, 25:489–495, 1844.

[82] L. Euler. Formulae generales pro translatione quacunque corporum rigidorum.

Novi Commentarii academiae scientiarum Petropolitanae, 20:189–207, 1776.

[83] W.K. Clifford. A Preliminary Sketch of Biquaternions. *Proceedings of the London Mathematical Society*, 4(64,65):381–395, 1873.

[84] M.J.D. Hayes. Advanced kinematics: Geometry. Lecture Notes MECH5507, Department of Mechanical and Aerospace Engineering, Carleton Univerity, January 2020.

[85] A.J. Sommese and C.W. Wampler. *The Numerical Solution Of Systems Of Polynomials Arising In Engineering And Science*. World Scientific Publishing Co. Pte. Ldt., Hackensack, NJ, U.S.A., 2005.

[86] B. Odehnal, H. Stachel, and G. Glaeser. *The Universe of Quadrics*. Springer-Verlag GmbH, Berlin, Germany, 2020.

[87] H. Anton. *Elementary Linear Algebra*. John Wiley and Sons, Inc., New York, NY, U.S.A, 1987.

[88] D.C. Lay. *Linear Algebra and Its Applications*. Pearson Education Inc., 2012.

[89] J.K. Eberharter and B. Ravani. Curves and Surfaces on Study's Quadric. The Fifth International Conference on Curves and Surfaces, Saint-Malo, France, June 2002.

[90] J.M. Selig. On the Geometry of the Homogeneous Representation for the Group of Proper Rigid-body Displacements. *Rom. J. Techn. Sci. – Appl. Mechanics*, 58(1-2):153–176, 2013.

[91] A. Gfrerrer. Study's Kinematic Mapping — A Tool for Motion Design. In J. Lenarčič and M. M. Stanišić, editors, *Advances in Robot Kinematics*, pages 7–16. Springer, Dordrecht Netherlands, 2000.

[92] J.J. Craig. *Introduction to Robotics, Mechanics and Control,* 4^{th} Edition.

Addison-Wesley Publishing Co., Reading, MA, U.S.A., 2017.

[93] J. Denavit and R.S. Hartenberg. A Kinematic Notation for Lower-pair Mechanisms Based on Matrices. *Trans ASME J. Appl. Mech.*, 23:215–221, 1955.

[94] B.W. Mooring, Z.S. Roth, and M.R. Driels. *Fundamentals of Manipulator Calibration*. John Wiley & Sons, Inc., New York, NY, U.S.A., 1991.

[95] C.H. An, C.G. Atkeson, and J.M. Hollerbach. *Model-based Control of a Robot Manipulator*. The MIT Press, Cambridge, MA, U.S.A., 1988.

[96] S.A. Hayati. Robot Arm Geometric Link Parameter Estimation. *Proc. 22nd IEEE Conf. on Decision and Control, San Antonio, TX, U.S.A.*, pages 1477–1483, 1983.

[97] M.L. Husty, M. Pfurner, and H.-P. Schröcker. A New and Efficient Algorithm for the Inverse Kinematics of a General Serial 6R Manipulator. *Mechanism and Machine Theory*, 47:66–81, 2007.

[98] D. Cox, J. Little, and D. O'Shea. *Ideals, Varieties, and Algorithms: an Introduction to Computational Algebraic Geometry and Commutative Algebra,* 2^{nd} Edition. Springer, Berlin, Germany, 1997.

[99] F.S. MacAulay. Some Formulæ in Elimination. *Proceedings of the London Mathematical Society*, s1-35(1):3–27, 05 1902.

[100] D.A. Cox, J. Little, and D. O'shea. *Using Algebraic Geometry,* 2^{nd} Edition, Volume 185. Springer Science & Business Media, 2005.

[101] W.W. Adams and P. Loustaunau. *An Introduction to Gröbner Bases,* Volume 3. American Mathematical Society, 1994.

[102] S.S. Balli and S. Chand. Transmission Angle in Mechanisms (Triangle in Mech). *Mechanism and Machine Theory*, 37(2):175–195, 2002.

[103] A. Harnak. Über die Vieltheiligkeit der ebenen algebraischen Curven. *Mathematische Annalen*, 10:189–198, 1876.

[104] R. Bricard. Mémoire sur la théorie de l'octaèdre articulé. *J. Math. Pures Appl.*, 3:113–148, 1897.

[105] A. Dresden. *Solid Analytic Geometry and Determinants*. John Wiley & Sons, Inc., New York, NY, U.S.A., 1930.

[106] H. Hilton. *Plane Algebraic Curves*. Clarendon Press, Oxford, England, 1920.

[107] R. Cipolla and P. Giblin. *Visual Motion of Curves and Surfaces*. Cambridge University Press, Cambridge, U.K., 2000.

[108] C.M. Gosselin and J. Angeles. Graphical representation of the mobility region of planar and spherical four-bar linkages. *Mechanism and Machine Theory*, 22(6):557–562, 1987.

[109] C. M. Gosselin and J. Angeles. Mobility Analysis of Planar and Spherical Linkages. *Computers in Mechanical Engineering*, pages 56–60, July/August 1988.

[110] C.M. Gosselin and J. Angeles. Optimization of Planar and Spherical Function Generators as Minimum-defect Linkages. *Mechanism and Machine Theory*, 24(4):293–307, 1989.

[111] H.S.M. Coxeter. *Regular Polytopes, 3^{rd} Edition*. Dover Publications, Inc., New York, NY, U.S.A., 1973.

[112] B. Segre. *The Non-singular Cubic Surfaces; a New Method of Investigation with Special Reference to Questions of Reality*. Oxford, The Clarendon Press, 1942.

[113] R. Kraus. Die Doppelkurbel und ihre Geschwindigkeitsgrenzen. *Maschinenbau/Getriebetechnik*, 18:37–41, 1939.

[114] N. Rosenauer. Gelenkvierecke mit vorgeschriebenen Groesst und Kleinstwerten der Abtriebswinkelgeschwindigkeit. *Werkstattstechnik*, 38:25–27, 1944.

[115] F. Freudenstein. On the Maximum and Minimum Velocities and the Accelerations in Four-link Mechanisms. *Trans. ASME*, 78:779–787, 1956.

[116] L.I. Wu and S.H. Wu. A Note on Freudenstein's Theorem. *Mechanism and Machine Theory*, vol 33(1/2):139–149, 1998.

[117] A.S. Hall. *Kinematics and Linkage Design*. Prentice-Hall, Inc., Englewood Cliffs, N.J., U.S.A., 1961.

[118] G.S. Sutherland. Quality of Motion and Force Transmission. *Mechanism and Machine Theory*, 16:221–225, 1981.